The role of motion artefacts in fabric-embedded sensors

Michael, Brendan

Awarding institution:
King's College London

The Role of Motion Artefacts in Fabric-Embedded Sensors

Brendan Michael

A thesis presented for the degree of

Doctor of Philosophy

Supervised by:

Dr. Matthew J. W. Howard

Department of Informatics

Faculty of Natural and Mathematical Science

King's College London

September 2017

I hereby declare that except where specific reference is made to the work of others, the contents of this dissertation are original and have not been submitted in whole or in part for consideration for any other degree or qualification in this, or any other university. This dissertation is my own work and contains nothing which is the outcome of work done in collaboration with others, except as specified in the text and Acknowledgements.

Brendan Michael

September 2017

Acknowledgements

There are a number of people I would like to thank, who have helped and supported me throughout this degree.

Firstly, my supervisor Dr. Matthew Howard, for the invaluable advice, encouragement, and opportunities he has provided to me over the past years. I would also like to thank Dr. Thrishantha Nanayakkara, from whose discussions a number of fruitful research directions emerged. In addition, I am thankful for the help from Professor Sethu Vijayakumar, Dr Vladimir Ivan, and the rest of the SLMC.

I would also like to thank my colleagues at the RLL, CoRE, and King's, all of whom have been very helpful, full of advice, and friendly beyond all measure.

Abstract

Fabric-embedded sensors are of growing interest to studies requiring the measurement and analysis of human movement outside the laboratory environment. These small scale, minimally invasive sensors, can be used for medical applications such as clinical diagnostics and long-term rehabilitation studies, or other areas which require motion measurements, such as sports analysis or human-computer interaction. However, a major issue limiting their usage is the undesired effect of fabric motion artefacts corrupting movement signals.

In this thesis, the role of motion artefacts in these types of sensors is explored, with the aim of creating strategies to overcome these artefacts, and allow for accurate, long-term human motion sensing systems. To solve this problem, this thesis proposes treating motion artefacts as *stochastic perturbations* to the sensed motion, and utilising statistical learning approaches to develop artefact elimination and motion classification strategies. Treating motion artefacts in this way provides many benefits over analytical fabric modelling, as it removes the need to estimate physical quantities of the fabric. This thesis investigates the relationship between learning approaches and the unique problems posted by fabric motion artefacts. Methods that explicitly account for stochastic perturbations in the sensed signals are investigated include supervised errors-in-variables regression, and unsupervised latent space learning. In addition, the role that information contained within motion artefacts is investigated, in relation to distance based classifiers. In experiments, these methods are evaluated in a number of human motion tasks, including pose estimation and gait analysis. It is shown that these methods demonstrate improved prediction accuracy over

learning approaches that do not account for the unique problems of fabric motion artefacts, and are of a suitable computational complexity to allow them to be implemented in small-scale embedded fabric-sensing systems.

Contents

Chapter 1

Introduction

The analysis of human motion is often performed in a wide variety of fields, ranging from supporting clinical decision making, evaluating research hypothese, and providing user control for medical devices. The sensing apparatus often used for observing this user motion is generally comprised of high-accuracy motion capture technology. For example, camera based systems can be used to create biomechanical models of user motion, which can in turn used to evaluate causes of injury [1], or design controllers for operating prosthesis [2]. However, the high start-up and running costs of motion capture laboratories severely restricts their usage in both clinical evaluations and research studies. In addition, the fact that motion capture laboratories are comprised a large-scale equipment, and are installed in-place, means that they are unable to collect data outside the clinic. This means that data collected during laboratory based clinical trials (*e.g.,* evaluation of locomotion) may not be indicative of a user's real motion as seen outside the laboratory. In recent years, due to the availability of low-cost, low-power sensing systems (such as microelectromechanical systems [3]), there has been increased interest in using small scale sensors to monitor user motion outside the laboratory. Increasing, *portable sensors* have been investigated to determine their suitability to clinical human motion capture

tasks. These often comprise of sensor packages (*e.g.,* small boxes containing electronics) attached rigidly to the user via straps. More recently, the concept of *fabric-embedded sensors* has been approached, whereby sensors are integrated into items of clothing, through the use of knitting, and embroidery techniques. This approach allows for sensors to be worn unobtrusively, allowing for the long-term collection of data in natural non-clinical environments, such as the home.

While these new, soft sensing technologies offer significant potential for inexpensive and unobtrusive capture of human movement data, there remain a number of problems in their use. An important issue, is that of how to deal with motion artefacts corrupting data recordings, as caused by the unpredictable motion of fabric sensors with respect to the body (see Fig. 1.1). Previous fabric systems have attempted to solve this problem by fitting sensors tightly to the body (e.g., by use of straps or other tight-fitting garments [4]). However, this is unsatisfactory if sensors are to be incorporated in an unobtrusive way, into everyday items of clothing.

To address this issue, this thesis focuses on the motion artefact problem in fabric-embedded sensors, with the aim of understanding the role that these artefacts play. With this in mind, two main research questions are investigated, to discover both how to minimise the effect of these artefacts while following the guiding principle of non-invasiveness, and also how to exploit the effect of these artefacts in user motion classification systems.

Specifically, the first aim in this thesis is to investigate how to overcome the issue of fabric motion introducing errors into the observed signal. In this statistical methods from the errors-in-variables field are used to learn models of the wearer's movement that eliminate the effects of fabric motion artefacts. The proposed approach is computa-

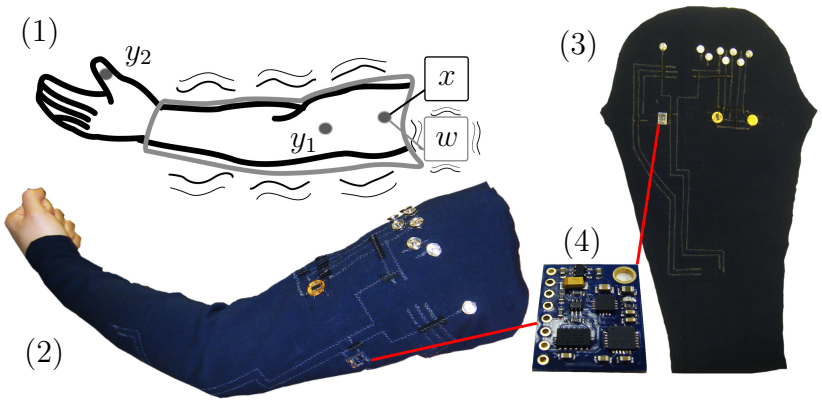

Figure 1.1: (1) Prediction of wearer movement at different points on the body (e.g., forearm y_1, fingertip y_2) based on sensor readings. Fabric motion with respect to the body introduces unpredictable artefacts into e-textile sensor readings w as compared to those derived from a rigidly attached sensor x. (2) Sleeve with embedded sensors. (3) Disassembled sleeve showing connections made with conductive thread. (4) Inertial measurement unit embedded on fabric.

tionally efficient, and can be easily implemented in an embedded system for on-board (*i.e.,* on-wearer) prediction of movements. As part of this, extensive experiments are performed, learning and predicting human motion movement from motion corrupted physical e-textile devices. These experiments indicate superior performance as compared to standard learning approaches, presenting a method for learning and predicting user motion from fabric embedded sensors.

Secondly, research into the role that fabric material parameters play in statistical classification systems is performed. This is in contrast to the first goal of eliminating motion artefacts, and provides a complementary look at how useful information of the body can be infer from analysis of the clothing. In this analysis, experimental evaluations are performed, and demonstrate that the motion of the fabric can contain useful information about the motion of the body, allowing the fabric itself to be used as a signal processing device.

1.1 Summary of Major Contributions

In this section, a summary of the major thesis contributions and published work is presented.

1.1.1 Eliminating Fabric Motion Artefacts with Statistical Learning

This thesis presents the first analysis of motion artefacts in fabric-embedded sensor systems. Specifically, in Chapters 3 and 4, the use of supervised statistical learning is presented as a method for overcoming these motion artefacts. An analysis of how motion artefacts can affect commonly used statistical learning methods is first presented, and it is shown that the standard learning assumptions are not compatible with the sources of error found in fabric-embedded systems. As such, a non-parametric *errors-in-variables* method is then described for learning body motions while explicitly accounting for these errors, and experimental evaluations are performed highlighting its superior performance over standard learning. These methods for solving the motion artefact problem are then generalised to unsupervised learning, through the use the latent space learning method, *Unsupervised Kernel Regression*. This allows for the prediction of body movement from fabric-embedded sensors by dealing with problems that arise when learning, in real-world motion tasks involving variations in user motion (*e.g.,* changes in locomotion speed).

Publications

- Michael, Brendan, and Howard, Matthew. "Eliminating motion artifacts from fabric-mounted wearable sensors." Humanoid Robots (Humanoids), 2014 14th IEEE-RAS International Confer-

ence on. IEEE, 2014.

- Michael, Brendan, and Howard, Matthew. "Learning Predictive Movement Models from Fabric-mounted Wearable Sensors." IEEE Transactions on Neural Systems and Rehabilitation Engineering 24.12 (2016): 1395-1404.

- Michael, Brendan, and Howard, Matthew. "Gait Reconstruction from Motion Artefact Corrupted Fabric-Embedded Sensors." IEEE Robotics and Automation Letters, Accepted/In Press, (2018)

1.1.2 Using Fabric Motion Artefacts as Information in Activity Recognition

In Chapter 6, analysis of the physical parameters of fabric is examined in relation to fabric motion and its affect on distance based classifiers. This empirical evaluation presents the first use of fabric motion as an additional source of information in activity recognition tasks. Fabric motion data is collected during a constrained motion task from fabric-embedded accelerometers, and statistical analysis is performed to examine the similarity of motions when using the additional information provided by the motion artefacts. These results show that exists a trade-off between additional information and extraneous motion, and this effect is evaluated in an online motion classification task using distance based classifiers, including *Support Vector Machines* and *Discriminative Regression Machines*.

Publications

- Michael, Brendan, and Howard, Matthew. "Activity Recognition with Wearable Sensors on Loose Clothing", PLOS One. 12, 10

(2017)

1.2 Thesis Outline

In this section, an outline of the thesis is presented.

Chapter 2

In this chapter, an analysis of the current uses of human motion analysis is presented, both in terms of laboratory based systems as well as portable sensors, contextualising the role of fabric-embedded sensors in this field.

- Review of motion analysis in the clinical domain, in terms of kinematic analysis for health-related studies.
- Review of clinical sensing apparatus, its limitations, and a review of the recent portable sensor data collection methods.
- Characterisation of fabric sensor, highlighting their current use as minimally invasive, continuous healthcare data collection systems.
- Review of of the sources of motion artefacts present in fabric sensors, and comparison to artefacts seen in clinical data acquisition systems
- In-depth analysis of the limitations of clinical-based artefact removal methods, when applied to fabric sensors.

Chapter 3

In this chapter, the role of motion artefacts in fabric sensors is specifically reviewed, exploring the use of both hardware design and signal processing methods for removing these artefacts.

- Comparison of motion artefact removal methods for fabric sensor systems, in terms of hardware based considerations and explicit modelling of fabric.

- In-depth analysis of the feasibility of statistical signal filtering for artefact removal, outlining common methods from the literature, highlighting limitations.

Chapter 4

In this chapter, the use of errors-in-variables statistical learning is presented as a method for overcoming the motion artefact problem. Experimental evaluations are presented demonstrating improved prediction accuracy over learning approaches that do not account for the unique problems of fabric motion artefacts.

- Basis for artefact removal by the application of statistical learning techniques in estimating motion.

- Developed method for viewing artefacts as stochastic perturbations to the sensed motion, and utilising errors-in-variables learning.

- Experiments presented in body-pose estimation highlights enhanced performance over standard learning techniques.

Chapter 5

In this chapter, the methods for solving the motion artefact problem presented in Chapter 4 are generalised to allow for the prediction of body movement from fabric-embedded sensors.

- Extension of learning body motion while treating motion artefacts as stochastic perturbations to the sensed motion

- Basis presented for the *unsupervised latent space learning* of human motion from fabric sensors, allowing for autonomously recalibration, and artefact elimination

- Experiments in gait sensing demonstrates elimination methods can be calibrated solely by the user motion, and are an effective method for handing artefacts experienced in everyday motion.

Chapter 6

In this chapter, a novel approach of using the fabric itself as a signal processing device is presented.

- Analysis of fabric as a *feature space mapping system* for classification systems.

- Characterisation of material properties in relation to sensed motion similarity.

- Experimental evaluations examining the affect of fabric motion on learning statistical classification models, showing enhanced predication accuracy in constrained tasks.

Chapter 7

In this chapter, conclusions and directions for future research is presented.

Chapter 2

Measuring Human Motion with Wearable Sensors

2.1 Introduction

In this chapter, the current state of the art in sensing for human motion modelling is reviewed to provide a background to research discussed in this thesis.

In this, an overview of *current research in the development and role of wearable sensors* is presented, contextualising the novel contributions. This is comprised of two constituent parts, a discussion on standard motion monitoring in the clinical environment, and the state of the art in fabric-embedded sensors.

The literature is then reviewed to discuss the issue of *motion artefacts* in fabric sensing systems. In this, existing solutions currently used for clinical motion capture are presented, and limitations in their applicability to human motion modelling using fabric sensors is discussed. Specifically, the failure of these methods to deal with the highly complex nature of fabric and its material properties is outlined.

2.2 Measuring Human Motion

This section outlines the current usage of motion data in both the clinical and research domains, and corresponding methods for obtaining these measurements. This is with the aim of providing a foundation for the later discussion of how these measurements can be obtained with wearable sensors, and associated problems.

2.2.1 Motion Analysis Overview

Information about human motion is of great interest to a variety of fields, including clinical decision making (*e.g.,* determining rehabilitation progress [5]) and hypothesis evaluation in research (*e.g.,* understanding causes of injury [1] or pathways of neurodevelopment [6]). Data collected during real-time can also be used as part of a feedback scheme for many end-user applications, such as the control of medical devices (*e.g.,* prosthesis [2] and exoskeletons [7]) and individualised statistics (*e.g.,* personalised healthcare tracking [8]).

In all of these fields, the overall aim is to capture accurate information about a user's motion. In the laboratory or studio environment, a variety of devices are available for taking such measurements, with the most commonly measurements sensed being the kinematics and dynamics associated with motion, such as walking, posture, or grasping. Data collected for understanding motion are commonly in the form of time-series measurements of: (i) positional data of segments of the body (*e.g.,* limbs or joint angles), often collected via camera-based optical motion capture [9] or internal measurement units [10], (ii) applied force, such as ground reaction force [11], or electric potentials in muscles associated with muscular force [12], or (iii) physiological and biochemical changes (*e.g.,* electrocardiogram (ECG) for cardiovascular related conditions, or pulse oximetry for blood oxygen saturation [13]).

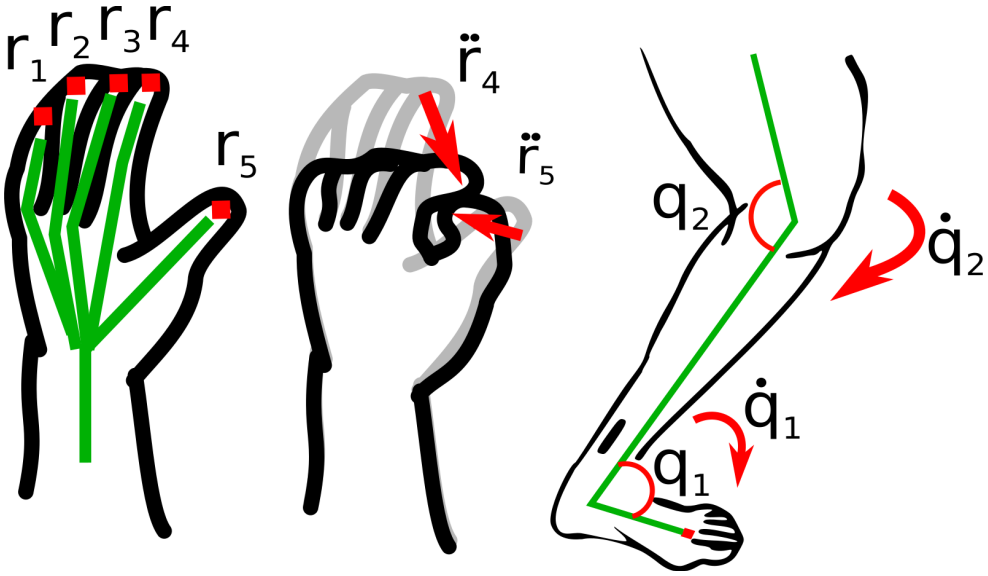

Figure 2.1: Common measurements in kinematics analysis can include position (r), linear accelleration ($\ddot{r}$), joint angle (q) or angular velocity ($\dot{q}$).

2.2.2 Kinematic Analysis

The most commonly measured feature in human motion analysis is of the kinematics of body segments. This characterises both the linear and angular motion of body segments, and can include the position of limb segments (*e.g.,* fingertips $\mathbf{r}$), joint angles (*e.g.,* knee or ankle $\mathbf{q}$), or their derivatives (Figure 2.1). Through knowledge of a user's kinematics, identification of the role of individual body segments during motions can be used to infer factors associated with that motion (*e.g.,* the relationship between injury and joint angles during sports [14]).

Example: Kinematic Analysis for Injury Prevention

To highlight the importance of accurate kinematic measurements of the body, a brief example is presented here outlining a commonly used technique for the objective analysis of workplace based ergonomics, the Rapid Upper Limb Assessment (RULA) [15].

In this technique, static measurements of the joint angles of a user's

upper limbs, neck, trunk and legs are made while the user performs tasks, and holds postures. For example, this could involve the user performing a workplace based task, such as assembling a component on a workbench, which may involve bending of the trunk and neck, and repositioning of the arms during the task.

Observed measurements are then given a score based on the RULA scale, such that postures that are known to cause musculoskeletal injuries (*e.g.,* excessive ulnar or radial deviation of the wrist) score highly, while postures that give minimal risk score low. Through this method, postures can be assessed for potential for injury, by identify the muscular effect required to maintain the posture. This allows for modifications of user posture (*e.g.,* by altering the workbench height) such that tasks can be performed with minimal risk to injury, based on the observed kinematic analysis.

2.2.3 Clinical Methods for Motion Capture

To be able to perform motion analysis tasks such as the RULA procedure described above, objective measurements of the kinematics and the dynamics of the body must be recorded, such as limb positions, joint angles, or applied forces. In the clinic these measurements can be taken quickly and inexpensively via a *pen and paper method*, whereby the clinician records static measurements of joint angles, or range of motion (*e.g.,* using a handheld goniometer [16]). However, while such methods are inexpensive and can be performed quickly, they lack precision [17], and are not easily generalisable to the measurement of movement tasks (*e.g.,* measuring the range of motion of a joint during walking).

As such, a number of objective techniques for the high-precision capture of human kinematics and dynamics have been developed. A brief

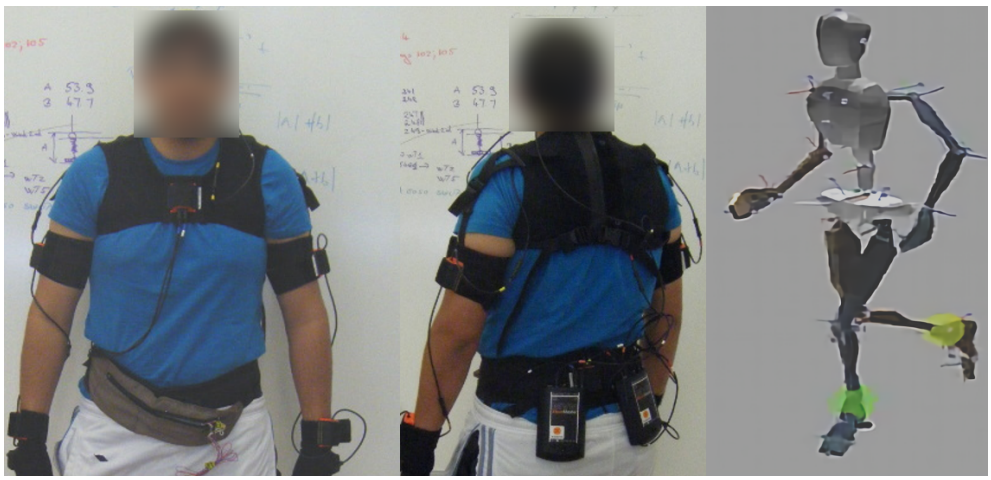

Figure 2.2: Inertial sensors MVN Biomech fully body motion capture system, and estimated biomechanical model.

discussion of different motion capture techniques is presented here to highlight current approaches in the clinical environment.

Goniometers

The simplest and most inexpensive technique for measurement of a patient's kinematics is though the use of a goniometer to directly measure a joint angle. For this, a goniometer is attached at the joint between two limb segments, with the axis of the goniometer aligned to the joint axis. Changes in the joint angle proportionally change the angle of the goniometer, which through the use of an in-built potentiometer, can be used to continuously measure the change in angle.

From these measurements, gait information can be determined including the duration of gait phases and the angular velocity of the joint [18]. However, due to their relatively simplistic design, goniometers suffer from a number of disadvantages, including excessive fitting and aligned time prior to data collection, patient encumbrance, and due to their hinge design, restriction to use in basic, single plane joint angles [19].

More recently, direct measurements of joint angles has also been per-

formed using using optical fibres to infer angle change with greater sensitivity [20], however these systems are still susceptible to the same positioning limitations as seen in goniometers.

Imaging Methods

To accurately measure human body motion, the use of image based motion capture systems has several advantages over direct measurement of joint angles, including the ability to measure multiple positions simultaneously without the need to attach measurement devices to the patient.

These imaging techniques involve the use of one or more cameras to track positions of limb segments during motion, and construct a kinematic structure based on this data [21]. This can be performed by tracking either markers placed on the body [22, 23, 24] (*e.g.,* Vicon Vero, Vicon Motion Systems Ltd. or OptiTrack, NaturalPoint Inc.), or by estimating limb segments from markerless video capture [25, 26, 27] (*e.g.,* Kinect, Microsoft Corporation or Basler Aviator, Basler AG). However, while these methods are suitable for measuring complex movements with a high sensitivity, the cost for such apparatus (and associated clinic space required) remains high, even with low-cost "in-home" markerless systems such as the Microsoft Kinect previously mention. However, limitations in this approach include marker or limb occlusion (resulting in line-of-sight issues), and the fact that measurements are made relative to an absolute coordinate frame defined by the camera system. This means that recording is restricted to the camera's fixed location, limiting the environment in which measurements can be taken (*i.e.,* only in the clinic).

For greater precision, magnetic field tracking [28, 29, 30] (*e.g.,* Liberty, Polhemus or Aurora, NDI Medical) has also been used to track individ-

ual positions. In this an external magnetic field is generated, and positional data of sensors placed on the body is estimated based on field strength measurements. Due to the magnetic field generation, these systems often only measure within a small range (often less than one metre volume), however can have much greater sensitively that image based methods.

Due to the high precision in estimating user kinematics, these apparatus are also used as the gold-standard with which to compare new sensing systems [9].

Inertial Sensors

Due to the problems of portability in image based measurement systems, internal measurement units are also commonly used to measure human kinematics [10] (*e.g.,* MVN Biomech, Xsens Technologies BV or IGS-Cobra Wireless Suit, Synertial Labs). In this, small-scale low-power microelectromechanical sensors (MEMs), often referred to inertial measurement units (IMUs), can be used to give instantaneous linear acceleration (accelerometers) or rotational velocity (gyroscopes), in their own three dimensional local coordinate system. This means that these sensors can make measurements without an external reference, allowing for a greater portability.

For this, IMU position and rotation is estimated from the observed measurements through integration methods [31], and body segment position and rotation is estimates from a combination of these IMUs, with a priori defined biomechanical models. An example of the MVN Biomech system is shown in Figure 2.2, showing 8 of the 17 required sensors for motion capture, and estimated skeleton model.

While IMU methods allow for an expanded environment, the accuracy of these measurements are often lower than image based sensors. This

can be due to a number of factors, including the fact that sensor position and movement during gait analysis can introduce errors into the estimation procedure, and the biomechanical estimation model itself must be sufficiently complex to estimate the segment kinematics from the IMU measurements [32].

Force Transducers

Alongside understanding the spatial properties of motion, it is also clinically important to measure the dynamics of motion, *i.e.,* the forces exerted by the body. This encompasses static forces (*e.g.,* force applied when holding a position), or dynamic forces (*e.g.,* those applied during gait).

To measure these forces in the clinical environment, measurements of the exerted force are often taken relative to an external body. Force transducers can be used to this effect, by providing an electrical signal proportional to an applied force, for example, by measuring the deflection within the sensor given an applied force. This is commonly performed by the use of piezoelectric or piezoresistive sensors, which change their electrical potential or resistive properties given an applied force.

In the clinical environment, force platforms are often used to quantity body forces, including the use of instrumented treadmills [33] or stairs [34] for use in gait studies. However, not only is there a high initial start-up and operational cost, the restriction to artificial environments (*e.g.,* in the case of gait studies, treadmills), means that measured forces can differ from those applied during everyday motion [35], resulting in reduced information for clinical decision making.

Electromyography

Direct measurement of the electrical activity associated with a contracting muscle can also be used to understand about force application [36, 37], in a technique known as electromyography (EMG). In this, the electrical potential of a muscle of interest is measured either invasively via intramuscular needles, or more commonly non-invasively via surface electrodes on the skin surrounding the muscle [38].

EMG provides a more intuitive way of investigating dynamics tasks [39], by explicitly measuring muscular response. In addition, the simplicity of measuring electrical potential allows for the design and use of low-cost sensors, and minimal training to collect data.

However, EMG suffers from practical restrictions that limits its applicability, and often requires repeating measurements. This includes both intrasubject [40] and interrater [41] variability, and poor reliability [42].

2.2.4 Kinematic and Dynamic Modelling of Motion

Measurements of the kinematic and dynamics of movement can provide useful information for understanding about patient motion [43], for example, to quantify patient recovery progress against functional assessment targets [44]. In this section, a brief overview of kinematic and dynamic modelling of motions is presented.

Kinematic and dynamic *biomechanical models* provides a means to use these measurements to investigate factors influencing motion, by estimating segment and joint forces associated with that motion. For example, by using a kinematic description of the body (*i.e.,* a defined geometry of the limb segments and and interactions), and body measurements, modelling can be used to find biomechanical features that relate to disease [45], or effects of changing prosthesis design on gait

[46]. Additionally, the use of biomechanical models allows for the estimation of forces in human movement that are difficult to measure directly, such as joint torques, centre of mass movement [47], or stress distributions [48].

Link segment models (LSMs) [19] are a commonly used method for estimating forces and torques, by finding an inverse dynamics solution from observed measurements. Simple models can be used to model a partial representation of the body for constrained movements, *e.g.,* the forces acting only in one plane of a single joint during a sit-to-stand exercise. More complex model can reprepresent a full kinematic description of the body, *e.g.,* estimating 3D forces [49] on a full body model with sufficient degrees of freedom to model walking. Anatomical geometery can also be included in the representation of the model by tracking markers placed on limb segments [50].

More specifically, a link segment model is defined as segments of fixed point masses, connected by hinge joints, with a priori defined lengths and moments of inertia [19]. Joint forces and torques can be predicted by using this model definition, by applying mechanical laws to the segments and joint kinematic measurements (*e.g.,* position, velocity), and measured external forces acting on the model (*e.g.,* gravity and ground reaction force). While these simple models have been shown to be a useful tool for investigating force control in motion tasks, limitations in this approach include the lack of accuracy when measurements are not representative of user motion (*e.g.,* in the case of soft-tissue artefacts [51] or marker placement errors [52]).

To overcome such issues, more advanced models include the use of optimal control studies to model dynamic gait data solely from the kinematics [47] (removing the need to capture environmental interaction forces), or by taking a probabilistic approach to account for uncertainty

in issues such as marker tracker [53], variability in kinematics [54], or uncertainty in the inverse dynamics [55]. The modelling of additional body characteristics, such as muscle stiffness [56], or representing moments generated by antagonistic muscle pairs [57].

2.2.5 Portable Sensors

Despite there being a wide range of technologies now available for capturing body motion and associated biosignals, there currently exists a number of topical problems that limits their usage in both the research and clinical domains. These problems include: (i) limited access to facilities for patients, even in the developed world [58] [59] (ii) the requirement that positional sensors (*e.g.,* magnetic field tracking, or optical camera methods) have a static point of reference with which to estimate changes in movement, limiting the observable environment (often in a single room with limited real-world interactions), (iii) occlusions of body parts in camera-based systems when the user leaves the field-of-view, or is obscured by other objects in the environment, (iv) limitations of magnetic field tracking including their inability to be used in conjunction with other magnetic sensitive medical apparatus (*e.g.,* pacemakers), or environmental inference in the local magnetic field, (v) limited time in which to collect data (*e.g.,* only for an hour every few months), (vi) high per patient cost of using this equipment [60] (and associated training / maintenance).

To address these issues with clinical based motion capture systems, there has been a recent interest in the development of sensing apparatus that can collect data over long-term periods of time, outside the laboratory environment (*e.g.,* in the home), without the need for specialist operators to configure and assist with data collection. While it has been proposed to use *in-home* video motion capture systems for

capturing positional data [61, 9] (*e.g.,* finger positions, as seen in Figure 2.1), these systems are still limited to data capture in one location (*e.g.,* a single room), and require video processing, a computationally costly exercise limiting real-time applicability. In addition, the use of cameras in the home may not been seen as an acceptable solution due to privacy and security constraints.

In an attempt to solve this, there has been great interest in using *portable sensors*, that can be carried or worn by an individual during everyday activities, and capture continuous body-related data. With the increasing life expectancy rate in developed countries, wearable sensing systems have the promise to provide quantitative movement data for use in the rehabilitation of patients [62], or the detection of disease specific conditions [63].

While early designs [64] were often cumbersome and had limited functionality, advances in the manufacture of microelectromechanical systems (MEMS) [65, 3] has enabled the development of very small form factor inertial sensors. In comparison to laboratory motion tracking equipment (*e.g.,* cameras or high-accuracy IMUs [10]), these small sensors are very inexpensive [66], ranging between $10 to $200.

Primarily, these sensors rely on measuring derivatives of position (*i.e.,* velocity or acceleration) via accelerometers or gyroscopes [67]. These IMUs do not require an external reference frame (*e.g.,* magnetic base station or cameras) with which to track positional changes, but instead take measurements of the current (history-independent) velocity or acceleration. IMUs can also be used for obtaining positional estimates [68], via tracking the change in measurements (while ensuring that sensor drift is accounted for).

Due to this ability to capture motion outside the laboratory environment, these types of sensors have found usage in a large number of re-

search studies investigating autonomous long-term data collection. To highlight the new research and clinical opportunities presented by these sensors, a number of systems are presented here. This includes (i) providing user feedback for at-home rehabilitation exercises [69, 70] (ii) assessing treatment progress for neurological conditions (*e.g.,* Parkinson's Disease) [71, 72, 73] and post-surgery monitoring [74], or (iii) the control of medical devices such as prosthetics [75] or assistive-grasping gloves [76].

2.2.6 Fabric Sensors

These portable sensor implementations present a promising solution to the problem of continuous healthcare data collection systems. However, even sensors designed for use outside the laboratory environment suffer from the traditional design principle of fitting electronics into ever smaller rigid boxes [77]. This can present a number of practical problems which limits their applicability, including: (i) size and weight of sensors affecting user movements (undesirable for analysis/diagnostic studies), which means that often sensors are placed in alternative, less desired positions [78], (ii) sensors being visually obtrusive (detrimental to patient experience [79]), (iii) user discomfort when recording over a continuous time-period lasting days or even weeks [78], (iv) the daily reattachment of sensors can result in inconsistent positions/orientations [80].

A natural solution to these problems is to incorporate such sensing systems into items already in use by patients. As such, sensors would be minimally invasive, both in terms of visual obtrusiveness and their limited additional influence on user movement. Often, these sensors are incorporated into commonly used electronic devices, such as wrist-worn watches [82] or mobile phones [83], however, these approaches are lim-

Figure 2.3: Fabric sensors, including a) small scale IMU embedded into fabric using conductive steel thread, b) flexible circuitry for muscular activity monitoring, c) jogging leggings using fabric sensors for collecting data outside the laboratory [81].

ited to sensing in one location (*e.g.,* the wrist), and cannot provide accurate information on other areas of the body (*e.g.,* gait from a wrist-worn device).

An emerging technology that extends the minimally invasive ideology, is the use of *fabric-embedded sensors*, also known as *e-textiles*. In this, sensors themselves either made out of fabric, and embedded with clothing items [84], or small sensors are embedded into items of fabric (such as clothing [4]). Examples of these sensors can be seen in fabric-devices used for data collection in this thesis, in Figure 2.3.

These modern, small scale embedded sensors use intergrated circuits (such as inertial measurement units) which are commercially available at low prices and measure only millimetres in size [85]. The recent development of these small-scale sensors has allowed for the timely investigation of creating measurement systems for monitoring bodily move-

ment, while minimising both physical and visual invasiveness. As these sensors are inexpensive and non-invasive, they can also be used to collect data prior to a diagnosis. For example, in the clinical setting, people 'at-risk' of a particular disorder can, by wearing these systems, provide a continuous stream of healthcare progression and recovery data to a clinician, which can be used to both understand disorder progress and provide an early warning if signs of a disorder are observed.
This integration of sensors into items of clothing takes advantage of the many benefits of textiles, including durability, conformity to the human body [77], and wash-ability (important for longer term data collection, with some sensors, *e.g.,* Figure 2.3(B), also having waterproofing properties). This provides a sensing platform suitable to long-term data collection studies [86] (*e.g.,* studies lasting periods of weeks or even months). Not only is user discomfort minimised with these soft-sensors, but it also means that the attachment of sensors can be performed easily by the user, by simply donning the garment. Consistent placement of sensors on a garment allows for sensor positioning without specific anatomical knowledge (*e.g.,* in the case of fabric based electrodes [87, 88]). These small-scale, unobtrusive fabric based sensors have also found utility in a number of research studies that were previously limited not by user discomfort, but where portable sensors alter the natural user motion, such as during respiration analysis [84, 89, 90] (*e.g.,* for sleep-studies, where uncomfortable strap-on sensors can alter sleep patterns), and running or other high-energy activities [91, 92, 93].
With this goal in mind, there exists a number of research designs for fabric structured sensors. While the design and manufacture of these sensors are outside the scope of this thesis, some brief examples are discussed here to contextualise the work presented. This includes including printing circuitry onto fabric [94] piezoelectric yarn-based strain

sensors for cardio-respiratory studies [90], 3D trunk motion analysis [95] or joint analysis [96], knitted electrodes for electromyography monitoring [88], or even cantilever-based fabric motion sensors [86]. In addition to this, fabrics are often used alongside standard sensor components (such as integrated circuits), allowing for the embedding of non-fabric sensors into textiles. Examples of this include accelerometers and wireless components attached to fabric electrodes, stored in on-body fabric packages [97] or plastic casings [98], or using conductive thread to sew components into clothing [4] [99, 100].

Due to the use of kinematic analysis as the primary means of inferring human motion (see §2.2.2), the research performed in this thesis is primarily concerned with those fabric-sensors that measure the same. In this, IMU sensors are used to collected measurements body linear accelleration, and angular velocity, using small scale accelerometers and gyroscopes. Due to reasons of frame independence (as discussed in §2.2.5) these sensors are particularly suited to collecting data outside of a laboratory environment, and can transmit data through a number of digital communication methods (*e.g.,* serial peripheral interface bus (SPI), or inter-integrated circuits (I2C)).

Specific examples of the IMUs that can be embedded into garments includes the ADXL345 tri-axel accellerometer [101] or the ITG-3200 tri-axel gyroscope[102]. While both kinematic measurements are easily obtained, different IMUs are suited to different tasks in human motion measuring, with accelerometers generally used to detect dynamic changes in motion (*e.g.,* impact forces in walking), while gyroscopes are used to detect angular changes (*e.g.,* joint movements).

2.2.7 Fabric Actuation

While outside the scope of this thesis, it is important to mention the current research in actuation systems designed for use with fabrics, which are often used alongside such fabric sensors. These actuators are designed to be embedded into fabric for use in wearable systems such as exoskeletons or prosthetic devices. Some examples of this include using shape-memory materials for controllable bending [103][104], pneumatic [105, 106] or Bowden cable-based [107] gait-assistance exosuits, soft-humanoid robotics [108], pressure controllable spacesuits [109] and cardiac actuation [110]. Due to the greater complexity in actuation (and limited mechanical force in fabrics), these systems often rely on a combination of hard electronic components coupled with fabrics.

2.3 Motion Artefacts in Fabric Sensors

The research discussed in §2.2 highlights the vast range of uses that fabric sensors have found, both in the research and clinical domains. These small-scale monitoring systems can allow for data to be collected outside of a laboratory environment, with systems able to record human motion in areas such as the home, over long-term time periods. However, one of the key problems consistently faced by these systems, is how to deal with motion artefacts corrupting observed signals, compromising their effectiveness for activity recognition and monitoring [111]. In this section, the topic of motion artefacts in wearable sensors will be discussed, including a outline of the sources of these artefacts, and how current artefact mitigation strategies could be applied to fabric sensors. While this thesis is primarily focused on the role of artefacts in fabric sensors, these artefacts also affect to varying de-

grees larger-scale non-fabric sensors (*i.e.,* portable sensors), and therefore this section discusses these artefacts in the context of both sensor types.

Initially, to illustrate this problem, an example of a common motion sensing task is presented. In this, the aim becomes to predict some measurements (*e.g.,* the position of a end-effector for a prosthetic hand, or the optimal velocity for an assisted gait device (see §2.2)), based on observed readings from a sensor located somewhere on the body (*e.g.,* muscular activity). These predictions can be made by computing the forward kinematics, given an analytic model of the system. However, this is generally a difficult task due to the need to acquire a precise analytical model of the interaction. In general, this is solved by instead using statistical machine learning to model the mapping from the sensed readings to the desired predictions, from a set of calibration data.

However, while these approaches are appropriate to situations with well-defined analytical interactions, or highly accurate measurements, errors in predictions can be made if observed measurements are significantly different from the actual state of the body. Causes of incorrect measurements are numerous (*e.g.,* electrical noise), however, predominately these errors are caused by *wearer motion* disturbing the sensing system.

These *motion artefacts* caused by the movement of a wearer are of varying severity depending on a number of factors (*e.g.,* type of motion sensed, positioning of sensors). As such, in the following section the sources of motion artefacts are described, with which to provide a starting point to understanding the effect of these artefacts on sensing systems.

2.3.1 Sources of Motion Artefacts in Fabric Sensors

This error between the sensed motion and the true underlying movement is prevalent in portable wearable sensing systems. These motion artefacts can be caused by a number of sources, including user motion temporarily causing sensors to loose contact with the body (*e.g.,* in the case of electrode contact in EMG)[112, 113, 114, 115], movement of intertial sensors causing misalignment of axes [116, 117, 32], or muscular cross-talk [118]. Sensors attached rigidly to the body (*e.g.,* via straps or elastic), can be perturbed by user motion, and shift their position depending on user action or body positioning [119]. In fabric based sensors however, the loose coupling between the fabric and the body can often magnify these errors. For example, sensors attached to standard garments (such as a t-shirt) can show alignment errors between the sensor and body. In [120], it is seen that the deviation between the true sagittal angle of the forearm during an arm raising task, and that measured from a sensor embedded into the sleeve, was up to 55°. This was due to fabric slack resulting in the embedded sensor becoming misaligned from the arm. Additionally a similar measurement error was seen during an arm rotation task, again due to the loose sleeve being only loosely couple to the arm, and not following arm rotation. This can severely affect motion analysis techniques reliant on accurate data. This introduction of fabric into the sensing problem brings with it additional issues, such as the increased deformation and slack [121] compared with sensor movement on human skin. This can increase the loss of contact between the sensor and the body, and can impede motion capture systems that are relient on consistent positioning, *e.g.,* artefacts in fabric respirometers, generated from speaking [84] or breathing [90]. In addition, their material properties can be affected by hysteresis

creating signal drift (*e.g.,* in wearable goniometers [96]), circuit instability (*e.g.,* short circuiting in yarns [122]), or even general fabric movement caused by textile/body interaction (*e.g.,* in piezoresistive bending sensors [95, 123]).

2.3.2 Eliminating Motion Artefacts in Clinical Systems

To investigate this problem of motion artefacts in fabric sensors, first a discussion on how artefacts can be eliminated from high-precision motion capture systems is given. In these systems, there are a number of sources of measurement error that influence both the quality of the sensed signal, and can distort later modelling (such as limb segment estimation in Figure 2.2). These sources can include external magnetic fields influencing magnetic position trackers (*e.g.,* electrical equipment, metallic objects) or occlusions of the sensed target for camera based visual tracking methods. However, the major source of these errors [124] are caused by the undesired motion of the sensing apparatus with regards to the sensed body, known as *soft tissue artefacts* [124]. These artefacts are especially prevalent in apparatus that requires the attachment of sensors to the body (*e.g.,* camera markers or IMUs). In this, artefacts are caused by the additional motion of the skin (on which the markers are placed) relative to the underlying bone on which the kinematic model is based. The magnitude of these artefacts depends on a number of factors, including the type of movement measured [125], the location of sensors (*e.g.,* soft tissue mass can have greater extraneous motion during task performance [126]), or even the subject-dependent structure of the tissue [127].

To attempt to solve this soft tissue motion artefact problem, commonly techniques use a *cluster of markers* approach, whereby arrays of visu-

ally tracked markers (generally three or more [128]) are attached to a body segment. From this cluster, estimation of the underlying kinematic model (*i.e.,* joint angles and bone positions) is made by tracking the displacement and deformation of this cluster. This includes techniques that remove local deformation errors by estimating mean best-fit measurements of a cluster during a time-series [129], modelling the non-rigid motion of the skin [130], or using optimisation methods to find joint models that best describe the observed sensor motion data [131].

However, direct application of these techniques can prove problematic in fabric sensor systems where tracking fabric displacement and deformation is not possible. This can be due to a number of factors, including (i) tracking multiple positions on the fabric to estimate deformation requires either an external reference (*e.g.,* a camera) negating the portable benefits of fabric sensors, or a large array of IMU based sensors, increasing garment weight (and therefore increasing invasiveness), and (ii) modelling the dynamic structure of the fabric is a much more computationally intensive task than body modelling, and would not be suitable to low-cost embedded systems.

2.4 Conclusion

In this chapter, the role of human motion monitoring in the clinical and research domains has been discussed. In this, it has been highlighted that there is a need for portable, small-scale sensing apparatus to allow for motion sensing outside the laboratory environment. Sensing devices that aim to fill this gap have been discussed, highlighting the broad range of applications these devices can be used for. The concept of fabric-embedded sensors has been discussed as an approach to making these systems minimally invasive, and data collection as simple

as possible for the end-user.

In detailing these systems, a recurrent problem was discussed, that of the effect of motion artefacts on human motion monitoring systems. It was noted that these problems occur in all forms of wearable sensing apparatus, and are especially prevalent in fabric sensing systems due to the complex dynamics of the substrate. In order to have accurate sensing systems that fully make use of the advantages offered by fabric, it is necessary to eliminate these errors from the measurement systems. In the next chapter, current approaches that attempt to solve this problem are outlined. This includes sensor design methodologies that have been used to minimise motion artefact generation, and the use of statistical signal processing techniques to remove artefacts from existing signals.

Chapter 3

Handling Motion Artefacts

3.1 Introduction

In this chapter, the role of *motion artefacts in wearable sensing systems* is specifically reviewed through examination of existing literature, with an emphasis on current artefact mitigation strategies. In this area, two main approaches to this problem are discussed, firstly studies that use *hardware design* to pre-emptively minimise artefacts before data collection will be reviewed, and secondly a review is carried out of studies that employ *signal processing and modelling* techniques to remove existing errors in the data. While this thesis mainly focuses on fabric-embedded sensing systems, on-body portable sensors will be discussed alongside fabric-embedded systems throughout this chapter, as many of the motion artefacts and artefact mitigation methods are seen in both. The material reviewed in this chapter will form the basis for which to present the novel contributions in later chapters.

3.2 Hardware Design Considerations

The problem of undesired fabric motion in e-textile data acquisition is often minimised by ensuring that there is minimal extraneous move-

ment of the fabric (*i.e.,* there a strong coupling between the body and the clothing) [132, 4, 91]. This can be done by fitting garments tightly to the body (*e.g.,* by embedding sensors into undergarments such as vests).

This approach however is unsuitable if sensors are to be incorporated into everyday items of clothing (*e.g.,* shirts, trousers). While close-fitting garments can be suitable for specific task monitoring (*e.g.,* sports), in general, clothes are worn loosely, and do not follow the strict contours of the body. Populations that can benefit greatly from personal sensing apparatus (*e.g.,* the elderly, suffers of neurological conditions, or people undergoing physical rehabilitation), can also find it difficult to put on close-fitting garments [133]. In addition, fabric exhibits material properties such as slack, stretch, or folding, meaning that strong coupling to the area of interest (*e.g.,* finger joint tracking [93, 134]) is not always possible, with sensors shifting during joint movement.

3.3 Explicit Modelling of Fabric

One approach to deal with fabric motion in everyday garments, is to explicitly model the wearer/fabric interaction dynamics. This is often performed in the animation field [135], to generate realistic fabric motion based on the wearer's movement. This can include physics based approaches, such as mass-spring or particle systems [136, 137] or explicitly computing estimates of the geometric behaviour of wrinkles in clothing [138].

However, the explicit modelling of fabric during motion is a complex procedure, requiring extensive information of the interaction mechanics (*e.g.,* how the fabric conforms to the wearer at different positions on the body during movements), and a suitably detailed model to represent these interactions [139].

The computational demands of predicting on such a model require the use of dedicated hardware, often costly graphical processing units [140], making this modelling unsuitable for a light-weight, embedded wearable system. In addition, the large number of fabric parameters in clothing (*e.g.,* thickness, weave pattern, looseness and flexibility), affects the wearer/fabric interaction in different ways depending on their internal fabric, or fibre structure [141]. Models formed in this way therefore, are restricted to a particular class of fabric, and would necessitate re-modelling for using different clothing items.

3.4 Filtering

A popular method for removing motion artefacts from signals obtained from wearable sensors, is to use techniques from the signal processing domain to remove unwanted features of an observed signal. These methods are aimed not at *preventing* motion artefacts (see §3.2), but predicting motion artefact-free measurements from observations. Generally, filtering in wearable sensors can be subdivided into two main branches. Firstly, hardware-based filtering can be used to remove artefacts and increase signal quality before reaching a digital device (such as a PC base-station [142]), and requires that additional circuitry (*e.g.,* capacitors and resistors) be designed and incorporated into a wearable sensing system prior to data collection. However, this requires the explicit tuning of filter parameters by adjusting circuit components (*e.g.,* resistance), and does not allow for simple modification of these parameters without hardware redesign. As such, digital filters are often employed instead, where a signal is instead filtered after acquisition without the need for additional hardware (however, at at higher computational cost). Due to this ability to implement more complex, tunable filters that have greater applicability to statistical algorithms, this

section will focus on digital filters.

3.4.1 Overview of Linear Digital Signal Processing

The most common approach for signal filtering is the *linear filter*, whereby a discrete-time observed measurement $\mathbf{w}_t \in \mathbb{R}^{\mathcal{K}}$ (*e.g.,* a joint position) can be defined as [143]:

$$\mathbf{w}_t = \mathbf{B}_t \mathbf{x}_t + \boldsymbol{\varepsilon}_t \tag{3.1}$$

where $\mathbf{x}_t \in \mathbb{R}^{\mathcal{I}}$ is the (unobserved) information containing signal generated at the current time, $\boldsymbol{\varepsilon}_t \in \mathbb{R}^{\mathcal{I}}$ denotes additive noise on $\mathbf{x}_t$ and $\mathbf{B}_t \in \mathbb{R}^{\mathcal{K} \times \mathcal{I}}$ is the measurement model matrix (also commonly known as the gain, parameter matrix, or weighted coefficients).
The transition from one discrete-time state to the next is then defined as:

$$\mathbf{x}_t = \mathbf{A}_{t-1} \mathbf{x}_{t-1} + \boldsymbol{\epsilon}_{t-1}, \tag{3.2}$$

where $\mathbf{A}_t \in \mathbb{R}^{\mathcal{I} \times \mathcal{K}}$ is the process transition matrix, and $\boldsymbol{\epsilon}_t \in \mathbb{R}^{\mathcal{I}}$ denotes process noise.
Given this setup, the problem then becomes the optimal selection of parameter matrices $\mathbf{B}$ and $\mathbf{A}$, such that an estimate of a noise-free signal $\tilde{\mathbf{x}}$ is obtained from measurements $\mathbf{w}$, in such a way that the extraneous noise is removed, and important information contained in the signal is retained. Alternatively, artefact detection methods can be applied to find and discard entire measurements that exhibit motion artefacts, for example through the use of classification methods such as neural networks [144]. However, due to the fact that the fabric-based motion capture systems are used during movement (and as such the majority of measurements will contain artefacts), discard the majority of these measurements neglects the useful information contained

within.

For the mitigation of motion artefacts, these common approaches to linear filtering is generally categorised into the following major types: bandpass filtering, adaptive filtering and Bayesian inference. These methods, and their suitability to the motion artefact problem, are discussed here to provide context for the novel approaches outlined in later chapters of this thesis.

3.4.2 Bandpass Filtering

Bandpass filtering is one of the most commonly used, and simplest approaches to removing undesired noise from the a motion signal, seeing usage in many wearable sensor implementations [145, 146, 132, 71, 147]. In this setting, methods such as the Butterworth Filter [148] are applied to observed measurements to remove or attenuate sections of the signal that contain frequencies outside of a desired range. For example, in electromyography studies [114], where the signal of interest has a known frequency range, bandpass filtering can be used to suppress unimportant frequencies while retaining those that correspond to the signal of interest.

However, while this method is well suited to certain domains where the frequency spectrum of the noise and motion signal are known a priori, (*e.g.,* where the sources of the artefacts are well understood) this solution is generally not applicable to systems where either (i) the frequencies of the motion artefact are either not known or too varied to filter via a spectral analysis, or (ii) the frequencies of the motion artefacts and desired motion signal overlap [149] [84], such that important information is lost during filtering. As such, bandpass filtering is generally only used as an pre-processing stage in wearable sensor filtering, to limit the range of possible errors. After applying this method, more

advanced techniques are employed to perform more precise filtering.

3.4.3 Adaptive Filtering

A popular method [150, 91, 151, 152, 153, 154] for filtering signals where *a priori* spectral information is not available, is to use filters that remove noise in the observed signal, by updating (adapting) its own filtering parameters over time. This *adaptive filtering* [155] is performed by iteratively updating filter parameters, such as the measurement model matrix $\mathbf{B}_t$ (see §3.4.1), so that the error between the measurement $\mathbf{w}_t$ and a secondary reference signal $\mathbf{s} \in \mathbb{R}^{\mathcal{S}}$ is minimised:

$$\arg\min_{\mathbf{B}} \|\mathbf{s}_t - \mathbf{B}_t^\top \mathbf{w}_t\|^2. \tag{3.3}$$

As the noise free signal $\mathbf{x}$ is not measurable, there is a key assumption that the underlying motion $\mathbf{x}$ is uncorrelated to the motion artefact, and that the motion artefact is correlated in some way to the reference signal $\mathbf{s}$. This correlation assumption allows for $\mathbf{s}$ to be used as an input to the adaptive filter, in order to identify and remove the artefacts that are also observed in the measured signal $\mathbf{w}$.

In wearable sensors, this approach is often used to remove electrical noise in physiological measurements (*e.g.,* EMG, or ECG). This can be done by using a reference signal representing powerline interference at another position on the body [156]. This is commonly performed by placing an additional electrode on an area of the body that will also contain electrical noise (*e.g.,* the hip), but is independent of the muscular electrical potential associated with the measured movement (*e.g.,* arm abduction).

Artefacts caused by user motion (*e.g.,* loss of contact between sensors and skin during motion) can also be mitigated with adaptive filters [150, 157], by using additional sensors to detect significant user mo-

tion, and attenuate the corresponding observed measurement. For example, in studies collecting EMG measurements, where the user must remain static for accurate measurements, undesired user motion can be detected using additional accelerometers. Note that this approach is not appropriate for motion capture as described in this thesis, due to the dynamic nature of user movement, and non-invasive approach of minimising the number of sensors.

Example: Least Mean Squares

To illustrate this technique, the well-known stochastic gradient descent algorithm Least Mean Squares (LMS) [158] is briefly presented as a solution to this learning task. As the error function (3.3) is convex, the algorithm estimates a parameter matrix that minimises the error in the prediction.
In this algorithm, the signal is filtered by first initialising the parameter matrix $\mathbf{B}$ to some small value, then by:

(i) estimating the motion artefact free signal $\tilde{\mathbf{x}}_t$, as the parametrised observed measurement:

$$\tilde{\mathbf{x}}_t = \mathbf{B}_t^T \mathbf{w}_t, \tag{3.4}$$

(ii) computing the error between this estimate and the reference signal $\mathbf{s}$, to evaluate the performance on the chosen parameters:

$$\tilde{\boldsymbol{\varepsilon}}_t = \mathbf{s}_t - \tilde{\mathbf{x}}_t, \tag{3.5}$$

(iii) and finally updating the filter parameters proportionally to this error:

$$\tilde{\mathbf{B}}_{t+1} = \tilde{\mathbf{B}}_t + \mu\tilde{\boldsymbol{\varepsilon}}_t\mathbf{w}_t, \tag{3.6}$$

with the learning rate controlled by the parameter μ.

While adaptive filtering techniques such as LMS are commonly used in removing motion artefacts, they suffer from a number of problems in relation to its implementation in fabric sensor systems. Firstly, the reliance on additional sensors for the parameter adaptation increases overhead, which is a troubling problem in fabric embedded systems, where physical space and both computational and electrical power are limited. In addition, for many fabric sensors that monitor human motion, the assumption of uncorrelated artefacts with the motion signal does not hold. For example, when using fabric sensors (*e.g.,* an embedded accelerometer) to monitor body kinematics, the fabric motion (and therefore the motion artefact) is correlated to the motion of the body. This is also seen in the case of muscle signals interfering in ECG studies [159]).

While there exist adaptive algorithms to take account of this correlation [160], these often require additional assumptions of the correlation, and have increase computational complexity.

3.4.4 Bayesian Inference

As discussed in §2.3.1, the sources of motion artefacts in wearable sensors are varied, with signal corruption ranging from electrical noise, vibrations and external influences (such as air currents). The factors are very difficult to model as a deterministic system, due to the sheer number of possible factors, and complex dynamic processes involved (e.g. fabric motion under wind).

An alternative to attempting to create deterministically models that

capture this noise, is to apply probabilistic filtering methods [161, 162, 163, 164, 165, 166]. In this, observed measurements are assumed not to be deterministic, but instead are drawn from a distribution of possible values. These methods, derived from Bayes' Theorem, are often used in filtering to provide continuous updates to filter parameters, to maximise prediction likelihood.

This method can be described by the process in which estimates of the noise-free signal are made through application of Bayes' rule [143]:

$$p(\mathbf{x}_t|\mathbf{w}_t) = \frac{p(\mathbf{w}_t|\mathbf{x}_t)p(\mathbf{x}_t)}{p(\mathbf{w}_t)}, \tag{3.7}$$

where $p(\mathbf{x}_t)$ is the prior estimation of the noise-free signal, $p(\mathbf{w}_t|\mathbf{x}_t)$ is the likelihood of the observed measurement given this signal, and $p(\mathbf{w}_t)$ is the normalisation constant.

From this posterior, Bayesian filters can employ a recursive filtering step, that not only makes a measurement prediction based on previous estimations (see the adaptive filter (§3.4.3)), but also updates this prediction given new data. This can be summarized in the prediction and update steps, given as [143]:

(i) Prediction:

$$p(\mathbf{x}_t|\mathbf{w}_{1:t-1}) = \int p(\mathbf{x}_t|\mathbf{x}_{t-1})p(\mathbf{x}_{t-1}|\mathbf{w}_{1:t-1})d\mathbf{x}_{t-1}, \tag{3.8}$$

(ii) Update

$$p(\mathbf{x}_t|\mathbf{w}_{1:t}) = \frac{p(\mathbf{w}_t|\mathbf{x}_t)p(\mathbf{x}_t|\mathbf{w}_{1:t-1})}{\int p(\mathbf{w}_t|\mathbf{x}_t)p(\mathbf{x}_t|\mathbf{w}_{1:t-1})d\mathbf{x}_t} \tag{3.9}$$

In practice however, instead of recomputing the probability distributions for new measurements, closed-form models are often used that capture an estimation of the distributions. An example of this is presented below.

Example: Kalman Filter

In the Kalman filter, linear Gaussian models are used to describe both the dynamics of the system, as well as the relationship between the observed measurement and the true signal. As such, the noise in the state transition (3.2) is assumed to be generated from a Gaussian distribution [143] $\boldsymbol{\epsilon}_t \in N(0, \mathbf{Q}_{t-1})$, with a prior on the state given as $\mathbf{x}_0 \in N(\mathbf{m}_0, \mathbf{P}_0)$. The measurement model is described similarly to (3.1), with measurement error also being Gaussian distributed $\boldsymbol{\varepsilon}_t \in N(0, \mathbf{R}_t)$. From posterior estimates using the Kalman filter, useful statistics about the signal prediction can be obtained. Most commonly, estimates of both the maximum likelihood signal $\mathbf{m}_t$, and the corresponding covariance matrix $\mathbf{P}_t$ are obtained, allowing for not only prediction, but also a confidence of the accuracy.

Given these assumptions on the distribution of the errors, and their corresponding covariances, prediction update stages are then given as:

(i) Prediction:

$$\begin{aligned} \tilde{\mathbf{m}}_\mathbf{t} &= \mathbf{A}_{t-1}\mathbf{m}_{t-1}, \\ \tilde{\mathbf{P}}_\mathbf{t} &= \mathbf{A}_{t-1}\mathbf{P}_{t-1}\mathbf{A}_{t-1}^T + \mathbf{Q}_{t-1} \end{aligned} \tag{3.10}$$

(ii) Update

$$\begin{aligned} \mathbf{m}_t &= \tilde{\mathbf{m}}_t + \mathbf{K}_t(\mathbf{x}_t - \mathbf{B}_t\tilde{\mathbf{m}}_t) \\ \mathbf{P}_t &= \tilde{\mathbf{P}}_t - \mathbf{K}_t\mathbf{S}_t\mathbf{K}_t^T \end{aligned} \tag{3.11}$$

with the Kalman gain given as $\mathbf{K}_t = \tilde{\mathbf{P}}_\mathbf{t}\mathbf{B}_t^T + \mathbf{S}_t^{-1}$, and $\mathbf{S}_t = \mathbf{B}_t\tilde{\mathbf{P}}_t\mathbf{B}_t^T + \mathbf{R}_t$.

While taking probabilistic estimates of the maximum likelihood is advantageous over deterministic filtering systems, Bayesian inference

methods suffer from a number of issues which limit their usage in wearable sensors systems. Care must be taken when modelling the expected distributions. For example, incomplete *a priori* knowledge of the noise covariance matrices used as part of the prediction and update steps ($\mathbf{P}, \mathbf{R}$) can result in poor precision and biasing of filters [167]. Tuning these filter parameters can be a time consuming and computationally costly process, which limits applicability to low-cost fabric systems (*e.g.,* through a grid-search over configurations [168]). Crucially, human motion in natural environments (*e.g.,* outside a controlled laboratory) will consist of a number of dynamic interactions and changes in motion. As such, the distributions of noise errors do not remain static, and can vary depending on factors such as environmental interaction [169] (*e.g.,* external stimuli), or changes in motion [169] (*e.g.,* user locomotion speed [170]).

In probabilistic estimates, there are also explicit assumptions on the type of noise distribution, for example in the Kalman filter outlined above where noise models are assumed to be linear mean-zero Gaussian. While this is often an appropriate approximation, in fabric sensing systems where the motion of the fabric (*i.e.,* the noise) is coupled with the motion of the body, non-Gaussian distributions that arise in the body kinematics (*e.g.,* forearm position given upper arm position [171]) may also emerge in the fabric motion, requiring either prior analysis of the expected fabric model, or estimations of the distribution from the data (*e.g.,* through random sampling [172]).

3.5 Conclusion

In this chapter, the application of commonly used motion artefact elimination methods as been discussed in relation to fabric sensors. In this, it has been shown that there are a number of incompatibilities between

these methods and the fabric sensors, limiting their usage. Standard filtering requirements, or error minimisation techniques (*e.g.,* the cluster of sensors method discussed in §2.3.2), rely on assumptions that do not hold in fabric-embedded systems.

For example, many methods require either multiple sensors situated on garments, which is incompatible with the aim of creating minimally invasive sensing systems. Hard assumptions about the artefact/body motion correlation can also presents problems for fabric-embedded sensors, where, (i) all sensors are coupled with each other due to their placement on the deformable surface of the fabric, (ii) the motion of the fabric (and thereby the artefact) is correlated with the motion of the body (*i.e.,* there is no reference signal available to adaptive filters that is decoupled from the noise-free signal).

More specifically, there are a number of limitations to applying standard filtering techniques to fabric sensors. Firstly, the assumption of linearity between the noise-free signal and the observed measurement, and between the state transitions, does not hold in the case of deformable free-flowing fabric. As such, non-linear implementations [173] must be used, where (3.2) is instead replaced by $\mathbf{w}_t = f(\mathbf{A}_{t-1}\mathbf{x}_{t-1}) + \boldsymbol{\epsilon}_{t-1}$, where $f(\cdot)$ is a non-linear mapping. Not only is this a more complex and computationally costly implementation, but the large number of fabric parameters (*e.g.,* flexibility, weave, thickness) that can alter the fabric motion (*i.e.,* introduce noise), means that *a priori*tuning (*e.g.,* estimation of the noise distributions) becomes a challenging task. Even for a single type of textile, measurement and transition matrices will not remain static during sensor use, and many vary at each-time step in user motion (*e.g.,* change of locomotion type).

A corresponding problem is the assumption that the state transitions ((3.2)) can be modelled as a Markov chain, where information con-

tained in the current state is sufficient to make a new prediction. This is generally not the case in filter design, and estimations are often made using information from multiple previous measurements and corresponding predictions. Often, techniques such as the standard *difference equation*[174] are used to make predictions based on historic parameter matrices. However, in the case of fabric motion, this state estimation becomes an even more challenging task, where due to the deformable structure and strong sensitivity to environmental influences and initial conditions, the dynamic behaviour of the fabric can mean memory based estimation systems may have difficulty with the stochastic motion of the fabric.

In the next chapter, a detailed look at how information regarding the unique properties of the motion artefact problem in fabric sensors can be incorporated into signal processing approaches in order to solve the problem of motion artefacts.

Chapter 4

Learning Human Motion Models from Motion Artefact Corrupted Data

4.1 Introduction

In this chapter, a closer look is taken at the application of statistical machine learning for solving the motion artefact problem. This is presented in two parts, firstly, a novel approach of treating motion artefacts as stochastic perturbations to the sensed motion is presented. For this, an analysis of the implications that motion artefacts have on commonly used learning approaches is presented, outlining shortcomings that make these approaches unsuitable to fabric motion artefacts. Secondly, it is proposed to use learning methods that explicitly takes into account the role of motion artefacts in signal generation. Existing approaches from the *errors-in-variables learning* field are applied in this chapter for the first time to fabric motion artefacts. This methodology is analysed, and experiments are performed demonstrating its superior performance in constrained human motion modelling tasks. Finally, a

discussion is presented outlining the usage of this learning approach in real-world wearable motion capture systems, to prepare the way for later contributions in this thesis.

Publications

- Michael, Brendan, and Howard, Matthew. "Eliminating motion artifacts from fabric-mounted wearable sensors." Humanoid Robots (Humanoids), 2014 14th IEEE-RAS International Conference on. IEEE, 2014.

- Michael, Brendan, and Howard, Matthew. "Learning Predictive Movement Models from Fabric-mounted Wearable Sensors." IEEE Transactions on Neural Systems and Rehabilitation Engineering 24.12 (2016): 1395-1404.

4.2 Learning Fabric Motions

In the absence of a detailed model of the wearer/fabric interaction dynamics §3.3, and poor applicability of statistical filtering §3.4, the approach presented for the first time in this thesis, is to use statistical learning techniques to form a predictive model of the wearer's motion, from noisy observed measurements. Addressing the problem in this way provides many benefits over analytical fabric modelling, since it allows unpredictable motion artefacts to be treated as stochastic perturbations to the underlying motion. It removes the need to estimate physical quantities such as mass and fibre structure of the fabric, and through use of simple parametric models, can be computationally very inexpensive.

For this approach, this chapter investigates the use of **generalised linear models** for learning the statistical relationship between the

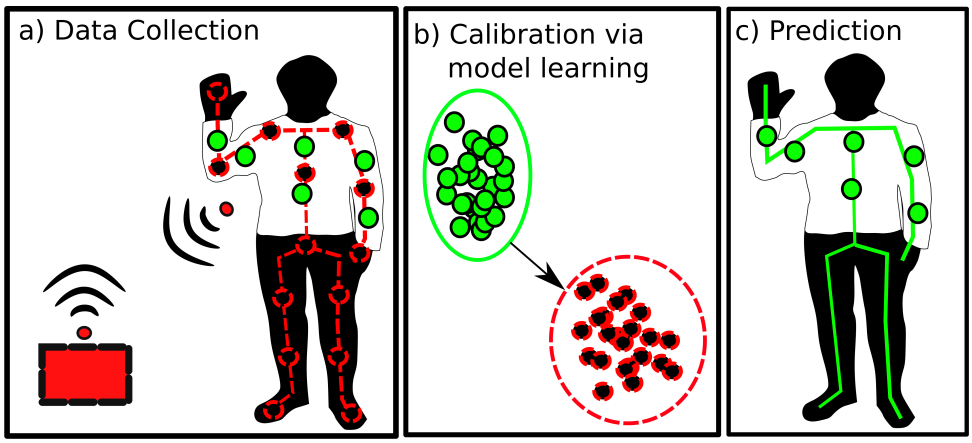

Figure 4.1: Stages of learning body motions. a) Data is collected by a high-fidelity motion capture system (*e.g.,* wireless IMUs attached rigidly to the body (red circles)), and a biomechanical model (red dashed structure) is computed at a base PC. Concurrently fabric-embedded sensors (green circles) collect similar movement data. b) A calibration model accounting for motion artefacts is learnt between the two datasets. c) The high-fidelity system is discarded, and predictions of the body (green solid structure) are made solely through application of the model and measurements from the fabric sensors.

wearer, and the worn fabric devices, while in the presence of motion artefacts. This allows for the analysis of the effect of motion artefacts on motion modelling approaches.

To apply such an approach, a calibration stage is required in which data from the target quantity $\mathbf{y} \in \mathbb{R}^{\mathcal{J}}$ and the fabric sensor readings $\mathbf{w} \in \mathbb{R}^{\mathcal{K}}$ are gathered for training the model. In the setting considered here Figure 4.2, such data may be gathered by subjecting the system to various movements while data is recorded both from the fabric sensors and from a sensor measuring the target quantity.

Note that, since the latter is only needed temporarily (i.e., during the calibration), a larger, rigidly-attached sensor can be used, that may otherwise not be suitable for long-term use. For example, one might choose to use a more intrusive, but higher fidelity motion capture sensor to obtain high quality readings, knowing that once the calibration is complete, the rigid sensor may be discarded, in favour of the predictions obtained from the fabric sensor readings.

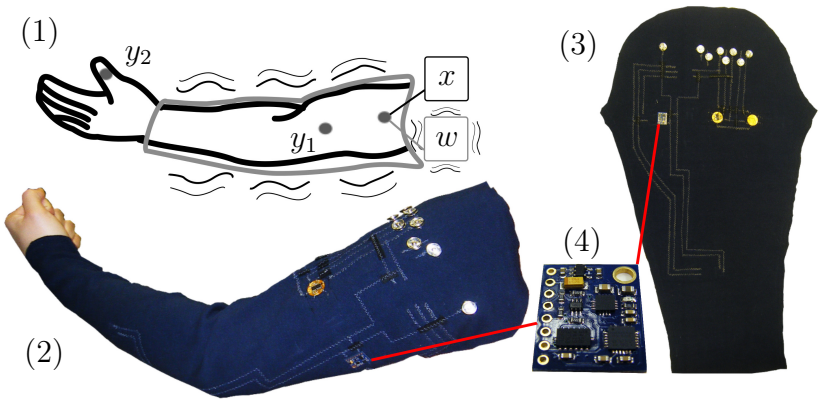

Figure 4.2: (1) Prediction of wearer movement at different points on the body (e.g., forearm y_1, fingertip y_2) based on sensor readings. Fabric motion with respect to the body introduces unpredictable artefacts into e-textile sensor readings w as compared to those derived from a rigidly attached sensor x. (2) Sleeve with embedded sensors. (3) Disassembled sleeve showing connections made with conductive thread. (4) Inertial measurement unit embedded on fabric.

4.3 Standard Least Squares Estimators

While the approach described above is appealing for dealing with fabric-mounted sensor data, close examination of the usual assumptions underlying standard learning suggest its direct application may be problematic. This is due to an important mismatch in the sources of error expected by these approaches, and those actually encountered in the data.

Specifically, the standard assumption made by such techniques is that data are generated according to a model of the form

$$\mathbf{y} = f(\mathbf{x}) + \boldsymbol{\epsilon} \tag{4.1}$$

where $\boldsymbol{\epsilon}$ denotes additive noise on $\mathbf{y}$ and f denotes the functional relationship between the sensed inputs $\mathbf{x} \in \mathbb{R}^{\mathcal{I}}$ and the target outputs $\mathbf{y}$. Given samples $\{\mathbf{x}_n, \mathbf{y}_n\}_{n=1}^{\mathcal{N}}$ the goal of the learning approach is to form an estimate of the function f.

A common approach for this is to minimise the sum of the squared

residuals

$$S_o = \sum_{n=1}^{\mathcal{N}} (\mathbf{y}_n - \tilde{\mathbf{y}}_\mathbf{n})^2 \tag{4.2}$$

where $\tilde{\mathbf{y}}_\mathbf{n}$ denotes the prediction of the model on the nth data point.

A convenient class of function approximators are the generalised linear models

$$\tilde{\mathbf{y}} = \boldsymbol{\phi}(\mathbf{x})^\top \tilde{\boldsymbol{\theta}} \tag{4.3}$$

where $\boldsymbol{\phi}(\cdot) \in \mathbb{R}^\mathcal{J}$ is a suitable feature vector or set of basis functions, such as Gaussian radial basis functions or polynomials and $\tilde{\boldsymbol{\theta}} \in \mathbb{R}^\mathcal{J}$ is the parameter. Note that, for convenience, here it is assumed that $\boldsymbol{\phi}(\cdot)$ contains the term $\phi_\mathcal{J}(\cdot) := 1$ to encode any constant offset in the target function (4.1).

The optimal choice for the parameter (with respect to (4.2)) is the least squares estimator:

$$\tilde{\boldsymbol{\theta}} = \frac{\sum_{n=1}^{\mathcal{N}} (\boldsymbol{\phi}(\mathbf{x}_n) - \boldsymbol{\phi}(\boldsymbol{\mu}_\mathbf{x}))(\mathbf{y}_n - \boldsymbol{\mu}_\mathbf{y})}{\sum_{n=1}^{\mathcal{N}} (\boldsymbol{\phi}(\mathbf{x}_n) - \boldsymbol{\phi}(\boldsymbol{\mu}_\mathbf{x}))^2}, \tag{4.4}$$

where $\boldsymbol{\mu}_\mathbf{x}$ and $\boldsymbol{\mu}_\mathbf{y}$ are the mean of $\mathbf{x}$ and $\mathbf{y}$ respectively. This is often given in matrix form as,

$$\tilde{\boldsymbol{\theta}} = (\boldsymbol{\Phi}^\top \boldsymbol{\Phi})^{-1} \boldsymbol{\Phi}^\top \mathbf{y} \tag{4.5}$$

where $\boldsymbol{\Phi} := (\boldsymbol{\phi}_1^\top, \cdots, \boldsymbol{\phi}_\mathcal{N}^\top)^\top \in \mathbb{R}^{\mathcal{N} \times \mathcal{J}}$ is the data matrix, containing independent sample features $\boldsymbol{\phi}_n := \boldsymbol{\phi}(\mathbf{x}_n)$ on each column.

An alternative to learning a global function is to fit spatially localised low order polynomials [175] (often linear or quadratic [176]) in the original input space. This nonparametric estimation method allows for improved scalability in terms of the dimensionality of the data, does not require biases on the data to be specified [177] (*e.g.,* the parametric form of the data), and also avoids the problems of global interference

[178]. A weighting function is used to determine a sample's contribution λ_n to the parameter estimation of a model, generally based on the input's distance from the centre of the region $\mathbf{c}_i \in \mathbb{R}^{\mathcal{I}}$.
As such, instead of minimising the sum of squared residuals (4.2), the objective function for local learning minimises

$$S_{ow} = \sum_{n=1}^{\mathcal{N}} \lambda_n (\mathbf{y}_n - \tilde{\mathbf{y}}_\mathbf{n})^2. \tag{4.6}$$

For each model, the diagonal weight matrix $\mathbf{\Lambda} \in \mathbb{R}^{\mathcal{N}\times\mathcal{N}}$ is formed for all samples, and the weighted least squares solution for the ith model becomes:

$$\tilde{\boldsymbol{\theta}}_i = (\mathbf{\Phi}^\top \mathbf{\Lambda}_i \mathbf{\Phi})^{-1} \mathbf{\Phi}^\top \mathbf{\Lambda}_i \mathbf{y} \tag{4.7}$$

In the case where $\mathbf{\Lambda} = \mathbf{I}$, this is equivalent to the least squares formulation (4.5).

4.4 Measurement Error in Learning Problems

In the context of fabric-based sensing, difficulties occur due to (4.1) being a poor model of the noise encountered in the data. As described in §2.3, the major source of noise in fabric sensor data is that of the motion of fabric with respect to the wearer, *i.e., noise on the inputs* $\mathbf{x}$. This has a number of implications with respect to the reliability of movement prediction models computed according to this standard approach. For example, ignoring these perturbations, and using the least squares estimate ((4.5),(4.7)) may result in (i) bias in the parameter estimation [179] (ii) loss of power in detecting relationships [180], and (iii) the masking of features in non-linear models.

As such, it is proposed to explicitly account for non-negligible noise in the *independent variables* $\mathbf{x}$ during learning and prediction. Specifically, the latter are assumed to be subject to additive noise $\boldsymbol{\varepsilon}$, that corrupt the sensor readings:

$$\mathbf{w} = \mathbf{x} + \boldsymbol{\varepsilon}. \tag{4.8}$$

In this, it is assumed that the noise is drawn from the Gaussian distribution with mean zero, and fixed variance, *i.e.,* $\boldsymbol{\varepsilon} \sim N(\mathbf{0}, \Sigma_{\varepsilon}^2)$. This assumption of a Gaussian noise distribution is used not only due to its analytical tractability (making it suitable for examining learning methods in this motion artefact context) but also due to its flexibility in practical applications when the actual distribution is not known [181]. This section analyses the effect that motion artefacts on the inputs $\mathbf{x}$ have in statistical learning.

Example: Parameter Bias in linear prediction

An initial problem commonly seen in learning problems involving measurement error, is that errors in the predictors causes biases in parameters during learning, resulting in an *attenuation* of the parameters towards zero [182]. Here, this attenuation is shown through analysis of the parameter estimation equations (4.4),(4.5).
For simplicity, this analysis assumes one-dimensional input data, with predictors x, prediction noise ϵ, and measurement noise ε being drawn from normal independent distributions:

$$(x, \epsilon, \varepsilon) \sim N((\mu_x, 0, 0), diag(\sigma_x^2, \sigma_\epsilon^2, \sigma_\varepsilon^2)). \tag{4.9}$$

In the noiseless setting, through application of (4.4) (where there is no feature space mapping, *i.e.,* $\boldsymbol{\phi}(x) = x$), error free inputs x are used to

learn the best linear estimate of the parameters $\tilde{\theta}_x$.

From this, it is seen that predictors and predictions in the noisy setting are distributed as as bivariate normal, with mean

$$E(y, x) = (\mu_y, \mu_x) = (\mu_x^\top \tilde{\theta}_x, \mu_x), \tag{4.10}$$

and covariance matrix,

$$\begin{bmatrix} \sigma_y^2 & \sigma_{yx}^2 \\ \sigma_{xy}^2 & \sigma_x^2 \end{bmatrix} = \begin{bmatrix} \tilde{\theta}_x^2 \sigma_x^2 + \sigma_\epsilon^2 & \tilde{\theta}_x \sigma_x^2 \\ \tilde{\theta}_x \sigma_x^2 & \sigma_x^2 \end{bmatrix}. \tag{4.11}$$

resulting in parameter $\tilde{\theta}_x$ expectation:

$$E(\tilde{\theta}_x) = \frac{\sigma_{yx}^2}{\sigma_x^2} = \tilde{\theta}_x. \tag{4.12}$$

However, when only error prone measurements w are available, (4.11) becomes,

$$\begin{bmatrix} \sigma_y^2 & \sigma_{yw}^2 \\ \sigma_{wy}^2 & \sigma_w^2 \end{bmatrix} = \begin{bmatrix} \tilde{\theta}_x^2 \sigma_x^2 + \sigma_\epsilon^2 & \tilde{\theta}_x \sigma_x^2 \\ \tilde{\theta}_x \sigma_x^2 & \sigma_x^2 + \sigma_\varepsilon^2 \end{bmatrix}, \tag{4.13}$$

and the parameter $\tilde{\theta}_w$ instead becomes,

$$E(\tilde{\theta}_w) = \frac{\sigma_{yw}^2}{\sigma_w^2} = \frac{\tilde{\theta}_x \sigma_x^2}{\sigma_x^2 + \sigma_\varepsilon^2} = \tilde{\theta}_w. \tag{4.14}$$

As such, the least squares regression of y on w produces a parameter estimate of not $\tilde{\theta}_x$, but $\tilde{\theta}_w = \tau \tilde{\theta}_x$, with τ (known as the reliability ratio [182]) defined as:

$$\tau = \frac{\sigma_x^2}{\sigma_x^2 + \sigma_\varepsilon^2} < 1 \tag{4.15}$$

This biasing of the parameter is clearly seen when estimating with ordinary least squares, seen in Figure 4.3 (left), where the estimator

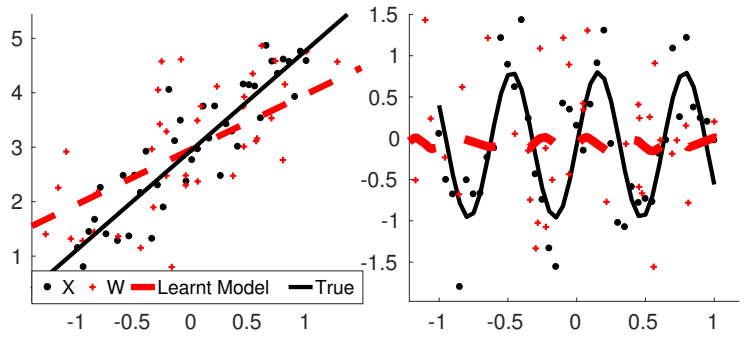

Figure 4.3: Effects of measurement error in simulation, for a linear function (left, $f_1 = \mathbf{x}^T\theta_x$) and nonlinear (right, $f_2 = sin(\mathbf{x}^T\theta_x)$). Measurements with additive noise only on the prediction x (black circles) can be used to fit the correct functional relationship using standard least squares (black line). However measurements containing noise also on the predictors w (red crosses), cause poor fitting (red dashed), as seen in (left) linear fitting, and (right) where the slope in a non-linear function attenuates towards zero.

learnt when using noisy measurements w, *attenuates* towards zero as the variance increases. This effect is particularly prominent in nonlinear problems, Figure 4.3 (right), where this measurement error not only biases the learning, but masks important features defining the functional relationship.

4.5 Orthogonal Regression

To deal with these problems, it is proposed in this thesis to explicitly account for non-negligible noise in the *independent variables* $\mathbf{x}$ during learning and prediction with fabric-embedded sensors. Given samples $\{\mathbf{w}_n, y_n\}_{n=1}^{\mathcal{N}}$, the task is to form a prediction model (4.3), that takes account of stochasticity both in $\mathbf{x}$ and y in the data.

This section outlines the first application of using learning methods from the *errors-in-variables* field to the problem of eliminating fabric sensor motion artefacts. In this, an analysis is first presented, highlighting the suitability of this novel approach, and forms the basis of the publications listed at the beginning of this chapter.

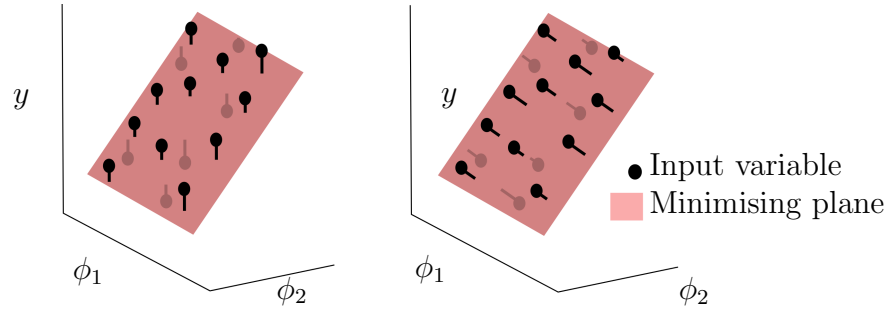

Figure 4.4: Fitting the model (4.1) with standard least squares (left) minimises the residuals due to error in the target variable y but ignores errors in the inputs. By minimising the residuals orthogonal to the fit, total least squares (right) reduces their effect.

4.5.1 Model Estimation through Total Least Squares

An intuitive approach to achieve this, is to modify the objective function (4.2) such that the parameter estimate minimises the squared residuals orthogonal to the predicted curve, an approach known as Total Least Squares (TLS) fitting [183, 184]. The following describes how TLS can be applied to fit a generalised linear model (4.3) given data $\{\mathbf{w}_n, y_n\}_{n=1}^{\mathcal{N}}$.

In particular, augmenting the feature vector [1] $\boldsymbol{\phi}(\cdot)$ with the targets y, (4.3) can be re-written

$$\boldsymbol{z}^\top \tilde{\boldsymbol{\omega}} = 0 \tag{4.16}$$

where $\boldsymbol{z}(\mathbf{x}, y) := (\phi_1(\mathbf{x}), \ldots, \phi_{\mathcal{J}-1}(\mathbf{x}), y)^\top \in \mathbb{R}^{\mathcal{J}}$ and $\tilde{\boldsymbol{\omega}} \in \mathbb{R}^{\mathcal{J}}$ is the vector of parameters.

In this augmented space, instead of minimising the residuals in y (as in (4.2)), the proposed approach minimises the sum of squared *orthogonal residuals*

$$S_t = \sum_{n=1}^{\mathcal{N}} d_n^2 \tag{4.17}$$

where d_n is the orthogonal distance from the nth data point to the

[1] Note that, to avoid biasing effects due to the mapping of $\boldsymbol{\varepsilon}$ into the feature space, the feature vector as far as possible should be chosen such that the distribution of $\phi_j(\mathbf{w})$ around $\phi_j(\mathbf{x})$ for $j \in 1, \cdots, \mathcal{J}$ is symmetric. In practice, this condition is not found to be crucial in obtaining a superior fit over approaches that ignore the input errors $\boldsymbol{\varepsilon}$.

plane defined by (4.16)

$$d_n = \boldsymbol{z}_n^\top \hat{\boldsymbol{\omega}} \tag{4.18}$$

with $\boldsymbol{z}_n := \boldsymbol{z}(\mathbf{w}_n, y_n)$ and $\hat{\boldsymbol{\omega}} := \tilde{\boldsymbol{\omega}}/||\tilde{\boldsymbol{\omega}}||$ (see Figure 4.4). It can be shown [183, 184] that the plane minimising (4.17) must pass through the centroid of the data

$$\bar{\boldsymbol{z}} := \frac{1}{\mathcal{N}} \sum_{n=1}^{\mathcal{N}} \boldsymbol{z}_n. \tag{4.19}$$

Hence, minimisation of (4.17) can be achieved by minimising its upper bound

$$\overline{S} = \sum_{n=1}^{\mathcal{N}} ((\boldsymbol{z}_n - \bar{\boldsymbol{z}})^\top \hat{\boldsymbol{\omega}})^2 \tag{4.20}$$

or in matrix notation

$$\overline{S} = ||\mathbf{Z}^\top \hat{\boldsymbol{\omega}}||^2 \tag{4.21}$$

where $\mathbf{Z} := ((\boldsymbol{z}_1 - \bar{\boldsymbol{z}})^\top, \cdots, (\boldsymbol{z}_{\mathcal{N}} - \bar{\boldsymbol{z}})^\top)^\top$.

This is equivalent to a low rank matrix approximation problem [185]:

$$\hat{\boldsymbol{\omega}} = \arg\min_{\hat{\mathbf{Z}}} ||\mathbf{Z} - \hat{\mathbf{Z}}||_F, \text{subject to } \text{rank}(\hat{\mathbf{Z}}) < \mathcal{J} - 1, \tag{4.22}$$

where F is the Frobenious norm.

The total least squares solution is retrieved by finding parameters where $\hat{\mathbf{Z}}^\top \hat{\boldsymbol{\omega}} = 0$, by forming the singular value decomposition of $\mathbf{Z} = \mathbf{U}\boldsymbol{\Sigma}\mathbf{V}^T$, where $\boldsymbol{\Sigma}$ is a diagonal matrix of the singular values, and $\mathbf{U}$ and $\mathbf{V}$ are matrices of the left and right singular vectors. The solution is retrieved by selecting elements of the right singular vector corresponding to the smallest singular value [186]:

$$\hat{\boldsymbol{\omega}} = \frac{-1}{V_{\mathcal{J},\mathcal{J}}} \mathbf{V}_{(\mathcal{J}_1,\ldots,\mathcal{J}_{\mathcal{J}-1})} \tag{4.23}$$

The intercept term is then formed as:

$$\hat{\omega}_0 = -\bar{\boldsymbol{z}}^\top \hat{\boldsymbol{\omega}}, \tag{4.24}$$

and the plane which minimises the squares residuals orthogonal to the predicted curve is given by:

$$\tilde{\boldsymbol{\theta}} = (\hat{\boldsymbol{\omega}}^\top, \hat{\omega}_0)^\top \tag{4.25}$$

Similarly to the standard approach §4.3, scalability can be improved by fitting spatially localised low order polynomials. The total least squares algorithm can be modified by the use of a weighting matrix $\boldsymbol{\Lambda}$, and the objective function (4.17) can be modified into the weighted objective function by minimising the weighted sum of squared orthogonal residuals [187]:

$$S_{tw} = \sum_{n=1}^{\mathcal{N}} \lambda_n d_n^2. \tag{4.26}$$

Then, instead of the plane passing through the centroid of the data (as in (4.19)), it must now pass through the weighted mean centre [187], denoted as

$$\bar{\boldsymbol{z}} := \frac{\sum_{n=1}^{\mathcal{N}} \lambda_n \boldsymbol{z}_n}{\sum_{n=1}^{\mathcal{N}} \lambda_n}. \tag{4.27}$$

The data matrix is formed as

$$\mathbf{Z} := ((\sqrt{\lambda_1}(\boldsymbol{z}_1 - \bar{\boldsymbol{z}}))^\top, \cdots, (\sqrt{\lambda_n}(\boldsymbol{z}_{\mathcal{N}} - \bar{\boldsymbol{z}}))^\top)^\top. \tag{4.28}$$

and the optimal solution retrieved by forming the singular value decomposition of $\mathbf{Z}$, and computing the parameters using equations (4.25)-(4.24). Similarly to the weighted least squares implementation in §4.3, if $\boldsymbol{\Lambda} = \mathbf{I}$, the weighted TLS formulation reduces to the global model.

4.5.2 Nongeneric TLS

In motion artefact data collected as part of this thesis, it is seen that the singular value decomposition of the data matrix $\mathbf{Z}$ can fail to produce a finite solution, or unstable results. Analysis of this data for the

first time in this thesis, shows that this may occur if the variance of the noisy measurements is excessively larger than the variance of the underlying (unobservable) motion, *e.g.,* in the case of very loose items of clothing. As, the diagonal matrix of singular values becomes incorrectly ordered, and therefore the incorrect orthogonal plane is selected.
In this thesis, it is proposed to account for this in fabric motion by choosing $\tilde{\boldsymbol{\omega}}$ as another right singular vector corresponding to a larger singular value (which is either not zero, or is above an acceptable value determined a priori) [188]. Here, the implementation of the nongeneric TLS solution selects the optimal singular vector through a cross validation process on the possible singular values. Spatially localised low order polynomials can also be fitted using the nongeneric TLS solution, by performing a cross validation on the singular values obtained from the process outlined in §4.5.1.

4.5.3 Weighting with Errors-in-variables

In this section, the problem of fabric measurement error in localised models is examined for the first time in this thesis, with practical conclusions drawn for use in fabric-embedded motion capture systems.
In spatially localised models, a weighting function is used to compute the contribution of a sample to a local model's parameter estimate, based on its distance in the input space from the model centre. For this, in ordinary least squares learning, a number of weighting functions have been proposed, such as the tricube or Gaussian functions, or a simply a piecewise discretisation of the space [189].
However, if the inputs are noisy, then some care must be taken into how these functions are chosen due to the difficulty in estimating the distance of samples $\mathbf{w}_n$ from nearby local models. If the distance calculation is incorrect, then noisy samples may be allocated to the wrong

local model (or over-weighted in the case of smooth weighting functions). In turn, this can affect the contribution of samples to the local model fit, thereby potentially reducing the quality of the overall fit. To see this, consider the task of learning a one dimensional function (see Figure 4.5 (left)) subject to zero-mean Gaussian noise on the inputs $\varepsilon \sim N(0, \sigma_\varepsilon^2)$, and using a simple piecewise weighting function

$$\lambda_{n,i} = \begin{cases} 0 & \|x_n - c_i\| > h \\ 1 & \|x_n - c_i\| \leq h \end{cases} \tag{4.29}$$

where c_i is the model centre and h is the bandwidth of the model. In this case, the probability that a given sample w_n is allocated to the correct model is

$$P(a \leq w_n \leq b) = \int_a^b \frac{1}{\sqrt{2\pi\sigma_\varepsilon^2}} N(x_n, \sigma_\varepsilon^2)\, \mathrm{d}x \tag{4.30}$$

where $a = c_i - \frac{h}{2}$ is the lower limit of the model, and $b = c_i + \frac{h}{2}$ is the upper limit. This equation can be evaluated by taking the difference between the cumulative distribution functions at b and a.
From (4.30), the probability of correct allocation depends on three factors: (i) the location of the model centre relative to x_n, (ii) the bandwidth of the model h, and (iii) the standard deviation of the input noise σ_ε^2. For instance, in this example, if the true input coincides with the ith model centre (i.e., $x_n = c_i$), and the bandwidth is equal to the noise standard deviation ($h = \sigma_\varepsilon^2$), the probability of w_n being correctly allocated to the model is $P = 0.383$. This probability increases to 1 as the bandwidth size increases (Figure 4.5, top right). On the other hand, if the true input is located on the boundary between two models ($x_n = c_i \pm h/2$), there is a maximum 0.5 probability of correct allocation (Figure 4.5, bottom right).

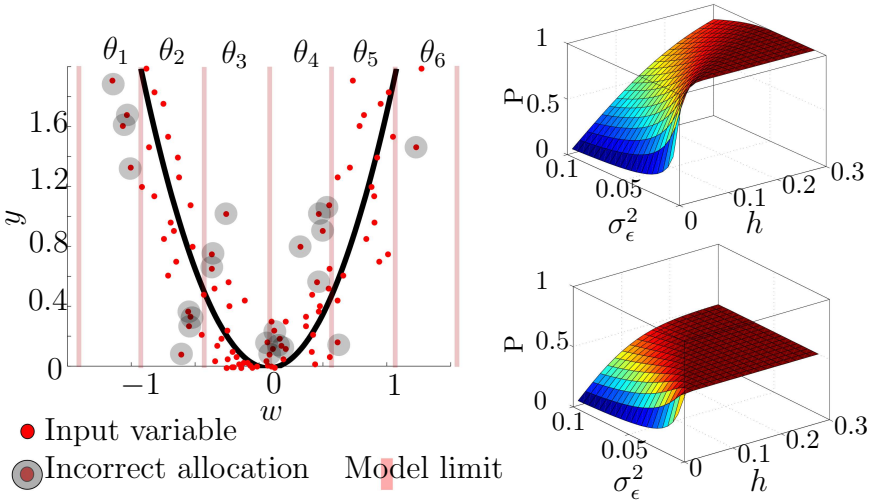

Figure 4.5: Incorrect model allocation using a piecewise weighting function, due to additive error on the input. (Left) Samples with noise on the input are denoted by red dots, samples circled are assigned to incorrect models (boundaries of model shown by light red vertical lines). Solid black line denotes true function. (Right) Probability of noisy sample being assigned to the correct model, when varying model bandwidth h and noise standard deviation σ_ε^2, given that (top) $\mathbf{x}_n$ is positioned at the centre of the model, and (bottom) $\mathbf{x}_n$ is positioned at the boundary of the model.

This problem is not limited to the piecewise model, since even with weighting functions such as the Gaussian [190]

$$\lambda_{n,i} = e^{-(\mathbf{w}_n - \mathbf{c}_i)^2 / 2h} \tag{4.31}$$

noisy samples may still be given excessive weight by incorrect (nearby) models (although, as the latter have weights decreasing asymptotically with distance, this tends to mitigate these problems).

Considering these factors, it would seem that the optimal approach would be to maximise the bandwidth of local models in order to minimise the probability of noisy samples being allocated to the wrong models. However, in the context of learning, excessively large bandwidths may also cause *over-smoothing* and thereby reduced accuracy of predictions. In practice, a trade-off must be made between the problems of model allocation and over-smoothing. In the experiments reported here, this is achieved through use of the Gaussian weighting

function (4.31), with the parameter h selected through cross-validation. The interested reader is referred to [191] for further discussion of the choice of weighting functions for use in nonparametric estimation with errors-in-variables.

4.5.4 Motion Prediction from Noisy Sensor Readings

Having learnt the model parameters $\tilde{\boldsymbol{\theta}}$, the next step is to form predictions based on incoming sensor readings.

In standard function approximation (see §4.3), the movement estimate $\tilde{y}^*$ for a given feature vector query point $\boldsymbol{\phi}(\mathbf{w}^*)$ in a global model is simply

$$\tilde{y}^* = \boldsymbol{\phi}^\top \tilde{\boldsymbol{\theta}} \tag{4.32}$$

while for the spatially localised models, $\tilde{y}^*$ is given as the normalised weighted sum of the predictions from all models [178]

$$\tilde{y}^* = \frac{\sum_{c=1}^{\mathcal{C}} \lambda_c \boldsymbol{\phi}^\top \tilde{\boldsymbol{\theta}}}{\sum_{c=1}^{\mathcal{C}} \lambda_c}. \tag{4.33}$$

However, because this fails to take account of the noise in $\mathbf{w}^*$, it can result in poor accuracy.

The ideal prediction would be obtained by directly feeding $\mathbf{x}^*$ to the model (4.1), but in the present context this reading is not directly accessible. It is therefore necessary to build an estimate $\tilde{\mathbf{x}}^*$ based on the data available.

In this thesis, it is proposed to achieve this through use of *replicate data* [179], whereby for any query point $\mathbf{x}^*$, the availability of $\mathcal{K}$ noisy replicates

$$\mathbf{w}_k = \mathbf{x}^* + \boldsymbol{\varepsilon}_k \tag{4.34}$$

is assumed within the test data. Under the assumption of zero-mean distribution of errors $\boldsymbol{\varepsilon}_k$ (4.8), this means that a simple estimate $\mathbf{x}^*$ can be obtained by taking the sample mean of the replicates over $\mathcal{K}$. This allows the final prediction to be made by using the feature vector $\boldsymbol{\phi}(\tilde{\mathbf{x}}^*)$ with equation (4.32) for global models, or equation (4.33) for local models.

Note that, in general, the accuracy of the prediction $\tilde{\mathbf{x}}^*$ depends on the number of replicate data available at that point. For sensors measuring continuous variables (as considered here), exact replicates $\mathbf{w}_k$ of sensor readings at a given $\mathbf{x}^*$ are unlikely to be available. However, in practice, a good estimate can still be found from approximate replicates (i.e., using samples $\mathbf{w}_n = \mathbf{x}_n + \boldsymbol{\varepsilon}_n$ where $||\mathbf{x}_n - \mathbf{x}^*||$ is small).

In the experiments reported here, approximate replicates are obtained by a heuristic binning procedure, whereby similar measurements are grouped together. For this, a $\mathcal{K}$-dimensional grid of bins is created, each with a fixed width. The training inputs are placed in bins according to their value. The query point $\mathbf{w}^*$ is placed in a bin, and the mean of that bin is used as the estimate $\tilde{\mathbf{x}}^*$.

4.6 Evaluation of Orthogonal Regression

In this section, the proposed approach is evaluated through a simulation study, and through an experiment on acceleration data from a fabric-embedded device.

4.6.1 Simulation

The goal of the first evaluation is to characterise the performance of the proposed approach for learning and predicting movements from noisy sensory inputs. For this, learning is tested on artificial data from

models with both linear and non-linear relationships between the input $\mathbf{x}$, the sensed $\mathbf{w}$, and the target quantity y. For example, $\mathbf{x}$ may represent the acceleration of a body segment (e.g., forearm), $\mathbf{w}$ the fabric sensor readings (e.g., from a shirt sleeve), and y the corresponding acceleration of another segment (e.g., hand), see Figure 4.2.

1-Dimensional Input

In this evaluation, a set of $\mathcal{N}$ points for training the model is generated as follows. As inputs to the model, first, a set of $\mathcal{M} = 50$ independent sample inputs are drawn from the uniform random distribution $x_m \sim U[-1, 1]$. Each of these is then corrupted with additive Gaussian noise. To simulate multiple sensor readings observed from the same true input, but with different noise corruptions at each sampling, this process is repeated $\mathcal{K} = 10$ times, to generate the matrix of data $\mathbf{W} \in \mathbb{R}^{\mathcal{M}\times\mathcal{K}}$, where each column of the matrix is a corruption of the true input,

$$w_{m,k} = x_m + \varepsilon_k \tag{4.35}$$

where $\varepsilon_k \sim N(0, \sigma_\varepsilon^2)$ and $\sigma_\varepsilon^2 = 0.15$.
The matrix of data is then transformed[2] to the vector of data $\mathbf{w} = vec(\mathbf{W})^T \in \mathbb{R}^{\mathcal{M}\mathcal{K}}$, where $\mathcal{M}\mathcal{K} = \mathcal{N}$.
At the same time, the corresponding target quantities y_n are computed for each of the readings w_n

$$y_n = y_{m,k} = f(x_m) + \epsilon_n \tag{4.36}$$

where $\epsilon_n \sim N(0, \sigma_\epsilon^2)$ and $\sigma_\epsilon^2 = 0.01$. In the following, results are reported for generative functions f that are (i) linear $f_1(x) = 1.5x + 3$,

[2]For further details on the *vec* transformation, the reader is directed to [192]

		Linear	Quadratic	Sinusoidal
LS	$\|\|\boldsymbol{\theta} - \tilde{\boldsymbol{\theta}}\|\|$	0.467 ± 0.053	3.188 ± 0.164	-
	NMSE	0.344 ± 0.043	0.736 ± 0.081	0.493 ± 0.041
TLS	$\|\|\boldsymbol{\theta} - \tilde{\boldsymbol{\theta}}\|\|$	0.189 ± 0.068	1.234 ± 0.368	-
	NMSE	0.067 ± 0.013	0.370 ± 0.136	0.265 ± 0.052

Table 4.1: Mean norm difference between estimated and ground truth parameters and normalised mean squared error (NMSE) in predictions $\tilde{y}^*$. Results are mean±s.d. over 20 trials.

(ii) quadratic $f_2(x) = 4x^2+0.75x+3$, and (iii) sinusoidal $f_3(x) = -0.3\sin(2.5x)$ in the inputs.

The resultant $\{w_n, y_n\}_{n=1}^{\mathcal{N}}$ are used to train the approximator (4.3) through the total least squares (TLS) method outlined in §4.5. For this thesis, this method was programmed according to definition as outlined in §4.5. For this, $\boldsymbol{\phi}$ is chosen according to the model (f_1, f_2 and f_3) used to generate the data. In particular, for f_1 and f_2 basis functions exactly capturing the parametric form of the model (e.g., for f_2, $\boldsymbol{\phi}(x) := (x^2, x, 1)^\top$) are used, while for f_3, a 3rd order polynomial basis is used to estimate the function. This is to test the case of underlying function being unknown. For comparison, identical models are trained on the same data through standard least squares (LS), using the approach outlined in §4.3 [3]. The procedure is repeated for 20 trials on different data sets.

Table 4.1 summarises the results. There, it can be seen that the parameters estimated by TLS for f_1 and f_2 are much closer to the ground truth, as compared to those learnt through standard least squares. This is reflected in the normalised mean squared error values (NMSE), that indicate good predictive accuracy of the models. Likewise, for f_3, TLS obtains lower NMSE than LS, despite the exact parametric form of the function being unavailable in this case.

[3]Note that the noiseless prediction method §4.5.4 is used only for models trained with TLS. The LS procedure does not make use of prior knowledge about noise on the inputs either in the training §4.3 or prediction stages.

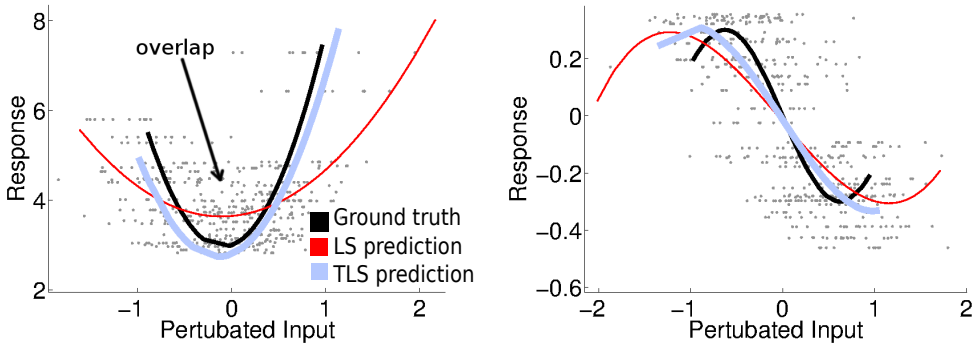

Figure 4.6: Ground truth (black function) and noisy measurements of points on this function (grey dots). Least squares (thin red) and total least squares (thick light purple) predictions overlaid on the ground truth f_2 (left), and f_3 (right) when learning on noisy measurements.

In order to evaluate the effectiveness of the estimation method for the predictors §4.5.4, the mean squared error (MSE) of the predictor residuals is computed. In the naive LS case, this is the residual of the noisy input $\mathbf{w}^*$ against the true input $\mathbf{x}^*$ and in the TLS case the residual between the estimated true input $\tilde{\mathbf{x}}^*$ and the true input. The mean results obtained from the linear data set are 0.146 ± 0.012 for the $\mathbf{w}^*$ MSE, and 0.015 ± 0.002 $\tilde{\mathbf{x}}^*$ MSE. Similar results are seen for the other functions in this experiment, as this procedure estimated the residuals independently of the prediction y^*. It can be seen from these results that the heuristic binning method outlined in §4.5.4 computes predictors $\tilde{\mathbf{x}}^*$ that are closer to the ground truth.

Interestingly, the worst performance for both methods is found when learning the quadratic function f_2. This appears to be due to the specific form of this function, where high input noise tends to cause overlap of data between the two 'arms' of the parabola, resulting in interference in learning (shown in Figure 4.6).

These results are verified by examining the prediction curves of the learnt models over the range of training data. In Figure 4.6, the predictions of the learnt TLS models for f_2 and f_3 are plotted, overlaid upon

the ground truth values, and those of standard LS[4]. It can be seen that the models learnt with TLS are in good agreement with the underlying ground truth functions. In contrast, those learnt through standard LS suffer a bias towards zero, causing attenuation of the predictions and thereby higher errors.

To further assess the performance of learning, the experiment is repeated, varying (i) the noise in the data, $0 \leq \sigma_\varepsilon^2 \leq 0.4$, and (ii) the number of replicates available, $1 \leq \mathcal{K} \leq 30$. Note that, the former corresponds to increasing the 'slack' of the fabric-mounted sensor (since looser coupling between sensor and wearer is likely to result in larger motion artefacts), while the latter corresponds to differences in the size and density of the data set recorded during the calibration stage, §4.2. The results for functions f_1, f_2 and f_3 are plotted in Figure 4.7. There, it can be seen that, as expected, there is a decrease in accuracy for both TLS and LS as the noise level increases. However, the divergence of the TLS and LS lines indicates a much quicker degradation of performance for the latter. For the concave function f_2, this is particularly pronounced, an effect that may also be attributed to the non-monotonicity of the function: increasing noise causes greater overlap of data from the two arms of the parabola resulting in greater interference during learning.

Looking at the learning curves for varying $\mathcal{K}$ (Figure 4.7, right), it can be seen that the error in the prediction NMSE for TLS drops rapidly as the number of replicates found in the data increases, levelling off at around $\mathcal{K} = 10$ for all functions. This suggests that the proposed approach is able to use the data efficiently to obtain a good fit. The LS line, in contrast, does not change significantly, despite the increase in

[4]Note that, for standard LS, the predictions extend over a wider range of inputs since the $w_n = x_n + \varepsilon_n$ usually extends beyond the maximum and minimum x_n due to the symmetrically distributed additive noise.

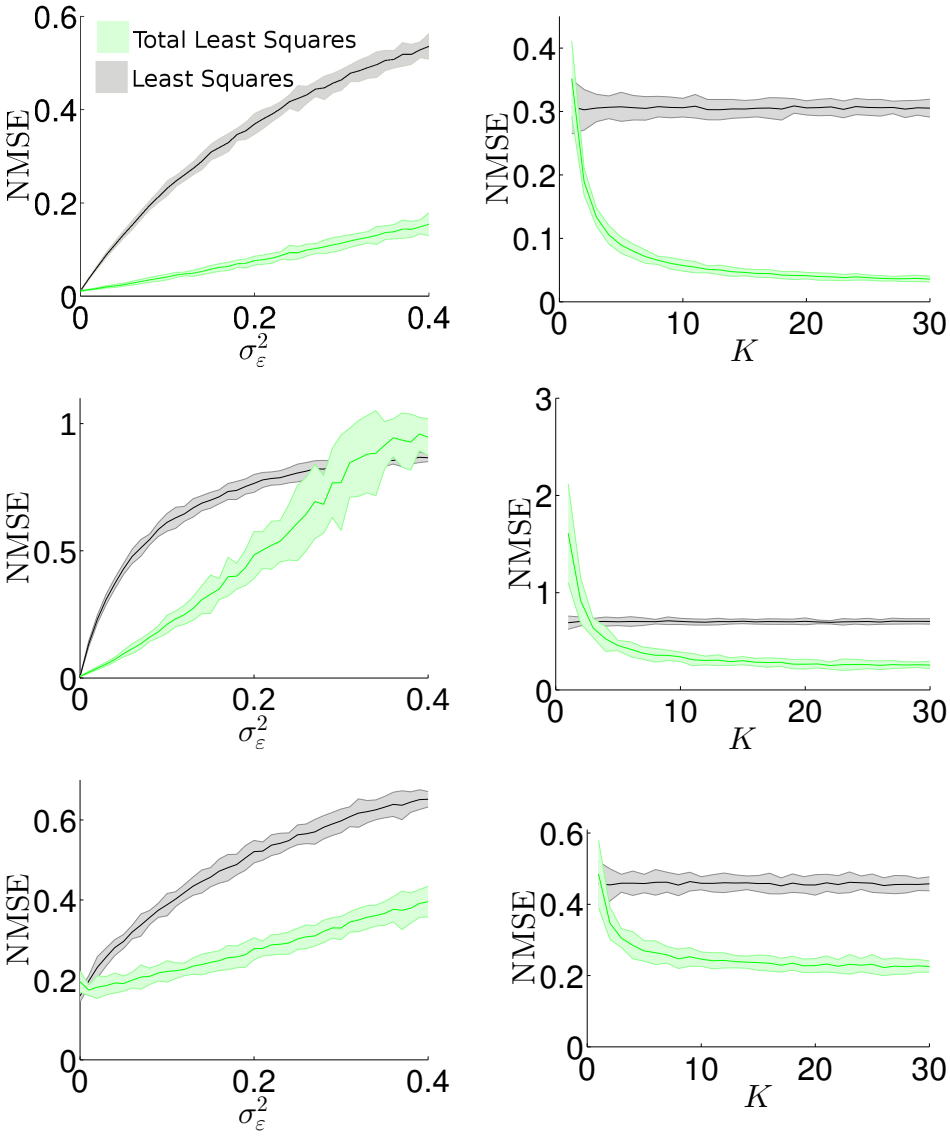

Figure 4.7: Effects of varying σ_ε^2 (left) and $\mathcal{K}$ (right) on NMSE for linear (top), quadratic (middle) and sinusoidal (bottom) functions when learning with least squares (black) and total least squares (light green). Shown mean± two s.d. over 20 trials.
the amount of data available.

Multi-Dimensional Input

In this section, the learning methods outlined in §4.5 are evaluated in a multi-dimensional setting. Higher dimensional problems are common in many applications, for example in the context of analysing human movement the input $\mathbf{x}$ may represent both the pitch and roll of the arm, from which the corresponding end-effector position is to be pre-

dicted.

Here, learning is evaluated on two nonlinear functions, namely,

$$f_1(x_1, x_2) = x_2^2 + 0.5x_2 + 1.5x_1^2 + 0.75x_1 + 3 \tag{4.37}$$

and

$$f_2(x_1, x_2) = x_1^2 - x_2^2 + \arctan(3x_1 + 4x_2). \tag{4.38}$$

These functions are chosen such that learning can be evaluated in functions with a relatively simplistic parametric form (f_1), as well as more complex structures (f_2).

The procedure is as follows. A set of $\mathcal{M} = 50$ training samples are drawn from the uniform random distribution $x_i \sim U[-1, 1]$, where $i \in \{1, 2\}$. For each of these, to simulate noise and motion artefacts, a set of $\mathcal{K} = 10$ readings are generated, corrupted with additive Gaussian noise

$$\mathbf{w}_n = \mathbf{w}_{m,k} = \mathbf{x}_m + \boldsymbol{\varepsilon}_k \tag{4.39}$$

where $\boldsymbol{\varepsilon}_k \sim N(\mathbf{0}, \sigma_\varepsilon^2 \mathbf{I})$ and $\sigma_\varepsilon^2 = 0.05$. At the same time, the corresponding target quantities y_n are computed for each of the readings $\mathbf{w}_n$

$$y_n = y_{m,k} = f(\mathbf{x}_m) + \epsilon_n \tag{4.40}$$

where $\epsilon_n \sim N(0, \sigma_\epsilon^2)$ and $\sigma_\epsilon^2 = 0.001$.

As in §4.6.1, the resultant $\{\mathbf{w}_n, y_n\}_{n=1}^{\mathcal{N}}$ are used to train the approximator (4.3) through both total least squares (TLS) §4.5, and the standard least squares (LS) outlined in §4.3. In this higher dimensional problem, local linear models are used to estimate the functional relationship due to their improved scalability in terms of data dimensionality. Local models are placed in an equally spaced 10×10 grid, covering the range of $\mathbf{w}$, with the width of each model selected a priori as $h = 0.05$ by

		Quadratic	Atan
LS	$\tilde{y}^*$ NMSE	0.321 ± 0.078	0.249±0.058
TLS	$\tilde{y}^*$ NMSE	0.191± 0.079	0.143±0.058

Table 4.2: Normalised mean squared error (NMSE) in predictions $\tilde{y}^*$, and normalised mean squared error in the predictors, for given functions estimated local linear models. Results are mean±s.d. over 20 trials.

a visual observation of the fit. The procedure is repeated for 20 trials on different data sets. Where necessary, the nongeneric TLS algorithm §4.5.2 is used to prevent numerical errors.

Table 4.2 summarises the results for the 2-dimensional input, and Figure 4.8 shows the surfaces estimated for f_1 and f_2, compared against the true surfaces. The normalised mean squared error (NMSE) values of the prediction are lower when using the local TLS models for both functions. This is consistent with the results shown in §4.6.1, even when estimating the function non-parametrically in a higher-dimensional space. For comparison, fitting a global quadratic model of f_1 with $\boldsymbol{\phi}(\mathbf{w}) := (w_1^2, w_2^2, w_1, w_2, 1)^\top$, the average NMSE value using LS is 0.328 ± 0.051 and using TLS is 0.077 ± 0.0027, indicating that the local TLS approach outperforms LS, even when the latter is provided with a priori information such as the correct parametric form of the model.

To examine the trade-off between model allocation and over-smoothing (ref. §4.5.3), the experiment for learning f_1 is also repeated while varying the model bandwidth h. Figure 4.9 shows the mean NMSE of the local TLS model for different levels of input noise $\sigma_\varepsilon^2 \in \{0, 0.02, 0.05, 0.1\}$ for $0.05 \leq h \leq 0.5$. As can be seen, for $\sigma_\varepsilon^2 = 0$, the optimal bandwidth with respect to minimising the NMSE is small, due to the local parameter estimate being a good fit from the local data. As the bandwidth increases, the NMSE begins to rise, as the estimated function becomes oversmoothed. At larger σ_ε^2, however, the optimal bandwidth

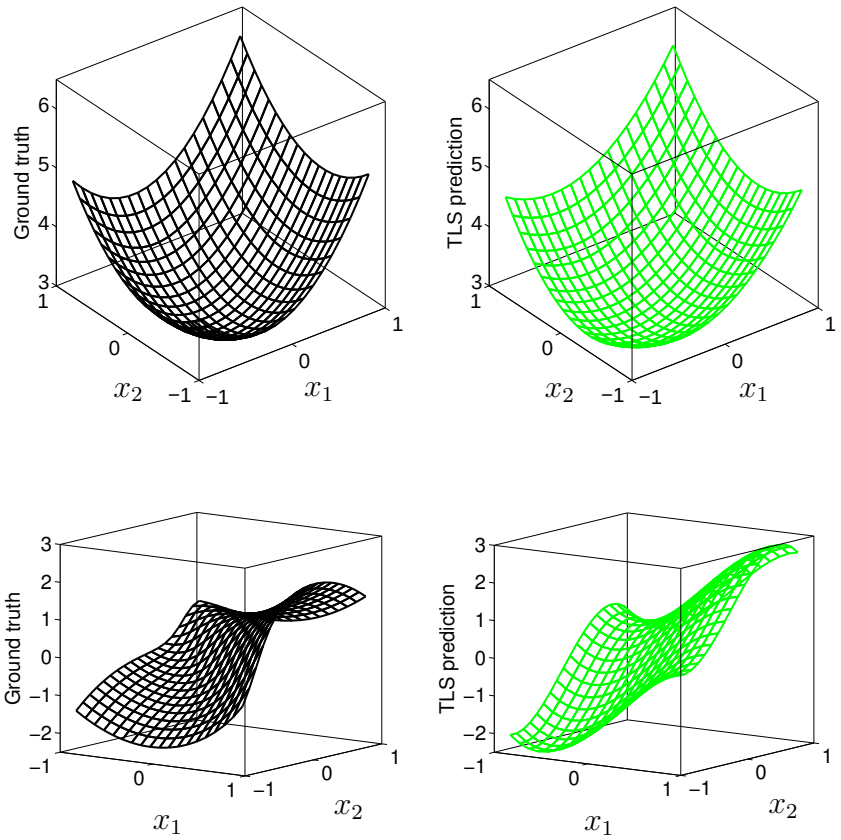

Figure 4.8: Functions f_1 (top) and f_2 (bottom), showing estimations using local linear TLS (right).

h increases (vertical black lines). This is consistent with the discussion in §4.5.3, which showed that models using smaller bandwidths would under-perform in the presence of measurement error, due to the problem of samples being wrongly allocated to nearby local models.

4.6.2 Experiment - Fabric Mounted Sensor

In this evaluation, the proposed approach is tested for learning from physical data with the goal of predicting the movement of an object through space from a fabric-mounted sensor. The experimental platform used is shown in Figure 4.10.

The platform consists of a pair of LilyPad ADXL335 tri-axial accelerometers mounted onto a plastic box. Of these, the first is attached rigidly,

Effect of weighting function bandwidth on accuracy

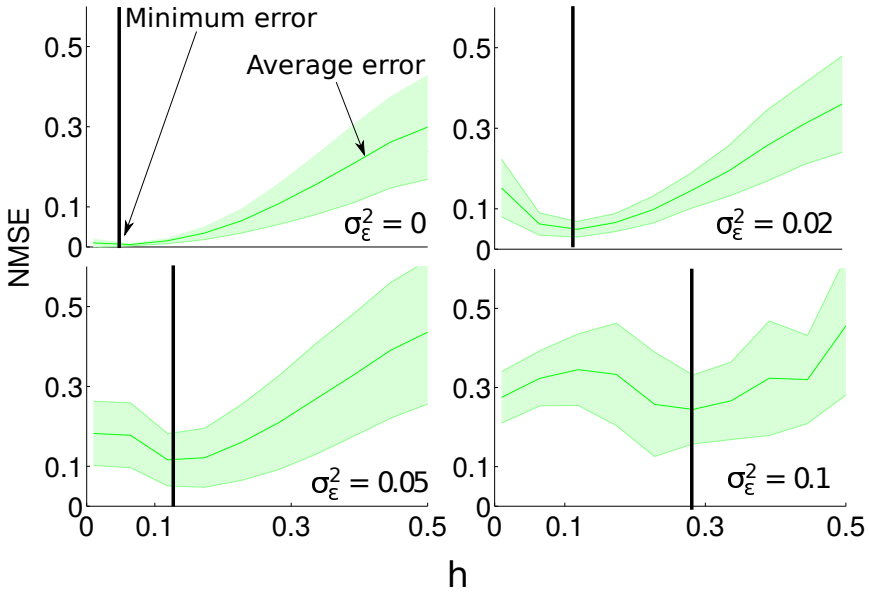

Figure 4.9: Effects of varying bandwidth (h) of weighting function on NMSE for f_1, when learning with total least squares, while varying amounts of measurement variance σ_ε^2. Black bar shows minimum NMSE value. Shown mean $\pm$ s.d. over 20 trials.

to provide a ground truth measurement of the box acceleration α, while the second is sewn onto a light-weight strip of cloth, and measures the fabric acceleration β. The cloth attachment is designed such that the slackness of the fabric s (defined as the maximum displacement from the box admitted by the fabric, see Figure 4.10) can be adjusted between $s = 0\,cm$ (taut against the box) and $s = 6\,cm$.

During motion, readings from the two sensors are sampled synchronously at a rate of $23\,Hz$ using an Arduino Uno (Atmega-328P microcontroller, 16-bit ADC), and sent wirelessly to a PC base-station for analysis. As the methods defined in this section do not utilize the fact that time-series data is being used, the sampling frequency does not need to be particularly high, and as seen in Figure 4.7, increasing the number of replicates available does not significantly improve performance.

The fabric-mounted sensor is connected to the Arduino using conduc-

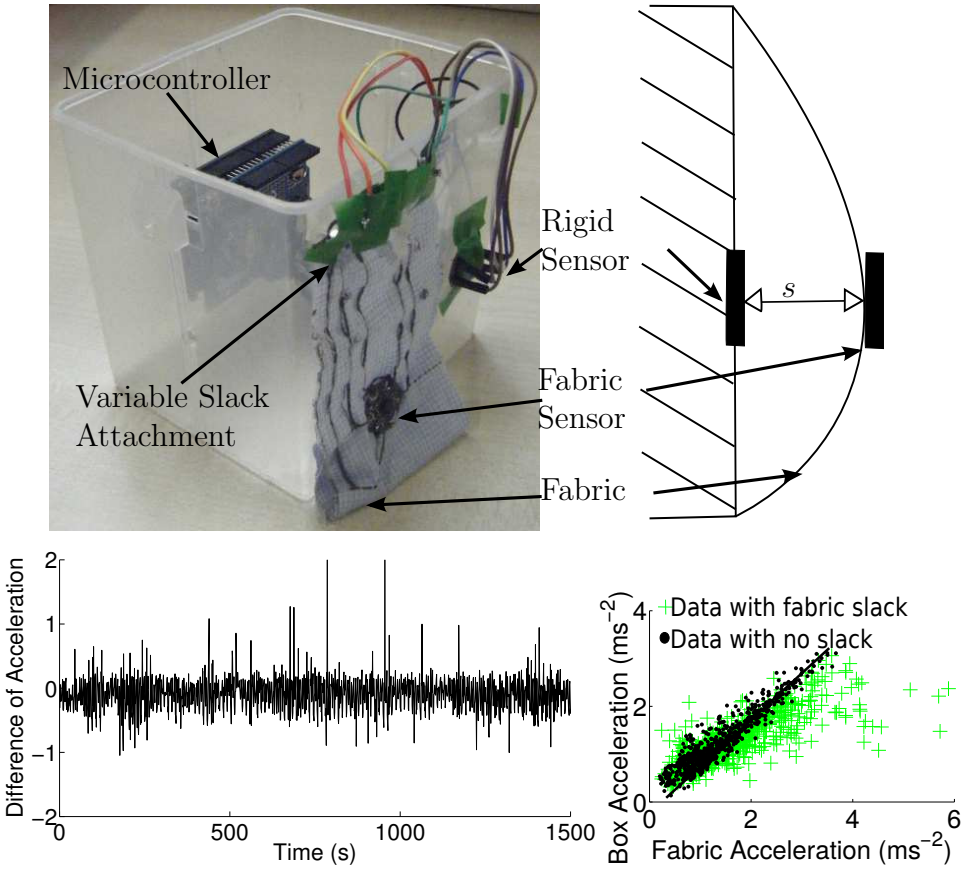

Figure 4.10: Experimental set up (top). Difference of fabric and box acceleration magnitude against time (bottom left). Plot of box acceleration magnitude against that of the box (bottom right) showing ground truth mapping (black line), data with no slack (black circles) and data with slack (crosses).

tive thread to ensure minimal interference with the fabric motion (as might occur, for example, with use of wiring). Note that, while this reduces invasiveness of the sensor, it also adds further noise to the sensor readings [193], making the learning task in this experiment especially challenging.

As data, signals from the two sensors are recorded during random shaking of the box in a single plane, for sessions of 60 s each. The raw signals are preprocessed by converting the ADC values to acceleration in g, and then computing the acceleration magnitude for each time step. The latter is commonly used in clinical movement recording studies [194] and is used in this experiment to verify the usefulness of the proposed approach in such settings. The resultant data $\{\alpha_n, \beta_n\}_{n=1}^{\mathcal{N}}$ con-

sists of $\mathcal{N} = 1350$ samples of box- and fabric-mounted sensor readings, respectively. These are randomly split into training and test data sets of equal size.

An sample data set is illustrated in Figure 4.10 (bottom left and right), for displacement $s = 6\,cm$. On the left, the difference between fabric and box acceleration magnitude is shown against time, showing a significant amount of noise, much greater than would be expected from ordinary electrical noise. On the right, the fabric acceleration magnitude is plotted against that of the box, for two different slacks. In this case, the sensors are calibrated against one another so that there exists an identity relationship between the two (black line). When the slack is zero ($s = 0\,cm$, black dots) the sensor readings lie closely along the line, however for greater slack ($s = 6\,cm$, green crosses) a much broader distribution of readings is observed.

For learning, the proposed TLS approach is then used to train a linear model $\boldsymbol{\phi} := (x, 1)^T$ mapping the measured fabric accelerations β to box acceleration α on the training data. Note that, at the prediction stage, exact replicates of the form (4.34) are not available for forming the estimate ε_n (ref. §4.5.4). Instead, approximate replicates are obtained by grouping similar values of β_n together into 350 discrete bins of equal size and spacing, and treating the data in these bins as the replicates. In the following, results are reported for 5 trials of this experiment, in which data is recorded at slackness levels $s = 0$, 2, 4, 5, and $6\,cm$. As a baseline for comparison, the experiment is also repeated using the same model but learnt through the standard LS approach (ref. §4.3). Predictions are made offline (i.e. not during motion), as is consistent with rehabilitation studies which monitor readings over a long-term period.

In an initial experiment, the identity function is learnt between the two

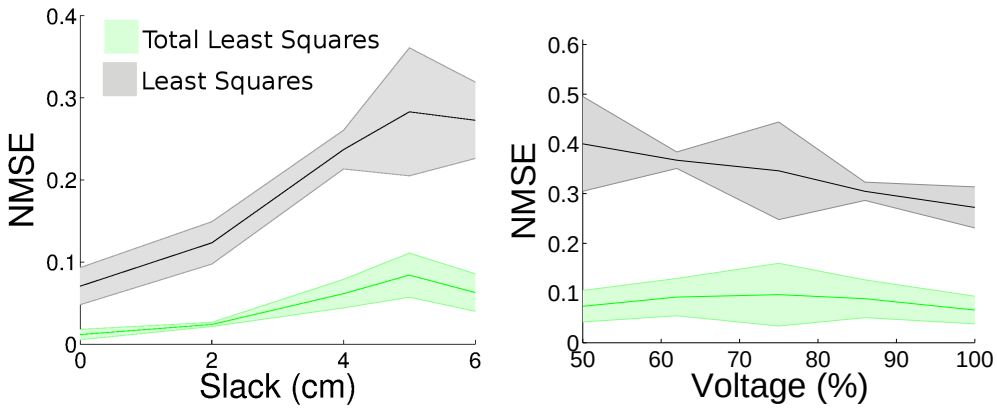

Figure 4.11: NMSE of least squares (black) and total least squares (light green) of box motion when varying fabric slacknesses (left) and fabric sensor voltage (right). Results are mean±s.d. over 5 trials.

calibrated accelerometers. These known parameters are used to verify that the estimated parameters are correct. These results are shown in Figure 4.11 (left) where the mean prediction NMSE of the LS and TLS models are plotted against the slackness s. There it can be seen that, as the slackness increases, there is a gradual decrease in accuracy for both methods. This is in agreement with the simulation study (see §4.6.1), where it is seen that increasing noise (motion artefacts) resulted in a similar trend. However, comparing TLS with the standard LS approach, it is seen that the proposed approach consistently outperforms the latter across the range of slacknesses, with a more gradual decrease in accuracy in the face of greater noise.

To further test performance, the experiment is also repeated using data from a decalibrated pair of sensors. This corresponds to the situation described in §4.2, where a temporary (potentially heterogeneous) sensor is used for gathering data in a calibration stage.

In this experiment, the same test platform in Figure 4.10 is used and data is collected following the same experimental procedure (with the slack of the fabric fixed at $s = 6\,cm$). However, to induce differences between the two accelerometers, the fabric sensor's input voltage is al-

tered with a potentiometer, reducing the strength of the signal[5]. In the following, results are reported for data collected when the fabric sensor is supplied with (i) 4.3V (100% normal operating voltage), (ii) 3.7V (86%), (iii) 3.2V (75%), (iv) 2.7V (62%), and (v) 2.2V (50%). Note that, decalibrating the sensors in this way induces a non-identity mapping between the sensors, so that, for example, when the fabric sensor operates at 2.15V, the readings of the box sensor readings should be approximately twice the magnitude of those of the fabric sensor.
In Figure 4.11 (right), the prediction NMSE of the test data against the fabric sensor input voltage are shown for 5 trials of this experiment. As can be seen, the proposed approach outperforms standard LS across the range of voltages (sensor calibration factors).

4.6.3 Pose estimation

In this section, the proposed learning approach is evaluated in a human motion context, by predicting the pose of an arm from a fabric embedded device. Pose estimation is particularly important in long-term rehabilitation studies, as it provides quantitative data on a patient's movement, which can be used to monitor progress. For this experiment, the orientation of a forearm is estimated using a sleeve (Figure 4.2), with an accelerometer embedded on the inner forearm of the sleeve. The sleeve is loose fitting, to induce motion artefacts.
The experimental setup is illustrated in Figure 4.12 (left). In this, the upper arm is placed flat on a surface, while the forearm segment is positioned at different angles around the elbow joint. Recordings are taken using the same accelerometer and Arduino as shown in §4.6.2, and a Hall rotary encoder (Melexis, MLX90316) is attached to the elbow, make an independent ground truth recording of the forearm seg-

[5]Note that, at each voltage, the sensors still have each axis calibrated at zero acceleration.

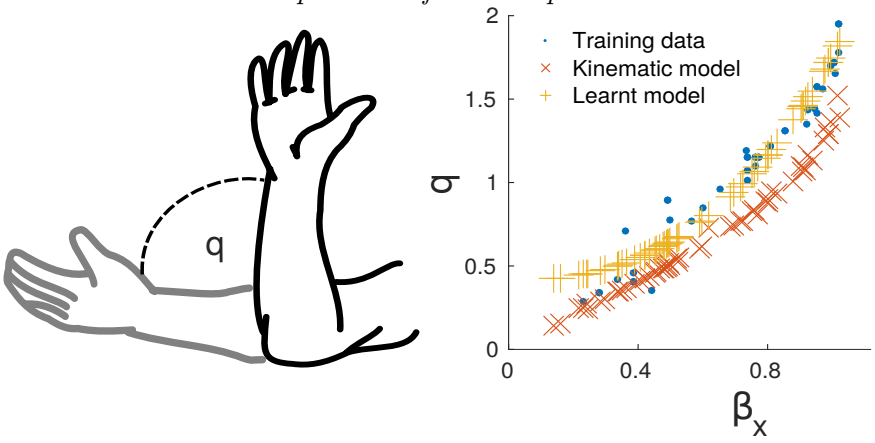

Figure 4.12: (Left) Arm segment measurement, (right) predictions of segment angle

ment orientation.

In this evaluation, predictions made using orthogonal regression techniques outlined in §4.5 are compared against the ground truth values from the encoder. To compare against this, predictions are also made using the standard regression setup §4.3, and a kinematic model of the orientation of the arm segment. Kinematic modelling of a single joint is a relatively simple computation often performed in human motion analysis, and is therefore a suitable contender against orthogonal regression for joint angle estimation.

This kinematic model of the arm orientation at rest is defined as:

$$q = tan^{-1}(\frac{\sqrt{1-\beta_x^2}}{\beta_x}), \tag{4.41}$$

where the subscripts denote the x-axis and z-axis of the tri-axel acceleration vector β. This is derived from basic trigonometry [195], and assumes the only acceleration recorded is due to gravity.

To evaluated the proposed method, the recorded pose data is first split randomly into independent training and testing sets of equal size. The standard and orthogonal non-parametric regression models are then learnt, using the x-axis acceleration as input data and the angle obtained from the calibrated Hall encoder as the predictor. Predictions

are made on the testing set of poses. This procedure is repeated 10 times.

These results for an example trial are shown in Figure 4.12. Here it is shown that the predictions made with the kinematic model have a large error in comparison to the true joint angle, and consistently underestimate this angle. This is due to the misalignment between the sensor and body orientations, due to the slack of the fabric. As such, as the kinematic modelling does not account for this error, and underestimates the angle. In comparison, the learnt model outperforms, even with the kinematic model being given the bias of being provided with a mathematical model of the mapping. This is also shown in the mean NMSE values of predictions, which for the naive model is 0.358 ± 0.044, the least squares model 0.079 ± 0.070, and total least squares model 0.073 ± 0.025.

4.7 Conclusion

The unsuitability of analytic modelling of fabric for the removal of motion artefacts, both from the view point of model identification and computational tractability, suggests the use of learning approaches to learn models of wearer movement from these noisy measurements. In this chapter, the application of statistical learning techniques in removing these motion artefacts has been investigated. It is seen, however, that commonly used non-parametric learning techniques need to be adapted to this problem, due to the mismatches in noise assumptions found in standard learning models.

With a view to this, it has been proposed to exploit statistical methods from the errors-in-variables field to deal with the effects of stochastic perturbations to the sensory inputs in clothing-based sensing. An approach to model estimation and movement prediction has been pre-

sented, based on the use of total least squares regression. This approach consists firstly of a calibration stage, in which data from the fabric sensor and a rigidly-attached sensor (*e.g.,* optical motion capture) are gathered. After this, the rigidly attached sensor can be discarded, and this model is used to make estimations of noise-free measurements solely from the fabric sensor.

Evaluation of the proposed approach in simulation has shown its ability to outperform standard regression in fitting non-parametric models in the face of significant input noise, and to efficiently make best use of replicate readings found in data. Experiments in learning and predicting joint angles using a fabric-embedded accelerometer and non-parametric implementation of the orthogonal regression method, enables the estimation of the motion of an object in space, and compensates for calibration mismatches. It is shown that it is always an improvement to apply orthogonal regression techniques over ordinary least squares. The computational efficiency of the proposed approach also makes it feasible for implementation onto an embedded device, making it an appealing option for the long-term gathering of data, e.g., in rehabilitation studies.

It is also seen that the assumption that motion artefacts are generated from a Gaussian distribution does not affect the learning nor prediction. In §4.6.3, it is seen during the non-parametric learning task that the measurements corrupted by motion artefacts no longer exhibit the mean-zero distribution property, as outlined in §4.4, with no adverse effect to the learning.

While the human motion capture experiments reported in this section are limited to single axis measurements, this approach demonstrates the suitability for dealing with fabric-mounted sensor data. The implementation described in this chapter can also be applied for learning

the body/fabric interaction in the presence of motion artefacts for more complex, multi-sensor motion capture problems. In the next chapter this is demonstrated by examining more complex human motion capture.

In a practical setting however (such as continuous measurement of daily activities), direct application of these methods becomes challenging. This is due to the requirement of a calibration stage, which limits the generalisability of the motion artefact elimination method. For example, changes in the user motion (*e.g.,* changing locomotion speed) alters the dynamics of both the body, and the mounting fabric, presenting additional challenges by requiring re-calibration. In the next chapter, as a solution to this problem, this orthogonal regression approach is incorporated into regression methods that allow for the learning of self-calibrating models of motion.

Chapter 5

Adaptive Motion Artefact Elimination

In the previous chapter, it was found that standard regression techniques performed poorly, due to the mismatches in noise assumptions found in standard learning models, and the artefacts introduced by the motion of the fabric. An approach to eliminating motion artefacts in constrained tasks was presented, using non-parametric statistical learning methods to model body movements, while viewing the motion artefacts as stochastic perturbations to the sensed motion.

In this chapter, this approach is generalised to allow for *unsupervised recalibration* of the motion artefact elimination approach, enabling the ability to deal with the wide range of human motion and wearer/fabric interactions that occur during everyday usage. This improves upon the approach outlined in §4.5, which while successful in learning body motions in constrained settings, requires that in order to correctly calibrate the fabric-embedded sensors to account for motion artefacts, a baseline (noiseless) dataset of the same motions be collected in a calibration stage prior to first-use (*e.g.,* through the use of a high fidelity motion capture system). This requirement limits applicability in

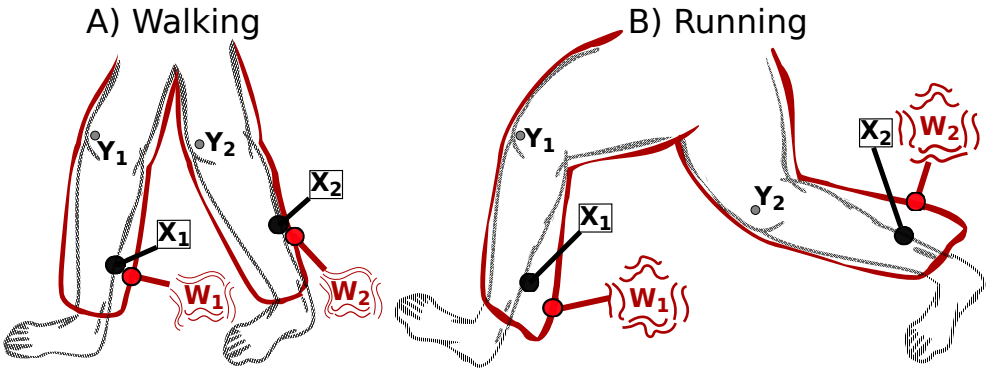

Figure 5.1: (A) Prediction of wearer movement (e.g. knee angle $\mathbf{Y}$) based on sensor readings. Fabric motion introduces artefacts into the e-textile sensor readings $\mathbf{W}$, compared to sensor fixed rigidly to the body $\mathbf{X}$. (B) Predictive models can be calibrated to estimate $\mathbf{Y}$ from $\mathbf{W}$, however variations in user locomotion (e.g. speed) varies the fabric dynamics, resulting in poorly calibrated models.

real-world motion capture tasks as, due to the large space of possible human motions (*e.g.,* walking at different speeds), the calibration approach would require the computation and switching between multiple models of fabric-body interaction.

To solve this problem, this chapter outlines the use of unsupervised learning methods to learn models of human motion solely from motion artefact corrupted signals, without the need of either a clinical calibration stage, nor the requirement to define discrete motions (*e.g.,* walking, running) prior to use. The learning approach is used successfully to extract dependency relationships from motion artefact corrupted signals observed from fabric-embedded sensors. The quality of these artefact free estimates are comparable to the results obtained from a calibrated model, showing the unsupervised learning model's generalization provides superior usability for continuous real-world gait analysis.

Publications

- Michael, Brendan, and Howard, Matthew. "Gait Reconstruction from Motion Artefact Corrupted Fabric-Embedded Sensors", (Ac-

cepted/In press) In : IEEE Robotics and Automation Letters, 2018

5.1 Problem Definition

The use of statistical errors-in-variables learning methods to eliminate motion artefacts §4 has been successful in learning body motions from fabric-embedded sensors. In this, a calibration procedure is performed between data obtained from the fabric embedded sensors, and a baseline (noiseless) dataset. After calibration noise-free predictions of the user motion can be made solely from the calibrated fabric sensor. However, this approach requires that, in order to correctly calibrate the fabric-embedded sensors to account for motion artefacts, *a baseline (noiseless) data set of the same motions be collected in a calibration stage prior to first-use* (*e.g.,* through the use of a high fidelity motion capture system).

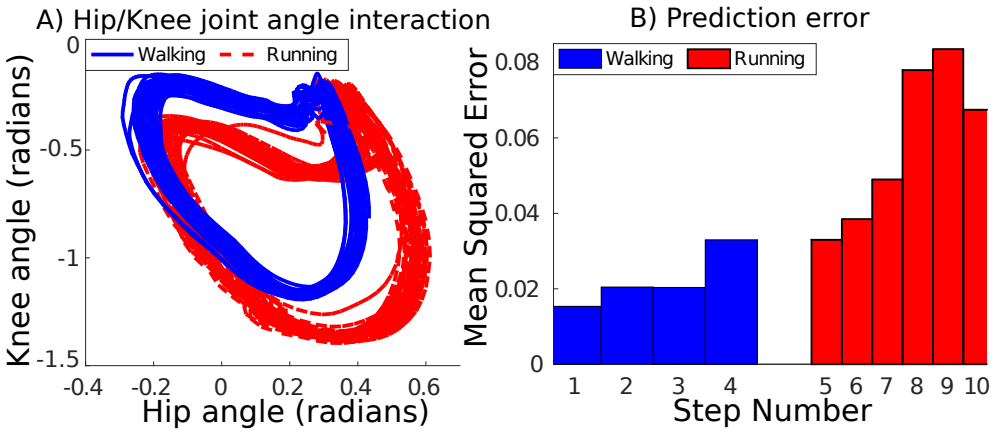

Figure 5.2: A) Hip/knee angle-angle plots (captured from high fidelity motion capture systems), showing gait changes between walking and running. B) Prediction error during walking and running from fabric-sensors, after using artefact elimination methods calibrated solely on walking data.

While this training session to calibrate the sensors is suitable for collecting future data about this single motion, it fails to address how variations in the user motion may affect the calibration procedure,

leading to poor generalizing capabilities. For example, fabric-embedded sensors calibrated in the clinic during a locomotion task (*e.g.,* Figure 5.1(A)) will experience motion artefacts within a range of amplitudes and frequencies, due to the motion of the fabric. However, even normal changes in a user's gait (*e.g.,* locomotion speed Figure 5.2(A)), can result in the behaviour of the fabric also being altered (Figure 5.1(B)), generating additional motion artefacts that are not solved by the initial calibration procedure.

5.1.1 Learning in Errors-in-Variables Regression

To illustrate the problem, consider the task of estimate noise free measurements $\tilde{\mathbf{X}}$ from motion artefact corrupted data $\mathbf{W}$ (see for full details §4.5). To make these predictions, one may learn a generalised linear model of the form:

$$\tilde{\mathbf{X}} = \mathbf{\Phi}(\mathbf{W})^{\top}\tilde{\mathbf{\Theta}}, \tag{5.1}$$

choosing the parameter matrix $\tilde{\mathbf{\Theta}}$ such that squared *orthogonal residuals* to the predicted curve are minimised.

While this learning approach is appealing for dealing with fabric-mounted sensor data, in a practical setting (such as continuous measurement of daily activities), the relationship between the motion of the body, and that of the fabric changes during use. The sources of these changes in fabric motion are various, and can include, (i) a change in wearer locomotion type altering the dynamics of the fabric, changing the frequency and amplitude of clothing movement [196], (ii) clothing being stretched over time, changing the amount of contact between the fabric and body (*i.e.,* greater artefacts), (iii) the wearer themselves varying movement behaviour, either due to gait disorders (*e.g.,* age associated decreased limb strength [197]) or exercise interventions [198].

As such, the assumption of there being *static* learnt parameters $\tilde{\mathbf{\Theta}}$ (which defines the relationship between fabric and body motion), is inconsistent with these sources of variation, and can result in poor prediction accuracy. For example, fabric-embedded sensors calibrated in the clinic during a locomotion task (*e.g.,* walking, Figure 5.1(A)) experiences motion artefacts within a range of amplitudes and frequencies, due to the fabric motion. However, even relatively small changes in a user's gait (*e.g.,* change in locomotion type Figure 5.2(A)), can result in the behaviour of the fabric also altering (Figure 5.1(B)), generating additional motion artefacts that are not covered by the initial calibration procedure. This problem is illustrated in Figure 5.2(B), where models calibrated (TLS fitting) on only one type of motion (walking), predict poorly when the user switches to running.

These modalities of motion are not just limited to gait, but can also be seen in other activities (*e.g.,* switching between swings in tennis [199]). A simple solution to dealing with these modalities, is to compute multiple models of motion, capturing a large range of possible human motions (*e.g.,* different walking modes), then switching to the desired calibration model depending on the user motion. However, not only does such an approach massively increase the clinical time spent capturing all these different motions, but an additional prediction system is required to determine what mode of the motion the user is currently doing.

It can be seen that the lack of ability in this stochastic learning approach to cope with different modalities of motion, limits its applicability in real-world fabric-embedded measurement systems.

5.2 Adaptive Learning

To deal with these problems, in this thesis it is proposed to learn user motion $\mathbf{X}$ from the noisy fabric-embedded signals $\mathbf{W}$, without relying on the collection of noiseless observations for calibration. This allows for models of motion to be recalibrated during use, adapting for changes in motion, environment, or fabric dynamics. This thesis proposed that this can be achieved by using: (i) *unsupervised learning* that exploits existing structure within the motion data to build regression models without user input, and (ii) *a lower-dimensional (latent) representation of the motion signals*, as an artefact elimination technique in the learning process.

In general, unsupervised non-linear dimensionality reduction techniques are used to discover hidden dependencies between variables within the latent data, thereby learning a manifold that captures relationships between recorded motion parameters (*e.g.,* joint interactions). After learning, new (noisy) measurements are then projected onto the lower-dimensional manifold, and noiseless reconstructions can then be made back in the original data space.

Specifically, this method proposed in this thesis for fabric-embedded sensors, solves the motion artefact problem by removing components of the noisy measurement that do not have a significant contributory role in the formation of the latent space manifold. An illustration of this is seen in Figure 5.3(A), where noisy complex data in a high dimensional space can be seen to mask any relationship between variables. After finding structure within a latent space representation of this data (Figure 5.3(B)), reconstructions can be made in the original data space (Figure 5.3(C)), with greater importance given to maintaining this learnt structure. In the context of motion artefacts, the artefacts themselves within the measurements have limited reconstruction

weight, when viewed in relation to the relationship between recorded motion parameters, and as such are discarded during reconstruction.

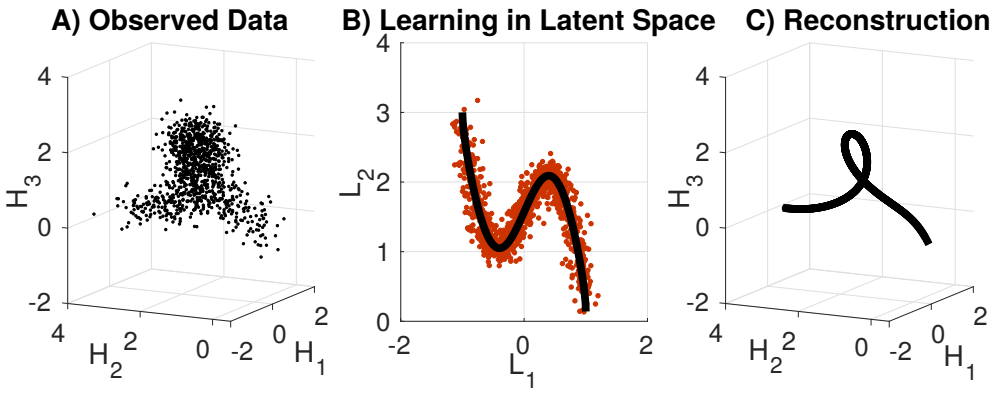

Figure 5.3: A) Illustration of complex data in an observed high (H) dimensional space. B) Finding existing structure within a lower (L) dimensional (latent) representation of the data, means that the structure of the manifold becomes clear. C) Reconstructing latent variables back to the observed data space removes components of the signal that have limited manifold contribution (*i.e.,* noise).

5.2.1 Manifold Learning

There exist a number of existing dimensionality reduction techniques that may be used to learn latent manifolds. For example, the commonly used Principle Component Analysis (PCA) converts data to a new coordinate system comprised of orthogonal axes (principle components), depending on the variance of the data. Axes with small amounts of variance can be discarded when reconstructing back to the original data space, as they have only limited contribution. However, in the context of human motion, where manifolds are potentially non-linear, many commonly used methods such as PCA or Linear Discriminant Analysis may not be suitable due to their linear assumptions. As such, non-linear methods, such as Kernel PCA [200], or Gaussian processes latent variable models (GPLVM) [201], are more suitable. While the method for motion artefact elimination presented in this chapter does not depend on any specific manifold learning technique, a key concern

is the the suitability of the method to the low-cost computational constraints of fabric-embedded devices.

To solve this problem, this paper uses the *Unsupervised Kernel Regression (UKR)* library from [202], due to its low computational cost for learning ($\mathcal{O}(\mathcal{I}\mathcal{N}^2)$ [202]) compared to other methods (*e.g.,* GPLVM is $\mathcal{O}(\mathcal{N}^3)$ [201]). In this, latent manifolds are learnt with automatic complexity control, and require minimal *a priori*specification (only latent space dimensionality and density kernel shape) [203]. The UKR computation also contains a number of useful tricks to optimise the training procedure, including making use of the kernel trick to apply learning to general Hilbert spaces, and performing leave-one-out cross-validation with no additional computational cost. In addition, to prevent the algorithm from falling into local minima, candidate solutions (such as linear manifolds obtained from principle component analysis or local linear embeddings) can be used to initialise the training. For further details of the optimisation methods, see [202].

UKR aims to find both a latent representation $\mathbf{S} = (\mathbf{s}_1 \dots \mathbf{s}_n) \in \mathbb{R}^{\mathcal{Q}\times\mathcal{N}}$ of the observed data $\mathbf{W}$, and a functional relationship $\mathbf{W} = f(\mathbf{S})$ between them. In this, $\mathcal{Q} < \mathcal{I}$, and $\mathcal{Q}$ can be selected by examining criteria such as reconstruction error [204].

In UKR, these reconstructions (also known as the *forward mapping*) are made by an approximation of the conditional expectation $\tilde{\mathbf{X}}$ using smooth kernel regression estimators (such as the Nadaraya-Watson estimator [205, 206]). Kernel-based estimates of the probability space densities are used to compute the prediction:

$$\tilde{\mathbf{X}} = f(\mathbf{S}) = \frac{\sum_{n=1}^{\mathcal{N}} \mathbf{w}_n K(\mathbf{s} - \mathbf{s}_n)}{\sum_{n=1}^{\mathcal{N}} K(\mathbf{s} - \mathbf{s}_n)} = \mathbf{W}\mathbf{\Phi}(\mathbf{S})^\top \tilde{\mathbf{\Theta}}, \tag{5.2}$$

where K is a kernel function. In the second equality, this is written as a weighted set of basis functions.

The latent variables themselves are found via a gradient-based training procedure, that minimises the *orthogonal data-space reconstruction error*:

$$R(\mathbf{S}) = \frac{1}{\mathcal{N}} \sum_{n=1}^{\mathcal{N}} ||\mathbf{w}_n - f(\mathbf{s}_n)||^2 = \frac{1}{\mathcal{N}} ||\mathbf{W} - \mathbf{W}\mathbf{\Phi}(\mathbf{S})^\top \tilde{\mathbf{\Theta}}||_F^2. \tag{5.3}$$

5.2.2 Motion Prediction from Noisy Sensor Readings

The learnt variables $\tilde{\mathbf{\Theta}}$ define the optimal latent space manifold for the data. Estimates of the noiseless measurements $\tilde{\mathbf{x}}$ can be made by first projecting the noisy measurement $\mathbf{w}^*$ (*e.g.,* motions captured from fabric-embedded sensors) onto this manifold, and then reprojecting this estimate back into the original data space.

Specifically, this is done by finding a latent space estimation $\tilde{\mathbf{s}}^*$ that minimises the (orthogonal) reconstruction error [207]:

$$\tilde{\mathbf{s}}^* = \arg\min_{\mathbf{s}} ||\mathbf{w}^* - f(\mathbf{s})||^2, \tag{5.4}$$

(this can be achieved via nonlinear optimisation (*e.g.,* a constrained nonlinear least squares algorithm [208], or back-propagation [202])).

From $\tilde{\mathbf{s}}^*$, an estimate of the noise free motion $\tilde{\mathbf{x}}^*$ is then made by application of (5.2) (*i.e.,* $\tilde{\mathbf{x}}^* = f(\tilde{\mathbf{s}}^*)$).

5.3 Evaluation

In this section, the proposed approach is evaluated through a simulation study, and through an experiment on gait learning from fabric-embedded devices.

5.3.1 Simulation

The goal of the first evaluation is to characterise the performance of the manifold learning approach for learning and predicting movements from noisy sensory inputs. For this, learning is tested on artificial data with additional noise between the sensed input $\mathbf{w}$ and the target $\mathbf{x}$. In this, $\mathbf{x}$ can represent joint angles as sensed from a high accuracy sensor (*e.g.,* a rigidly attached encoder), and $\mathbf{w}$ the fabric sensor reading of the same angles.

In this evaluation, a set of $\mathcal{N} = 200$ two-dimensional coordinates are sampled linearly from the unit circle, to form the matrix of noiseless measurements $\mathbf{X} \in \mathbb{R}^{2\times\mathcal{N}}$. To simulate readings sensed with noise corruption, $\mathbf{X}$ is corrupted by additive Gaussian noise $\mathbf{E} \sim N([\mathbf{0},\mathbf{0}], \Sigma_\varepsilon^2)$, where $\Sigma_\varepsilon^2 = 10^{-3}\mathbf{I}$, to generate the matrix of noisy data $\mathbf{W} = \mathbf{X} + \mathbf{E}$. The data are then randomly decomposed into independent training (70% of data) and testing data sets (30%) for learning, and shown in Figure 5.4(A).

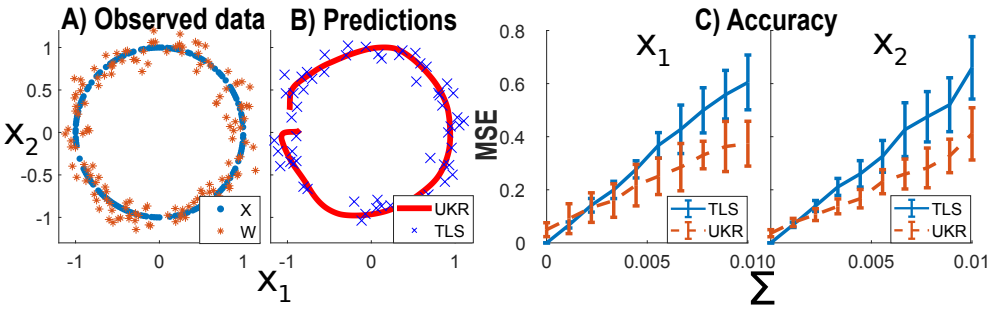

Figure 5.4: (A) Ground truth and noisy input data, (B) predictions using TLS estimator and manifold estimation with UKR, (C) NMSE of predictions at different noise levels (mean ± s.d. over 20 trials).

A one-dimensional ($\mathcal{Q} = 1$) UKR model is then trained using the "UKR toolbox" developed by [202]. For this, the noise corrupted training data $\mathbf{W}$ is used to fit a manifold in the data-space. No initialisation candidates are presented to the method, and both the default quartic kernel [209] and default number of back-propagation time-

steps (100) are used. For comparison, the supervised errors-in-variables model total least squares (TLS), is also learnt from both $\mathbf{W}$ and $\mathbf{X}$ using the approach outlined in [210]. As in the UKR model, no additional feature space mapping is performed (*i.e.,* the feature matrix is $\mathbf{\Phi}(\mathbf{W}) = \mathbf{W}$). This procedure is repeated on 20 independent data sets. The prediction results for one data set are shown in Figure 5.4(B). In this, it is seen that the learnt UKR manifold is a good fit to the noiseless unit circle, and that reconstructions made using UKR have eliminated the additive noise. This is reflected in the low mean squared error (MSE) between the UKR predictions $\tilde{\mathbf{X}}$ and the ground truth $\mathbf{X}$, averaging 0.37 ± 0.085 and 0.41 ± 0.098 for the respective axes, over the 20 trials. In comparison, predictions made using the TLS estimator have a larger error (0.64 ± 0.10, and 0.66 ± 0.12) and are seen to have a somewhat poorer fit.

To evaluate the robustness of the method, the experiment is repeated varying the additive noise Σ_ε^2 in the range $[0, 0.01]\mathbf{I}$, with prediction results shown in Figure 5.4(C). In this it is seen that initially, at low levels of noise, the error in both the TLS and UKR predictions remains low. As Σ_ε^2 increases there is, as expected, a larger error for both TLS and UKR. However, while prediction error for both models increases, the UKR error is less than TLS, indicative greater predictive accuracy at higher noise levels.

The results demonstrate that not only can a statistical model be designed to *account for motion artefacts without the need to calibrate with a noiseless data set*, but that these predictions can be more accurate than standard errors-in-variables techniques.

5.3.2 Experiment - Fabric mounted sensor during walking

In this evaluation, the proposed approach is tested in a real-world motion task, with the goal of estimating hip and knee angles during locomotion using fabric-embedded sensors.

The experimental platform for this experiment consists of two independent measuring systems ($M1$ and $M2$) used to obtain sagittal hip and knee angles, shown in Figure 5.5(A). These measurements are collected during walking from four healthy male participants, on a treadmill operating at a constant $1.2ms^{-1}$ (average speed for men age 20-29 [211]) for $20s$.

To obtain hip and knee joint angles, the relative orientation of the two segments forming the joint is computed. In $M1$, high-accuracy (noiseless) angular velocity measurements of the shank and thigh are obtained using the full-body Xsens motion capture system [212], which requires a prior calibration procedure involving measuring participant limb segment lengths, and performing poses. Measurements of the sensor angular velocities measurements are sampled at $140Hz$, and converted to thigh and shank segment angular velocities through the use of an inbuilt biomechanical model.

Simultaneously, a second data set is collected from $M2$, consisting of two ITG3205 tri-angle gyroscopes [213] embedded into the leg of a pair of loose trousers worn by the participant, sampling at a rate of $100Hz$. The gyroscopes are located on the mid-points of the upper and lower leg (to allow for measurement of both the hip and knee angle), and are connected to an Arduino Uno via conductive thread wiring sewn into the trousers to a belt pouch. Using conductive thread instead of standard wiring allows for natural motion of the fabric that is not impeded by wiring. Data is streamed via a serial connection to a PC

base-station for analysis. Note that unlike the Xsens system, there is no calibration from the sensor to segment coordinate frame, nor filtering, as this is included as part of the unsupervised learning process. For both systems, a cumulative trapezoidal numerical integration is performed on the limb segment angular velocities, to obtain estimates of the angular position of each limb segment. To determine initial joint orientation, participants momentarily stand still in an upright position at the beginning of each data recording. Integration drift is removed by subtracting the linear trend (found via a least squares fit) from the signal after data collection. Note, in a live-prediction setting, both the determination of initial joint orientation, and the removal of drift, can be solved by using on-sensor absolute orientation computation methods [68], or inexpensive orientation sensors (*e.g.,* the Adafruit BNO055 [214]). The relative orientation between the thigh and shank are then computed to estimate the knee angle. For the hip angle, the relative orientation between the thigh orientation and the vertical (as determined by the upright reference position) is used as a substitute for the pelvic-thigh relative orientation, as this is a reasonable approximation [215]. Data from the XSens system ($M1$) is then sub-sampled to $100Hz$ using a least-squares linear phase finite input response filter, forming the matrix $\mathbf{X} \in \mathbb{R}^{2\times 2000}$ for $M1$. Data from the fabric system $M2$ is stored in the matrix $\mathbf{W} \in \mathbb{R}^{2\times 2000}$. Motions are also split manually into individual steps for validation and visualisation, but this does not form part of the learning process.

An example of the body angles obtained from both systems is shown in Figure 5.5(B). In this, it is seen that the sensed motion of the fabric experiences additional noise, making for poor predictions of the underlying true body angles.

For learning, a leave-one-out cross-validation [216] is performed on the

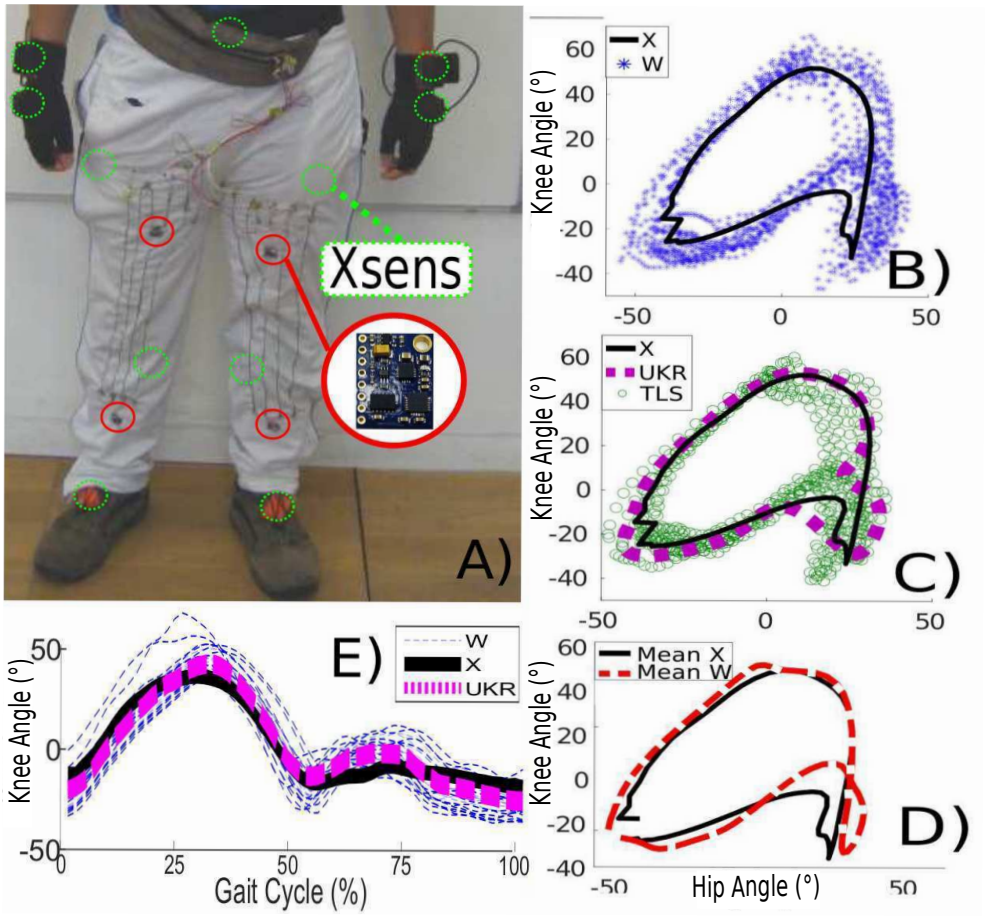

Figure 5.5: (A) Data collection equipment. Shown are Xsens trackers attached rigidly to the body under clothing (green dashed circles) and fabric-embedded gyroscopes (red solid circles). B) Measurements with motion artefacts (noisy) **W** compared to mean walking step **X**. (C) Predictions using TLS and UKR modles. (D) Mean of high quality (noiseless) measurements (**X**) and noisy data (**W**). (E) Knee angle during gait cycle, as measured from both systems, and predictions made with UKR.

recorded steps, exhaustively assessing the accuracy and robustness of the learning method. The proposed UKR approach is then used to learn the latent space representation of the motion-corrupted data **W**. As a baseline for this comparison, a supervised TLS model is also learnt using both the motion corrupted data **W** and noiseless samples **X**.

The predictions for both models are shown in Figure 5.5(C), for one participant. It is seen that the manifold learnt by UKR exhibits a good fit to the underlying body angle interaction pattern. The prediction re-

Table 5.1: Mean angle error (degrees°) in model prediction (mean ± standard deviation). Results for Participant 1 (P1) are over 30 steps, results for all are over four participants.

	Hip (P1)	**Knee (P1)**	**Hip (all)**	**Knee (all)**
Raw	10.68±9.42	4.26±9.05	10.52±10.16	5.52±10.59
UKR	0.72±7.21	1.08±10.1	0.36±0.29	0.74±0.42
TLS	0.78±6.33	0.75±9.88	0.48±0.35	0.63±0.38

sults of the UKR and TLS models are shown in Table 5.1. In this, it is seen that the average angle error for one participant remains low for both UKR and TLS modelling, in comparison to the raw noisy data. This low error is also seen across participants, demonstrating the generalisability of the method. These results show that UKR is able to make prediction estimates just as well as learning methods that explicitly account for errors-in-variables, but *without needing the set of noiseless body measurement for calibration.*

It should be noted that there is some error in the segment of the manifold corresponding to the foot-strike (Figure 5.5(C) lower-right corner), that results in the large standard deviation seen in Table 5.1 for participant one for both learnt models. This appears to be due to the high peak ground reaction force [217] causing a higher variability in the fabric motion at this point and, it is seen in Figure 5.5(B) that the motion of the fabric is shifted to one side of the walking step. This is also illustrated in Figure 5.5(D), where it is seen that the (noisy) mean walking step observed by the fabric embedded sensors is slightly shifted away from the ground truth step. As such, in this segment, the fabric exhibits a non-mean zero distribution of noise. This complex distribution of noise explains why UKR does not outperform TLS as previously seen during the simulation (§5.3.1). However despite this complex noise breaking the zero-mean noise assumption made by UKR, it still performs equally as well as the supervised learning techniques, without

requiring explicitly defined noiseless body motions.

5.4 Conclusion

In this chapter, the application of unsupervised non-parametric learning in estimating human motion through noise corrupted fabric-embedded sensors has been investigated. A major issue in the implementation of artefact elimination techniques in fabric-embedded sensors, is the ability to deal with the wide range of human motion and wearer/fabric interactions that occur during everyday usage. Using explicit calibration models (*e.g.,* motion capture) to create motion artefact elimination models is unsuitable due to the large number of calibrations that are required to capture all motions.

To address this, it has been proposed to exploit unsupervised statistical learning techniques to not only deal with the effects of stochastic perturbations in measurements, but allow for the automatic recalibration of artefact elimination models. In this, an approach to noiseless measurement reconstruction has been presented based on the use of unsupervised kernel regression for learning lower-dimensional, latent space representations of the noisy motion data. Evaluation of this approach in simulation has shown its ability to outperform supervised errors-in-variables models when explicitly accounting for noise in the independent variables. Experiments in learning human gait cycles has shown that it performs equally as well as the supervised learning techniques, without the need to explicitly perform a manual calibration stage. In principle, latent space representations can be used to overcome the problems of motion artefacts for any motion. However, the distribution of noise can play a role the accurate modelling and prediction of motions (see §5.3.2).

In the next chapter, a detailed look is presented about how the unique

material properties of fabric can affect motion monitoring tasks. This is with the aim to understanding the role that fabric has on sensing human motion, and how additional information contained in the motion of the fabric may find utility in human motion monitoring applications.

Chapter 6

Activity Recognition with Wearable Sensors on Loose Clothing

6.1 Introduction

In previous chapters, approaches have been presented to remove motion artefacts, in order to estimate measurements of human motion that are as similar as possible to the true body motion. However, this precludes the possibility that *the motion of the fabric itself may also contain valuable information about the wearer's body motion.* Fabric exhibits features which may, in fact, help in classifying wearer motions, including an increased range of motion and a deformable structure that allows for multi-directional movement, see Figure 6.1. In the performing arts, this is implicitly exploited for choreographed dance routines: Loose and free-flowing garments are used to exaggerate, emphasise, and express motions to a much larger degree than is possible solely with the human body [218]. Low stiffness materials such as nylon are often used to create a "floating" effect around a dancer, while stiffer fabrics such

as jersey grip the wearer [219]. Varying the physical design parameters of textiles to emphasise or suppress particular motion features has also been employed in systems such as vibration isolation (*e.g.,* by varying the knitting method to lower the resonant frequency of material [220]) and for structural deformation (*e.g.,* by introducing auxetic behaviour, whereby a material stretches perpendicular to an applied force [221]).

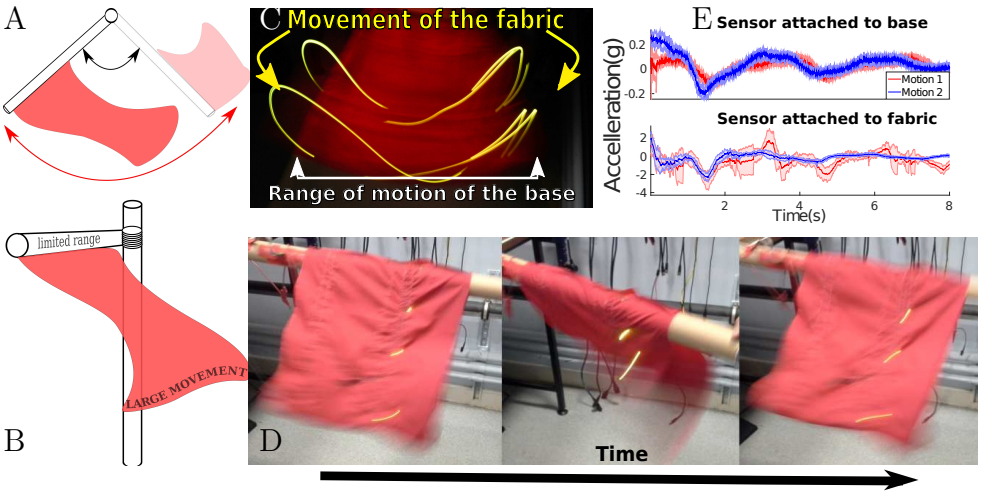

Figure 6.1: Effects of motion on fabric. The soft, deformable structure of the fabric allows for an increased range of motion **A**, **B**, as seen in LED trails from the top **C** , and side **D** of the fabric. Difference in motion signals in a comparison task **E** where motion sensors are located on both a rigid base, and loosely attached to the base via fabric (note the different vertical scales).

In this chapter, an experimental examination is performed into the role that the material parameters of fabric play in statistical classification systems. For this analysis, fabric is investigated as a *feature space mapping system*, characterised by its material properties. Experiments in this chapter demonstrate that the motion of the fabric can contain useful information about the motion of the body, allowing the fabric itself to be used as a signal processing device.

Publications

- Michael, Brendan, and Howard, Matthew. 'Activity Recognition with Wearable Sensors on Loose Clothing" In PLOS One. 12, 10. 2017

6.2 Background

To understand how best to exploit such effects in the context of wearable sensing, it is important to understand how the fabric moves when subject to user motion, and how this affects our ability to interpret sensed signals for motion recognition. In the performing arts, choreographers and clothing designers use fabric to best exhibit factors of motion they wish to emphasise. For example, natural materials that easily deform can be used to "catch" the air during motion [222] which allows for a large range of fabric motion from relatively little body motion. This use of the motion of the fabric does not just express the wearer's body motion on a larger scale (amplification), but selectively emphasises parts of the movement, creating complex motions that the human body could not perform on its own.

If these effects could also be exploited in motion recognition tasks, it may be possible to gain additional information for more robust classifications of movement tasks. To design a *sensing system* that also uses this effect, it is important to understand the role of the fabric parameters (*e.g.,* material properties such as weight) on motion recognition. One way to examine this relationship is to use detailed models of the fabric structure (§3.3), including the behaviour of individual yarns, to simulate interaction dynamics between wearer and fabric. However, as previously mentioned, such simulations are computationally expensive, and are of questionable accuracy due to the difficulty in determining

fabric parameters (*e.g.,* weave, thread tension, worn position) and external factors (*e.g.,* wind, humidity).

Alternatively, one can directly analyse data from a physical fabric system and use statistical learning methods to examine the effect of varying specific elements of the fabric structure. In a wearable sensing system, this can be used to both create models of the user's motion from sensed movements, and quantify recognition improvement when varying fabric designs. By statistically quantifying this accuracy, it can be shown explicitly which fabric parameters have the greatest influence in emphasising motion.

By far the dominant approaches to activity recognition in wearable sensing systems are distance-based statistical methods [223] such as K-Nearest-Neighbours or Support Vector Machines (SVM) [224]. In this setting, the sensed movement (*e.g.,* the sensed unidirectional acceleration of an arm during a reaching task) is recorded and represented as a fixed length vector $\mathbf{y} \in \mathbb{R}^{\mathcal{I}}$, where $\mathbf{y} := (y_1, y_2, \ldots, y_{\mathcal{I}})^T$, and y_t is the sensed reading at time t. In classification systems, these sample movements are then represented as points in some feature space $\boldsymbol{\phi} \in \mathbb{R}^{\mathcal{J}}$, and the contrast between these points is used to determine the class label, see Figure 6.2.

The key to success in such approaches is the selection of the feature space $\boldsymbol{\phi}$, which plays an important role in building good predictors[225]. To find features in the data that may result in highly accurate classifiers, processes such as *feature extraction* or *dimensionality reduction* can be used. For example, principle component analysis [226] is often used to decompose a data into a set of linearly uncorrelated variables, allowing for the removal of variables that only contribute minimally to describing the data. These features can also be selected a priori, for example in myopathic studies, decomposing raw electromyographic sig-

nals into frequency domain information often results in highly significant differences between healthy and myopathic patients, increasing the accuracy when diagnosing neuromuscular disorders [227].

In the context of fabric-based sensing systems, the fabric itself can be thought of as a feature space transformation from the wearer's body motion. This transformation is defined as the one-to-one mapping $\boldsymbol{\phi}(\mathbf{y}) : \mathbb{R}^{\mathcal{J}} \mapsto \mathbb{R}^{\mathcal{J}}$ between the sensed motion from the body and that of the fabric (note that in this approach, $\mathcal{J} = \mathcal{I}$). In other words, fixed-length motions $\mathbf{y}$ of a given type are collected and transformed into the feature space $\boldsymbol{\phi} = \boldsymbol{\phi}(\mathbf{y})$. Note that, by using the fabric as the feature space transformation, the transformation is obtained simply by placing sensors *on the fabric itself*, requiring no additional processing.

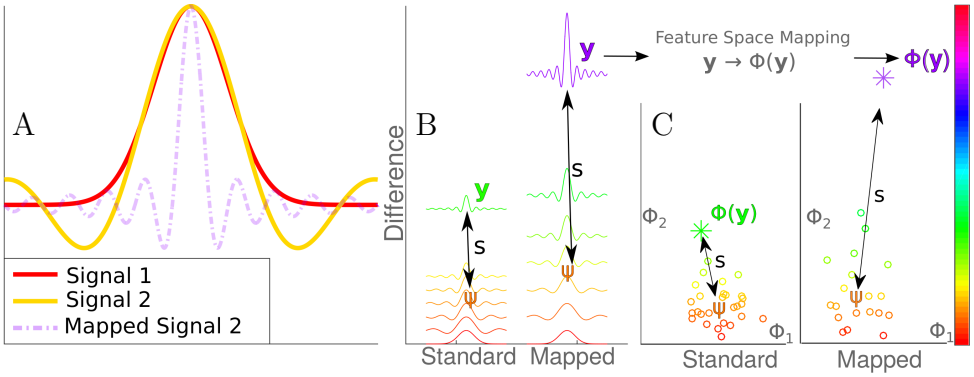

Figure 6.2: **A** Illustration of how two visually similar functions can be difficult to classify (signal 1 is the Gaussian function with $\mu = 0, \sigma = 2$, and signal 2 is $\text{sinc}(x)$). These signals can be more easily distinguished when one or the other signal is non-linearly transformed (Mapped Signal 2, is $\text{sinc}(4x)$)). **B** Visual illustration of the similarity s between a cluster mean $\boldsymbol{\psi}$ of one signal, and a new signal $\mathbf{y}$, for both the normal and mapped systems. **C** Similarity when representing signals as points in a cluster classification system.

To compute a classification model, $\mathcal{M}$ samples of motions $\boldsymbol{\phi}$ in the feature space are used to form a cluster $\boldsymbol{\Psi} \in \mathbb{R}^{\mathcal{I} \times \mathcal{M}}$, from which a single model representing the full data set is derived $\boldsymbol{\psi} \in \mathbb{R}^{\mathcal{I}}$ (*e.g.*, the mean of the cluster). The *similarity* s between $\boldsymbol{\psi}$ and a new feature-space-mapped motion sample $\boldsymbol{\phi}'$ scores the extent to which the latter

belongs to this cluster of motions. This is computed as the distance $s = d(\boldsymbol{\psi}, \boldsymbol{\phi}')$ according to some chosen metric (*e.g.,* the Euclidean or Mahalanobis distance [228]). A small value of s indicates that the new motion sample $\boldsymbol{\phi}'$ is a member of the cluster $\boldsymbol{\Psi}$, while a large value (a large *dissimilarity*) indicates that $\boldsymbol{\phi}'$ is a movement of a different type. The present study empirically investigates whether varying the structure of a fabric-based sensing system increases motion prediction accuracy due to selective emphasis of parts of the motion. A statistical approach is taken whereby the physical fabric motions are analysed through the statistical classification techniques described above.
For this, the data acquisition device shown in Figure 6.3(A) is used. In the experiments, motion signals are recorded, varying factors of the experimental setup, including types of fabrics used and similarities between motions. Given these motion signals, the *similarity* between types of motion is analysed, to determine which factors of the fabric influence motion prediction accuracy.

6.3 Experimental Design

6.3.1 Data Collection

The data acquisition device (Figure 6.3(A)) used in this study consists of a weighted pendulum (of length 57 cm), swinging freely in gravity on a single axis.
A fabric substrate (heavy weight jersey, two-way stretch, 95% cotton, 5% elastane, 18 cm length when taut), is attached to the tip of the pendulum. The device is instrumented by three inertial sensors (LilyPad ADXL335 tri-axial accelerometer) that simultaneously record the acceleration of different points on its length. These sensors are attached at (i) the tip of the rigid pendulum (denoted R1, 57 cm from the pivot),

(*ii*) in the centre of the fabric (F2, 66 *cm*) and (*iii*) at the tip of the fabric (F3, 75 *cm*).

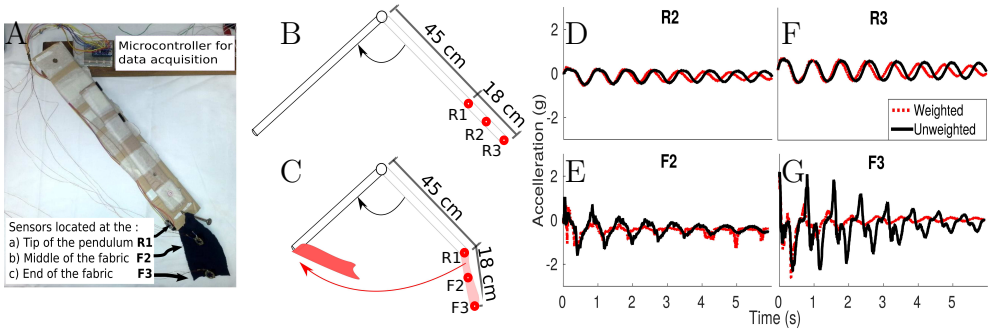

Figure 6.3: **A** Side-view of pendulum with attached fabric at tip. Sensors are placed at the tip of the pendulum, and on the body of the fabric. **B,C** Schematic of experimental setup. **D,F** Motion signals from both weighted and unweighted pendulum when sensor is attached rigidly to the pendulum at increasing distances from the axle. **E,G** Motion signals when sensor attached to the end of the fabric.

The accelerometers are sampled using an Arduino Nano (Atmega-328P microcontroller, 16-bit ADC), and readings are transferred to an attached PC base-station for analysis. The accelerometers are connected to the microcontroller by loose, thin, light-weight insulated copper wiring to ensure minimal interference with the motion of both the pendulum and fabric. All sensors are calibrated to one-another to remove inter-sensor variability, and collect data at 600Hz.

In each recorded motion, the pendulum is released from a static position (the horizontal), and data is recorded from all three sensors for 10 seconds. External environmental factors, such as vibrations and air currents, were minimised by performing the experiments in a closed laboratory. During motion, acceleration signals are collected from the axis parallel to the ground (when the pendulum is at rest) from all three sensors. Two sets of data are collected, in the first the pendulum is weighted with $3N$ at the tip, and in the second the weight is removed. This process of data collection is repeated to produce 10 in-

dependent motions per data set. All motion signals are converted to standard gravity, then time-synchronised. For each data set, a cluster of the 10 motions recorded over 6000 time-steps is then defined as the cluster matrix $\boldsymbol{\Psi} \in \mathbb{R}^{6000\times10}$, and the mean $\boldsymbol{\psi} \in \mathbb{R}^{6000}$ is taken to form the model of the motion.

6.3.2 Varying Fabric Material

To evaluate how the structure and physical properties of the fabric can influence the similarity score, the same experiment is repeated with several other commonly-used clothing materials, denim (98% cotton, 2% elastane), jersey, and roma (four-way stretch 74% polyester, 27% rayon, 3% spandex). The process is also repeated with the fabric replaced by a rigid element, with sensors R2 and R3 placed at identical distances to the pivot as F2 and F3.

6.3.3 Varying Pendulum Weight

To examine the effect of the motion itself, the experiment is repeated using the jersey material with pendulum weights varied between $0.5N$ to $3N$. This variation alters the speed of the pendulum, thereby generating different motion signals. In the context of wearable sensors monitoring human motion, this simulates the common task of a wearer performing tasks with different speeds (e.g. lifting weights for rehabilitation exercises [229]).

6.3.4 Statistical Analysis

To examine the similarity between different motions, these experiments compute the Euclidean distance between signals $\boldsymbol{\phi}$, normalised over the range of distances. One-way analysis of variance is performed using the Matlab R2016b statistics toolbox. Depending on the experiment, input

data is either motion signals $\boldsymbol{\phi} \in \mathbb{R}^{6000}$ or similarity scores s, and data is grouped according to their weight.

6.3.5 Motion Classification

To perform classification and prediction, classification methods are trained using the data collected from the fabric tipped pendulum, to predict whether the pendulum is swinging with or without a weight attached. In these experiments, support vector machines (SVM), (two-class, using the Matlab R2016b statistics and machine learning toolbox) and discriminative regression machines (DRM) [230] are used. For both competing methods, linear [224] and Gaussian kernels [190] are used, with the hyper-parameters *box-constraint* and *kernel scale* obtained via a five-fold cross-validation. Note that this implementation can be extended to the multi-class setting by using common ensemble techniques such as "one-vs-one" or "one-vs-all" [231].

For each of the three sensors, 10 samples of pendulum motion with a 3N weight and 10 samples without, are randomly segmented into two independent sets, a model training set consisting of 19 motion samples and an independent testing set consisting of one sample.

As is common in wearable prediction systems that work from continuous streams of data [232] (i.e. where it is not known when one motion finished, and another begins), an online learning and prediction method is used. In this, time-discrete segments of the motion signal are passed to the classifier as they are recorded. In this study, motion signals $\boldsymbol{\phi}$ are segmented into *windows* of size n (where $n < \mathcal{I}$). A small value of n signifies that only a small segment of the temporal motion signal is used to compute classification models and make predictions. As n increases (i.e. $n \to \infty$), more of the motion signal is used. Windows overlap by every $\frac{n}{2}$ time-steps, with predictions made every $\frac{n}{2}$ time-steps.

These windows can be defined as subsets of the full motion signal,

$$\mathbf{w} := [(\boldsymbol{\phi}_1, \ldots, \boldsymbol{\phi}_n)^T, (\boldsymbol{\phi}_{\frac{n}{2}}, \ldots, \boldsymbol{\phi}_{\frac{3n}{2}})^T, (\boldsymbol{\phi}_n, \ldots, \boldsymbol{\phi}_{2n})^T, \ldots]$$

To perform model training and prediction, initially the first n time-steps of the training data are used to train a classification model, and predictions are then made on the first n time-steps of the testing data. The window is then time-shifted forwards by $\frac{n}{2}$ time-steps, and process is repeated. This repeats until the end of the signal is reached. To ensure robustness of the modelling method, this online learning and prediction method is repeated 20 times, varying the motion sample used for the testing set.

With this experimental setup, the effect of the window size used to segment the motion data is examined, by evaluating the classifier accuracy for each sensor when varying the size of the window between 15 milliseconds, and 1.5 seconds. From this evaluation, a fixed window size is selected to examine the normal operation of the classifier.

6.4 Results

6.4.1 Effect on Sensed Motion Signal

To examine how sensed readings from fabric-embedded sensors can be exploited in wearable sensing systems, this section examines if significant differences between similar pendulum motions can be observed. Figure 6.3(D), the motion signal from sensor R3 (located further along the pendulum) is plotted.

It is seen that, as expected, increasing the distance from the axle increases the amplitude of the acceleration signal. This is due to the geometry of the set up; sensor signals have larger amplitude with in-

creased distance from the pivot (linear acceleration of the tip increases with pendulum length). To examine if the sets of weighted and unweighted signals are significantly different from each other, motion signals $\boldsymbol{\phi} \in \mathbb{R}^{6000}$ from each sensor is allocated to groups according to their weight. It is seen that there is no significant difference between weighted or unweighted motions observed either from sensors R1, R2 or R3 ($p > 0.75$). This shows that in this setup, attempting to predict if a motion is weighted or unweighted by using rigidly attached sensors, is a challenging task.

It is seen in Figure 6.3(E,G) that when the lower two sensors are mounted onto fabric, there is a much larger difference between the two signals compared to that seen with a rigid extension. The difference between motions is most noticeable in readings from the sensor mounted furthest from the fabric attachment point Figure 6.3(G), where different oscillatory patterns emerge between the motions due to changes in direction of the pendulum causing secondary swinging motions of the fabric. There is a significant difference between the two motions, for both sensors F2 and F3 ($p < 0.01$). From this, it can be seen that there are significant differences between motions, but only observed when sensing the motion of the attached fabric.

6.4.2 Effect on Classification Algorithms

To examine how these observations affect distance based classification algorithms, this section examines if contrasting motion signals observed from fabric-mounted sensors show greater *dissimilarity* than rigidly attached sensors. Greater dissimilarity between motions is increased by the enhancement of contrasting features, and is the underpinning factor in many commonly used classification algorithms. To examine this, the following experiments examine the similarity between the two sets of

motions.

Initially when observing motion signals from the rigid pendulum (Figure 6.4(A)), it is seen that the average similarity between the weighted and unweighted pendulum signals decreases as distance from the axle increases ($p<0.01$). However, this difference between motions is small, for all three sensors located rigidly on the pendulum. In comparison to this, there is a much larger difference between motion signals when observations are recorded using fabric sensors mounted onto jersey (Figure 6.4(B)).The greater distance between the two motions when using jersey indicates that the signals observed from fabric-mounted sensors are not only less similar (and thereby easier to distinguish in a classification system), but are more robust to in-class variance in the sensed readings, increasing the *confidence of the predictions*. The signals from sensors placed at the middle and end of the fabric also show more variance due to external environmental factors (*e.g.,* air movement, small variations in starting angle) causing greater spread in the data cluster.

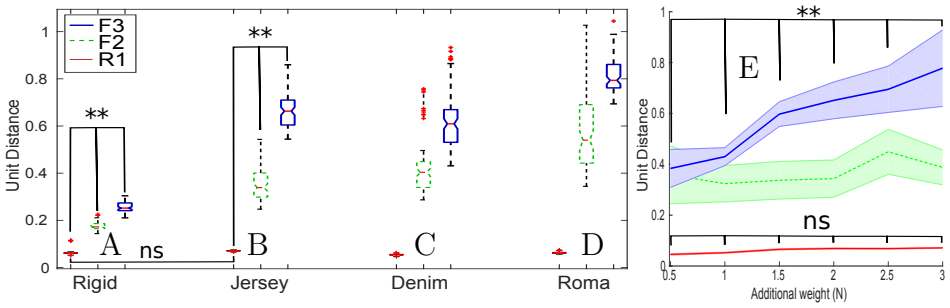

Figure 6.4: **A-D** Box plots of the difference between unweighted and weighted pendulum when using sensors located at the pendulum tip (red thin line), middle (green dashed), or end (blue thick line). **E** Difference for jersey when varying weights from $0.5N$ to $3N$.

One possible explanation for the difference between motions, is that the fabric significantly *alters* the motions of the pendulum (e.g. by increasing the air resistance and slowing down the pendulum). To evaluate this, similarity measurement are taken from the signals recorded from sensor R1, which is attached rigidly to the pendulum during all

experiments (including fabric-mounted ones). In this, it is shown there is no significant difference ($p>0.9$) in the similarity measures when using either a rigid pendulum or with a jersey tip. This indicates that the increase in distance is not caused by the additional fabric biasing the signal by altering the underlying pendulum motion.

6.4.3 Effect of Varying Pendulum Weighting

The similarity between motions when varying the pendulum weight (Figure 6.4(E)),

6.4.4 Fabric Structure and the Relationship to Similarity

In experiments varying the fabric material used, sensors placed on both the denim (Figure 6.4(C)) and roma (Figure 6.4(D)) result in a larger dissimilarity between motion classes than the rigid pendulum. It is seen that denim shows greater similarity than jersey or roma, due to the rigidity of denim damping the signal, and reducing the oscillatory effects of the fabric in motion. In contrast, the dissimilarity of the sensed motions from the sensor placed on the roma fabric is greatest (with the largest variance), due to the light, non-stiff structure of the fabric.

6.4.5 Activity Recognition

In a classification setting, the above suggests the surprising result that it should be *easier* to distinguish between different motions with a sensor mounted onto clothing, than one rigidly connected to the body. To evaluate this, classifiers are used to predict whether the pendulum is swinging with or without a weight attached, using the data collected

from the jersey tipped pendulum. In a motion recognition context, the sensors can correspond to sensors mounted on a loose area of a garment, such as a sleeve. In this context, sensors F2 and F3 correspond to mounting sensors at varying positions of the sleeve, while R1 (which is attached rigidly to the body) simulates a body worn sensor. Classification is performed using the traditional linear kernel, due to its simplicity in computing classification models (making it suitable for an embedded low-cost system), as well as its straightforward interpretation as a distance-based classifier. Models are also computed using the Gaussian kernel due to its common usage in activity recognition [233] and the discriminative regression machine (DRM), due to its suitability in dealing with similarities within classes of high-dimensional data with small sample sizes [230].

6.4.6 Effect of Window Size

Using the online classification system, the results for varying the size of the window are shown in Figure 6.5(A). Initially, it is seen that at a window size of $15ms$, the prediction accuracy from the rigidly attached sensor (R1) is approximately 40%, while the fabric-mounted sensors report accuracies of 70% and 75%. As the size of the window increases, the prediction accuracy also increases, as expected due to the additional information of the motion signal available to the classifier. The fabric-mounted sensors continuously predict at a greater accuracy than the body-mounted sensor. As the size of the window surpasses $300\,ms$, the body-mounted sensor predicts motions with 100% accuracy, while the fabric-mounted sensors F2 and F3 predict at 95% and 90% respectively. This result indicates that at small window sizes, where predictions can be made more rapidly with fewer computations, fabric mounted sensors outperform their body-worn counterparts. At

larger window sizes, where there are greater time-periods between predictions, the fabric-mounted sensors fall slightly short of the accuracies reported by the body-worn sensors.

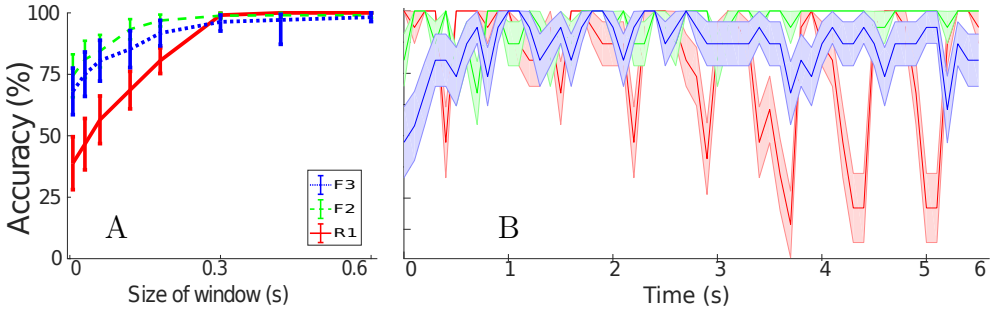

Figure 6.5: Mean accuracy of Gaussian SVM over 20 trials (± standard error) **A** when varying window size between 15 ms and 1.5 seconds, and **B** mean accuracy of online motion prediction with window size fixed at 250 ms, using data from the sensors attached to the pendulum and fabric. Similar results for both experiments are also seen for linear SVM, and both linear and Gaussian DRM.

6.4.7 Online Prediction

Closer evaluation of the classification results at a fixed window size of 250 ms is shown in Figure 6.5(B). In this, it is seen that on average the prediction accuracy using SVM from the rigidly attached sensor is $83.9 \pm 17.9\%$ (linear kernel) $84.1 \pm 20.6\%$ (Gaussian kernel), while the average accuracy from the sensor located in the middle of the fabric is $93.3 \pm 8.6\%$ (linear kernel) $95.9 \pm 6.1\%$ (Gaussian kernel). Predictions made using the DRM classification method, give accuracies from the rigidly attached sensor of $72.4 \pm 1.7\%$ (linear kernel) $80.3 \pm 18.1\%$ (Gaussian kernel), and for the sensor located in the middle of the fabric $90.6 \pm 9.1\%$ (linear kernel) $94.5 \pm 6.7\%$ (Gaussian kernel).

These results show that not only is the average prediction accuracy higher for the fabric-mounted sensors, but the lower variance in the predictions indicates that the classifiers used are more robust. This follows on from the similarity analysis (see above), which shows that the greater distance between types of motion signals from fabric-mounted

sensors results in a greater confidence when making predictions. It should also be noted that the body-mounted sensors (Figure 6.5(B)) demonstrate oscillating dips in prediction accuracy. This is due to pendulum moving in and out of phase between the weighted and unweighted motion signals (*e.g.,* at the apex of a swing, where the recorded acceleration is zero), resulting in high similarity between the signals. In contrast the fabric does not exhibit this effect, as the deformable structure of the fabric allows for complex movement in other axes, resulting in motion trajectories that are significantly dissimilar, at similar positions of the pendulum. The similar results seen in all three classification methods demonstrate that the exploitation of the fabric dynamics plays a greater role in achieving high accuracy, than the complexity of the classifiers used.

6.5 Conclusion

In this chapter, an empirical investigation into the the use of fabric-mounted sensors has been performed, to examine if the non-rigid, deformable nature of fabric can be exploited to provide additional information about a wearer's movement, enhancing activity recognition systems. The findings outlined here show that mounting MEMS inertial sensors onto loose fabric can lead a greater contrast between different types of measured motion. Even when signals from a rigidly attached sensor are not significantly different, the fabric's ability to deform in multiple directions allows for an increased range of motion, making it easier to distinguish between different motions. In motion classification tasks using streaming data, the use of fabric mounted sensors can result in a greater prediction accuracy, with smaller windows of data, allowing predictions to be made more quickly and at lower computational cost compared to the rigidly attached equivalent. This high

accuracy coupled with a relatively simple linear SVM classification algorithm, demonstrates that this approach of exploiting the dynamics of the fabric can enhance this classification accuracy with no need for greater computational power, even in comparison to using learning methods which explicitly account for high dimensional data and small data sets.

The effects seen in this chapter depend on factors such as the speed and amplitude of the motion and the material properties of the fabric such as its length and stiffness. However, it is robustly reproduced in a number of fabrics commonly used in ordinary clothing. Fabrics with a low stiffness flow more easily, subjecting sensors to greater accelerations. However, this low stiffness also means that the fabric motion is more sensitive to environmental factors (*e.g.,* air flow), and results in larger within-class variance. There is a trade-off between using motion artefacts to emphasise selective features, and limiting the effect of motion artefacts on the predictions. This is especially important when applying this method to real-world motion tasks, where poor control of this trade-off may result in highly unpredictable motion artefacts, masking the intended signal. Nevertheless, the experimental results on integrating sensors into deformable materials presents the first evidence that *noise and motion artefacts can be beneficial to motion recognition tasks*. With the advent of modern, model-free statistical approaches to activity recognition, requiring that motion artefacts always be eliminated is not only unnecessary, but *fails to exploit information implicit in the textile motion*.

In the context of real-world activity recognition, this method in its current form would find utility in classifying controlled motion tasks (e.g. rehabilitative weight-lifting exercises for muscle strengthening [229]). This approach shows a promising baseline for future work involving

unconstrained human motion. The exploitation of soft sensor deformation has wider implications outside the field of sensorised clothing. The observations reported here may also find utility in other soft sensing based applications, *e.g.,* healthcare monitoring devices such as sensorised mattresses for measuring cardiac and respiration during sleep [234], or capacitive textile sensors in car seating to capture whole body motion to detect impaired driving [235]. Not only would the ability to make sensitive predictions enhance current applications, but the revised view of utilising motion artefacts enables the development of systems previously thought to be too noise-corrupted.

In the next chapter, the findings of this thesis will be summarised, and directions for future work will be suggested.

Chapter 7

Conclusion

In this thesis, the role of motion artefacts in minimally invasive fabric-embedded sensors has been investigated. In this, it has been shown that these artefacts can severely limit the usage of such sensors in both the clinical and research domains, and that standard methods for account for these artefacts fail to address the unique aspects of the deformable fabric structure.

With an aim to understanding this role, this thesis investigates two aspects of this problem. Firstly, the use of statistical learning to eliminate the motion artefacts from sensed signals is investigated, and secondly, the role of fabric as a signal processing device to enhance statistical information is researched.

In Chapter 2, an analysis of the current uses of human motion analysis was presented, highlighting the issues that hinder both clinical and research directions. An introduction to the concept of both portable and fabric-embedded sensors was discussed, and the current state of the art was presented. As part of this, a common issue across sensor designs was observed, that of motion artefacts corrupting motion signals.

In Chapter 3, approaches to solving the artefact problem in fabric sensors was discussed in the context of the literature. In this, it was observed that standard methods fail to account for the unique aspects of

fabric, resulting in poor elimination of artefacts.

In Chapter 4, the use of statistical learning for solving this motion artefact problem is presented. In this, an analysis of how motion artefacts can affect standard statistical learning shows that noise assumptions on standard learning are not seen in this motion artefact problem, leading to poor learning accuracy. To solve this problem, a method is described accounting for stochasticity is the observed measurements in body motion learning problems. Experimental evaluations are performed to learn body motion from motion corrupted data, and show superior performance over standard learning techniques.

In Chapter 5, methods that account for errors in measurements are extended to learn generalisations of user motion, independently of any artefact elimination calibration stage. This allows for the real-time prediction of motion data given variations in both user motion and fabric properties. Experiments in this chapter demonstrates that these elimination methods can be calibrated solely by the user motion, and are an effective method for handing artefacts experienced in everyday motion.

Finally, in Chapter 6, a novel approach of using the fabric itself as a signal processing device is presented. This is with the aim of inferring additional information from the motion of the fabric, using the fabric as an additional feature space mapping in which to enhance classification techniques. Experimental evaluations on the material properties is performed to examine the affect of fabric motion on learning statistical classification models. In this, it is seen that noise and motion artefacts can be used to exploit information implicit in the textile motion, and that it is not always required to eliminate motion artefacts.

Limitations

While the approaches to dealing with motion artefacts in fabric embedded sensors presented in this thesis show improvement over existing methods, there exist limitations. It is important to be aware that the technical limitations of existing embedded computer systems, limit the applicability of these methods to partial body, constrained motion analysis. While this research presents experiments demonstrating that simple, clinically important measurements (such as joint angle tracking) can be successfully measured using the approaches outlined, full body, complex motion tracking cannot currently be performed on these embedded devices. To address this issue, the future works section of this thesis investigations possible methods for offloading both processing and prediction, allowing for the whole-body human motion capturing, and the handling of more complex fabric motions.

Future Work

The research presented in this thesis can be extended in a number of future directions.

Long-term Data Collection

In Chapters 4 and 5, experiments are presented to demonstrate that the proposed approaches to learning body motions from fabric-sensors is a feasible approach to overcoming motion artefacts. In Chapter 4, these experiments are limited to a simple arm pose estimation task. In Chapter 5, these experiments are extended to evaluate these methods in a more complex gait monitoring task, and also to investigate how adaptive learning techniques can be applied to account for user changes in motion during long-term use. However, further experiments

in longer-term studies can investigate the robustness of these methods in everyday tasks. For example, this can include the effect of higher impact activities (*e.g.,* running or other sports) on the motion artefact elimination methods, and well as the inclusion of time series analysis into the motion artefact problem. In addition, the evaluation of these methods in collaboration with clinicians (*e.g.,* the accuracy of a sit to stand assessment) would provide further insight into directions for this research.

Fabric Motion Analysis

In Chapters 4 and 5, motion artefacts are assumed to be stochastic perturbations to the body motion. In this, no assumptions are made by the learning algorithms presented about the statistical distribution of motion artefacts. However, as seen in Chapter 5, fabric motion during gait was seen to exhibit a non-zero mean distribution of noise. To improve modelling and prediction accuracy when learning user motions from fabric systems, the heteroscedastic nature of the motion artefacts can be investigated, in order to better account for the relationship between body motion and artefact generation.

Information Gain from Fabric Motion

The experimental analysis in Chapter 6 of fabric motion, and its role in feature space mapping for discriminant classifiers, will be extended to investigate its applicability in more complex human motion capture tasks. For this, the role of clothing motion in a fabric-embedded *sign language recognition* system is currently be investigated. Specifically, this involves similar constrained motions as seen in Chapter 6, with more complex generating movements, and greater class of motions. Analysis in this context will highlight possible future applications of

this research, as well as further investigate the limitations.

Learning with Biomechanical Models

In Chapter 5, unsupervised learning techniques are presented to learn generalisations of user motion without a calibration stage. Learning methods that allow for prior knowledge about motions or the body structure, could be incorporated into manifold learning [207]. This can be be investigated to enable not only noiseless measurement reconstruction, but the noiseless prediction of other points on the body (*e.g.,* predicting end-effector information from sensors mounted on the upper arm). The inclusion of biomechanical modelling could potentially allow for higher accuracy in motion artefact elimination, by providing further structure to data. While this will increase the complexity of the motion artefact elimination methods, computationally inexpensive biomechanical models could be embedded into fabric devices, or offloaded to computational base-stations (*e.g.,* via wireless).

Design Choices for Modelling

In this thesis, design choices for modelling and eliminating motion artefacts, have been to use computationally inexpensive modelling methods. This is with a view to implementing these models on embedded devices, which would not be able to support computationally expensive, higher accuracy modelling methods. However, practically, there exists as a spectrum of design choices that allows for the use of more complex models, with wearable devices. Examples include storing data for later use in offline processing or the real-time transmission of data to a wireless base-station for model computation. These offloading methods are commonly used in wearable sensing systems, both research and commercial [236], and future research should investigate using sim-

ilar design choices to allow for more complex modelling as would be required for full body motion capture systems. In addition, the use of off-board processing would enable the analysis of captured fabric motion, and the application of fabric modelling techniques (as seen in the animation field) to improve and update motion artefact modelling.

Alternative Sensors

In this thesis, the data examined in the context of the motion artefact problem has been primarily measurements of human kinematics, through the use of embedded IMUS. However, as outlined in §2, this is just one of many motion capture measurements useful in research or clinical domains. The application of the research methods presented in this thesis to other sensing systems, such as artefact problems with dry-electrodes [81] or biosignal monitoring [237], would highlight both relevant applications, as well as investigate sensor specific needs. In the former, solving this problem will involve the fact that motion artefacts in this setting are caused by both high impedance of the skin (which the approaches discussed in this thesis could mitigate), but also loss of contact between the skin and the sensor. As such, further analysis of this application would be required to highlight specific requirements.

Bibliography

[1] C. Charbonnier, F. C. Kolo, V. B. Duthon, N. Magnenat-Thalmann, C. D. Becker, P. Hoffmeyer, and J. Menetrey, "Assessment of congruence and impingement of the hip joint in professional ballet dancers: a motion capture study," *The American journal of sports medicine*, vol. 39, no. 3, pp. 557–566, 2011.

[2] A. H. Al-Timemy, G. Bugmann, J. Escudero, and N. Outram, "Classification of finger movements for the dexterous hand prosthesis control with surface electromyography," *IEEE Journal of Biomedical and Health Informatics*, vol. 17, no. 3, pp. 608–618, 2013.

[3] D. Yamane, T. Konishi, T. Matsushima, K. Machida, H. Toshiyoshi, and K. Masu, "Design of sub-1g microelectromechanical systems accelerometers," *Applied Physics Letters*, vol. 104, no. 7, p. 074102, 2014.

[4] R. Slyper and J. K. Hodgins, "Action capture with accelerometers," in *Proceedings of the 2008 ACM SIGGRAPH/Eurographics Symposium on Computer Animation*, pp. 193–199, Eurographics Association, 2008.

[5] A. W. Lam, D. Varona-Marin, Y. Li, M. Fergenbaum, and D. Kulić, "Automated rehabilitation system: Movement measurement and feedback for patients and physiotherapists in the reha-

bilitation clinic," *Human–Computer Interaction*, vol. 31, no. 3-4, pp. 294–334, 2016.

[6] A. Klin, D. J. Lin, P. Gorrindo, G. Ramsay, and W. Jones, "Two-year-olds with autism orient to non-social contingencies rather than biological motion," *Nature*, vol. 459, no. 7244, pp. 257–261, 2009.

[7] T. Lenzi, S. M. M. De Rossi, N. Vitiello, and M. C. Carrozza, "Intention-based emg control for powered exoskeletons," *IEEE transactions on biomedical engineering*, vol. 59, no. 8, pp. 2180–2190, 2012.

[8] S. K. Vashist, E. M. Schneider, and J. H. Luong, "Commercial smartphone-based devices and smart applications for personalized healthcare monitoring and management," *Diagnostics*, vol. 4, no. 3, pp. 104–128, 2014.

[9] A. Pfister, A. M. West, S. Bronner, and J. A. Noah, "Comparative abilities of microsoft kinect and vicon 3d motion capture for gait analysis," *Journal of medical engineering & technology*, vol. 38, no. 5, pp. 274–280, 2014.

[10] D. Roetenberg, H. Luinge, and P. Slycke, "Xsens MVN: full 6dof human motion tracking using miniature inertial sensors," tech. rep., Xsens Motion Technologies, 2009.

[11] C. M. O'Connor, S. K. Thorpe, M. J. O'Malley, and C. L. Vaughan, "Automatic detection of gait events using kinematic data," *Gait & posture*, vol. 25, no. 3, pp. 469–474, 2007.

[12] C. Castellini, E. Gruppioni, A. Davalli, and G. Sandini, "Fine detection of grasp force and posture by amputees via surface

electromyography," *Journal of Physiology-Paris*, vol. 103, no. 3, pp. 255–262, 2009.

[13] T. Pedersen, A. Nicholson, K. Hovhannisyan, A. M. Moller, A. F. Smith, and S. R. Lewis, "Pulse oximetry for perioperative monitoring," *The Cochrane Library*, 2014.

[14] T. E. Hewett, G. D. Myer, K. R. Ford, R. S. Heidt, A. J. Colosimo, S. G. McLean, A. J. Van den Bogert, M. V. Paterno, and P. Succop, "Biomechanical measures of neuromuscular control and valgus loading of the knee predict anterior cruciate ligament injury risk in female athletes," *The American journal of sports medicine*, vol. 33, no. 4, pp. 492–501, 2005.

[15] L. McAtamney and E. N. Corlett, "Rula: a survey method for the investigation of work-related upper limb disorders," *Applied ergonomics*, vol. 24, no. 2, pp. 91–99, 1993.

[16] M. Tousignant, L. de Bellefeuille, S. O'donoughue, and S. Grahovac, "Criterion validity of the cervical range of motion (crom) goniometer for cervical flexion and extension," *Spine*, vol. 25, no. 3, pp. 324–330, 2000.

[17] A. Burdorf, J. Derksen, B. Naaktgeboren, and M. van Riel, "Measurement of trunk bending during work by direct observation and continuous measurement," *Applied Ergonomics*, vol. 23, no. 4, pp. 263–267, 1992.

[18] F. R. Finley and P. V. Karpovich, "Electrogoniometric analysis of normal and pathological gaits," *Research Quarterly. American Association for Health, Physical Education and Recreation*, vol. 35, no. 3, pp. 379–384, 1964.

[19] D. A. Winter, *Biomechanics and motor control of human movement*. John Wiley & Sons, 2009.

[20] L. Bilro, J. Oliveira, J. Pinto, and R. Nogueira, "A reliable low-cost wireless and wearable gait monitoring system based on a plastic optical fibre sensor," *Measurement Science and Technology*, vol. 22, no. 4, p. 045801, 2011.

[21] T. B. Moeslund, A. Hilton, and V. Krüger, "A survey of advances in vision-based human motion capture and analysis," *Computer vision and image understanding*, vol. 104, no. 2, pp. 90–126, 2006.

[22] A. Leardini, M. Benedetti, L. Berti, D. Bettinelli, R. Nativo, and S. Giannini, "Rear-foot, mid-foot and fore-foot motion during the stance phase of gait," *Gait & posture*, vol. 25, no. 3, pp. 453–462, 2007.

[23] E. Mirek, M. Rudzińska, and A. Szczudlik, "The assessment of gait disorders in patients with parkinson's disease using the three-dimensional motion analysis system vicon.," *Neurologia i neurochirurgia polska*, vol. 41, no. 2, pp. 128–133, 2007.

[24] A. Rozumalski, M. H. Schwartz, R. Wervey, A. Swanson, D. C. Dykes, and T. Novacheck, "The in vivo three-dimensional motion of the human lumbar spine during gait," *Gait & posture*, vol. 28, no. 3, pp. 378–384, 2008.

[25] B. Rosenhahn, C. Schmaltz, T. Brox, J. Weickert, D. Cremers, and H.-P. Seidel, "Markerless motion capture of man-machine interaction," in *Computer Vision and Pattern Recognition, 2008. CVPR 2008. IEEE Conference on*, pp. 1–8, IEEE, 2008.

[26] S. Corazza, E. Gambaretto, L. Mündermann, and T. P. Andriacchi, "Automatic generation of a subject-specific model for ac-

curate markerless motion capture and biomechanical applications," *IEEE Transactions on biomedical engineering*, vol. 57, no. 4, pp. 806–812, 2010.

[27] E. Surer, A. Cereatti, E. Grosso, and U. Della Croce, "A markerless estimation of the ankle-foot complex 2d kinematics during stance," *Gait & Posture*, vol. 33, no. 4, pp. 532–537, 2011.

[28] R. W. Bohannon, S. Harrison, and J. Kinsella-Shaw, "Reliability and validity of pendulum test measures of spasticity obtained with the polhemus tracking system from patients with chronic stroke," *Journal of neuroengineering and rehabilitation*, vol. 6, no. 1, p. 30, 2009.

[29] D. Lawrence, S. Domone, B. Heller, T. Hendra, S. Mawson, and J. Wheat, "Gait adaptations to awareness and experience of a slip when walking on a cross-slope," *Gait & posture*, vol. 42, no. 4, pp. 575–579, 2015.

[30] J. King, E. Harding, and A. Karduna, "The shoulder and elbow joints and right and left sides demonstrate similar joint position sense," *Journal of motor behavior*, vol. 45, no. 6, pp. 479–486, 2013.

[31] P. G. Savage, "Strapdown inertial navigation integration algorithm design part 1: Attitude algorithms," *Journal of guidance, control, and dynamics*, vol. 21, no. 1, pp. 19–28, 1998.

[32] T. Seel, J. Raisch, and T. Schauer, "Imu-based joint angle measurement for gait analysis," *Sensors*, vol. 14, no. 4, pp. 6891–6909, 2014.

[33] J. Dingwell, B. Davis, and D. Frazder, "Use of an instrumented treadmill for real-time gait symmetry evaluation and feedback

in normal and trans-tibial amputee subjects," *Prosthetics and orthotics international*, vol. 20, no. 2, pp. 101–110, 1996.

[34] S. M. Reid, R. B. Graham, and P. A. Costigan, "Differentiation of young and older adult stair climbing gait using principal component analysis," *Gait & posture*, vol. 31, no. 2, pp. 197–203, 2010.

[35] J. R. Watt, J. R. Franz, K. Jackson, J. Dicharry, P. O. Riley, and D. C. Kerrigan, "A three-dimensional kinematic and kinetic comparison of overground and treadmill walking in healthy elderly subjects," *Clinical biomechanics*, vol. 25, no. 5, pp. 444–449, 2010.

[36] R. Bogey, J. Perry, and A. Gitter, "An emg-to-force processing approach for determining ankle muscle forces during normal human gait," *IEEE Transactions on Neural Systems and Rehabilitation Engineering*, vol. 13, no. 3, pp. 302–310, 2005.

[37] J. L. Nielsen, S. Holmgaard, N. Jiang, K. B. Englehart, D. Farina, and P. A. Parker, "Simultaneous and proportional force estimation for multifunction myoelectric prostheses using mirrored bilateral training," *IEEE Transactions on Biomedical Engineering*, vol. 58, no. 3, pp. 681–688, 2011.

[38] L. J. Hargrove, K. Englehart, and B. Hudgins, "A comparison of surface and intramuscular myoelectric signal classification," *IEEE transactions on biomedical engineering*, vol. 54, no. 5, pp. 847–853, 2007.

[39] A. Shafti, B. U. Lazpita, O. Elhage, H. A. Wurdemann, and K. Althoefer, "Analysis of comfort and ergonomics for clinical work environments," in *Engineering in Medicine and Biology So-*

ciety (EMBC), 2016 IEEE 38th Annual International Conference of the, pp. 1894–1897, IEEE, 2016.

[40] K. P. Granata, D. A. Padua, and M. F. Abel, "Repeatability of surface emg during gait in children," *Gait & Posture*, vol. 22, no. 4, pp. 346–350, 2005.

[41] P. Narayanaswami, T. Geisbush, L. Jones, M. Weiss, T. Mozaffar, G. Gronseth, and S. B. Rutkove, "Critically re-evaluating a common technique accuracy, reliability, and confirmation bias of emg," *Neurology*, vol. 86, no. 3, pp. 218–223, 2016.

[42] T. Lorrain, N. Jiang, and D. Farina, "Influence of the training set on the accuracy of surface emg classification in dynamic contractions for the control of multifunction prostheses," *Journal of neuroengineering and rehabilitation*, vol. 8, no. 1, p. 25, 2011.

[43] C. D. MacKinnon and D. A. Winter, "Control of whole body balance in the frontal plane during human walking," *Journal of biomechanics*, vol. 26, no. 6, pp. 633–644, 1993.

[44] D. Datta, R. Ariyaratnam, and S. Hilton, "Timed walking test—an all-embracing outcome measure for lower-limb amputees?," *Clinical rehabilitation*, vol. 10, no. 3, pp. 227–232, 1996.

[45] K. Deluzio and J. Astephen, "Biomechanical features of gait waveform data associated with knee osteoarthritis: an application of principal component analysis," *Gait & posture*, vol. 25, no. 1, pp. 86–93, 2007.

[46] B. Burkett, J. Smeathers, and T. Barker, "Optimising the transfemoral prosthetic alignment for running, by lowering the knee joint," *Prosthetics and orthotics international*, vol. 25, no. 3, pp. 210–219, 2001.

[47] M. L. Felis, K. Mombaur, and A. Berthoz, "An optimal control approach to reconstruct human gait dynamics from kinematic data," in *Humanoid Robots (Humanoids), 2015 IEEE-RAS 15th International Conference on*, pp. 1044–1051, IEEE, 2015.

[48] A. Gefen, M. Megido-Ravid, Y. Itzchak, and M. Arcan, "Biomechanical analysis of the three-dimensional foot structure during gait: a basic tool for clinical applications," *Journal of biomechanical engineering*, vol. 122, no. 6, pp. 630–639, 2000.

[49] M. De Looze, I. Kingma, J. Bussmann, and H. Toussaint, "Validation of a dynamic linked segment model to calculate joint moments in lifting," *Clinical Biomechanics*, vol. 7, no. 3, pp. 161–169, 1992.

[50] M. P. Kadaba, H. Ramakrishnan, and M. Wootten, "Measurement of lower extremity kinematics during level walking," *Journal of orthopaedic research*, vol. 8, no. 3, pp. 383–392, 1990.

[51] A. Peters, B. Galna, M. Sangeux, M. Morris, and R. Baker, "Quantification of soft tissue artifact in lower limb human motion analysis: a systematic review," *Gait & posture*, vol. 31, no. 1, pp. 1–8, 2010.

[52] J. L. McGinley, R. Baker, R. Wolfe, and M. E. Morris, "The reliability of three-dimensional kinematic gait measurements: a systematic review," *Gait & posture*, vol. 29, no. 3, pp. 360–369, 2009.

[53] J. E. Langenderfer, P. J. Rullkoetter, A. G. Mell, and P. J. Laz, "A multi-subject evaluation of uncertainty in anatomical landmark location on shoulder kinematic description," *Computer*

methods in biomechanics and biomedical engineering, vol. 12, no. 2, pp. 211–216, 2009.

[54] J. H. de Groot, "The variability of shoulder motions recorded by means of palpation," *Clinical Biomechanics*, vol. 12, no. 7-8, pp. 461–472, 1997.

[55] J. A. Reinbolt, R. T. Haftka, T. L. Chmielewski, and B. J. Fregly, "Are patient-specific joint and inertial parameters necessary for accurate inverse dynamics analyses of gait?," *IEEE transactions on biomedical engineering*, vol. 54, no. 5, pp. 782–793, 2007.

[56] M. Katayama and M. Kawato, "Virtual trajectory and stiffness ellipse during multijoint arm movement predicted by neural inverse models," *Biological cybernetics*, vol. 69, no. 5-6, pp. 353–362, 1993.

[57] M. Millard, M. Sreenivasa, and K. Mombaur, "Predicting the motions and forces of wearable robotic systems using optimal control," *Frontiers in Robotics and AI*, vol. 4, p. 41, 2017.

[58] B. Toro, C. J. Nester, and P. C. Farren, "The status of gait assessment among physiotherapists in the united kingdom," *Archives of physical medicine and rehabilitation*, vol. 84, no. 12, pp. 1878–1884, 2003.

[59] S. Reid, J. M. Held, and S. Lawrence, "Reliability and validity of the shaw gait assessment tool for temporospatial gait assessment in people with hemiparesis," *Archives of physical medicine and rehabilitation*, vol. 92, no. 7, pp. 1060–1065, 2011.

[60] S. R. Simon, "Quantification of human motion: gait analysis—benefits and limitations to its application to clinical prob-

lems," *Journal of biomechanics*, vol. 37, no. 12, pp. 1869–1880, 2004.

[61] C. D. Metcalf, R. Robinson, A. J. Malpass, T. P. Bogle, T. A. Dell, C. Harris, and S. H. Demain, "Markerless motion capture and measurement of hand kinematics: validation and application to home-based upper limb rehabilitation," *IEEE Transactions on Biomedical Engineering*, vol. 60, no. 8, pp. 2184–2192, 2013.

[62] B. Dijkstra, Y. P. Kamsma, and W. Zijlstra, "Detection of gait and postures using a miniaturized triaxial accelerometer-based system: accuracy in patients with mild to moderate parkinson's disease," *Archives of physical medicine and rehabilitation*, vol. 91, no. 8, pp. 1272–1277, 2010.

[63] S. T. Moore, H. G. MacDougall, and W. G. Ondo, "Ambulatory monitoring of freezing of gait in parkinson's disease," *Journal of neuroscience methods*, vol. 167, no. 2, pp. 340–348, 2008.

[64] S. Finger, M. Terk, E. Subrahamanian, C. Kasabach, F. Prinz, D. P. Siewiorek, A. Smailagic, J. Stivoric, and L. Weiss, "Rapid design and manufacture of wearable computers," *Communications of the ACM*, vol. 39, no. 2, pp. 63–70, 1996.

[65] N. Yazdi, F. Ayazi, and K. Najafi, "Micromachined inertial sensors," *Proceedings of the IEEE*, vol. 86, no. 8, pp. 1640–1659, 1998.

[66] T. J. Deyle, "Low-cost inertial measurement unit.," tech. rep., Sandia National Laboratories, 2005.

[67] S. Alper and T. Akin, "A single-crystal silicon symmetrical and decoupled MEMS gyroscope on an insulating substrate," *J. Microelectromech. Sys.*, vol. 14, no. 4, pp. 707–717, 2005.

[68] S. O. Madgwick, A. J. Harrison, and R. Vaidyanathan, "Estimation of imu and marg orientation using a gradient descent algorithm," in *Rehabilitation Robotics (ICORR), 2011 IEEE International Conference on*, pp. 1–7, IEEE, 2011.

[69] S. Ananthanarayan, M. Sheh, A. Chien, H. Profita, and K. Siek, "Pt viz: towards a wearable device for visualizing knee rehabilitation exercises," in *Proceedings of the SIGCHI Conference on Human Factors in Computing Systems*, pp. 1247–1250, ACM, 2013.

[70] M. Sung, C. Marci, and A. Pentland, "Wearable feedback systems for rehabilitation," *Journal of neuroengineering and rehabilitation*, vol. 2, no. 1, p. 17, 2005.

[71] S. Patel, K. Lorincz, R. Hughes, N. Huggins, J. Growdon, D. Standaert, M. Akay, J. Dy, M. Welsh, and P. Bonato, "Monitoring motor fluctuations in patients with parkinson's disease using wearable sensors," *IEEE transactions on information technology in biomedicine*, vol. 13, no. 6, pp. 864–873, 2009.

[72] B.-R. Chen, S. Patel, T. Buckley, R. Rednic, D. J. McClure, L. Shih, D. Tarsy, M. Welsh, and P. Bonato, "A web-based system for home monitoring of patients with parkinson's disease using wearable sensors," *IEEE Transactions on Biomedical Engineering*, vol. 58, no. 3, pp. 831–836, 2011.

[73] D. Giansanti, G. Maccioni, and S. Morelli, "An experience of health technology assessment in new models of care for subjects with parkinson's disease by means of a new wearable device," *TELEMEDICINE and e-HEALTH*, vol. 14, no. 5, pp. 467–472, 2008.

[74] O. Aziz, L. Atallah, B. Lo, M. ElHelw, L. Wang, G.-Z. Yang, and A. Darzi, "A pervasive body sensor network for measuring post-operative recovery at home," *Surgical innovation*, vol. 14, no. 2, pp. 83–90, 2007.

[75] M. Goršič, R. Kamnik, L. Ambrožič, N. Vitiello, D. Lefeber, G. Pasquini, and M. Munih, "Online phase detection using wearable sensors for walking with a robotic prosthesis," *Sensors*, vol. 14, no. 2, pp. 2776–2794, 2014.

[76] P. Polygerinos, Z. Wang, K. C. Galloway, R. J. Wood, and C. J. Walsh, "Soft robotic glove for combined assistance and at-home rehabilitation," *Robotics and Autonomous Systems*, vol. 73, pp. 135–143, 2015.

[77] E. R. Post, M. Orth, P. Russo, and N. Gershenfeld, "E-broidery: Design and fabrication of textile-based computing," *IBM Systems journal*, vol. 39, no. 3.4, pp. 840–860, 2000.

[78] M.-Z. Poh, N. C. Swenson, and R. W. Picard, "A wearable sensor for unobtrusive, long-term assessment of electrodermal activity," *IEEE transactions on Biomedical engineering*, vol. 57, no. 5, pp. 1243–1252, 2010.

[79] J. Cancela, M. Pastorino, M. T. Arredondo, and O. Hurtado, "A telehealth system for parkinson's disease remote monitoring. the perform approach," in *IEEE Engineering in Medicine and Biology Society*, 2013.

[80] T. Shany, S. Redmond, M. Marschollek, and N. Lovell, "Assessing fall risk using wearable sensors: a practical discussion," *Zeitschrift für Gerontologie und Geriatrie*, vol. 45, no. 8, pp. 694–706, 2012.

[81] R. R. Manero, A. Shafti, B. Michael, J. Grewal, J. L. R. Fernández, K. Althoefer, and M. J. Howard, "Wearable embroidered muscle activity sensing device for the human upper leg," in *Engineering in Medicine and Biology Society (EMBC), 2016 IEEE 38th Annual International Conference of the*, pp. 6062–6065, IEEE, 2016.

[82] U. Maurer, A. Rowe, A. Smailagic, and D. P. Siewiorek, "ewatch: a wearable sensor and notification platform," in *Wearable and Implantable Body Sensor Networks, 2006. BSN 2006. International Workshop on*, pp. 4–pp, IEEE, 2006.

[83] E. B. Hekler, M. P. Buman, L. Grieco, M. Rosenberger, S. J. Winter, W. Haskell, and A. C. King, "Validation of physical activity tracking via android smartphones compared to actigraph accelerometer: laboratory-based and free-living validation studies," *JMIR mHealth and uHealth*, vol. 3, no. 2, 2015.

[84] O. Atalay, W. R. Kennon, and E. Demirok, "Weft-knitted strain sensor for monitoring respiratory rate and its electro-mechanical modeling," *IEEE Sensors Journal*, vol. 15, no. 1, pp. 110–122, 2015.

[85] InvenSense, *MPU-6500 Product Specification*. InvenSense, 2013.

[86] Y. Wei, R. Torah, K. Yang, S. Beeby, and J. Tudor, "Screen printing of a capacitive cantilever-based motion sensor on fabric using a novel sacrificial layer process for smart fabric applications," *Measurement Science and Technology*, vol. 24, no. 7, p. 075104, 2013.

[87] M.-S. Poboroniuc, D.-C. Irimia, A. Curteza, V. Creţu, and L. Macovei, "Improved neuroprostheses by means of knitted tex-

tiles electrodes used for functional electrical stimulation," in *Electrical and Power Engineering (EPE), 2016 International Conference and Exposition on*, pp. 320–325, IEEE, 2016.

[88] A. Shafti, R. R. Manero, A. Borg, K. Althoefer, and M. Howard, "Embroidered electromyography: A systematic design guide," *IEEE Transactions on Neural Systems and Rehabilitation Engineering*, 2016.

[89] S. D. Min, Y. Yun, and H. Shin, "Simplified structural textile respiration sensor based on capacitive pressure sensing method," *IEEE Sensors Journal*, vol. 14, no. 9, pp. 3245–3251, 2014.

[90] A. Atalay, O. Atalay, M. D. Husain, A. Fernando, and P. Potluri, "Piezofilm yarn sensor-integrated knitted fabric for healthcare applications," *Journal of Industrial Textiles*, p. 1528083716652834, 2016.

[91] Y.-D. Lee and W.-Y. Chung, "Wireless sensor network based wearable smart shirt for ubiquitous health and activity monitoring," *Sensors and Actuators B: Chemical*, vol. 140, no. 2, pp. 390–395, 2009.

[92] X. Guo, Y. Huang, X. Cai, C. Liu, and P. Liu, "Capacitive wearable tactile sensor based on smart textile substrate with carbon black/silicone rubber composite dielectric," *Measurement Science and Technology*, vol. 27, no. 4, p. 045105, 2016.

[93] S. Coyle, D. Morris, K.-T. Lau, D. Diamond, and N. Moyna, "Textile-based wearable sensors for assisting sports performance," in *Wearable and Implantable Body Sensor Networks, 2009. BSN 2009. Sixth International Workshop on*, pp. 307–311, IEEE, 2009.

[94] A. Tognetti, F. Lorussi, R. Bartalesi, S. Quaglini, M. Tesconi, G. Zupone, and D. De Rossi, "Wearable kinesthetic system for capturing and classifying upper limb gesture in post-stroke rehabilitation," *Journal of NeuroEngineering and Rehabilitation*, vol. 2, no. 1, p. 8, 2005.

[95] M. I. Mokhlespour Esfahani, O. Zobeiri, B. Moshiri, R. Narimani, M. Mehravar, E. Rashedi, and M. Parnianpour, "Trunk motion system (tms) using printed body worn sensor (bws) via data fusion approach," *Sensors*, vol. 17, no. 1, p. 112, 2017.

[96] A. Tognetti, F. Lorussi, G. Dalle Mura, N. Carbonaro, M. Pacelli, R. Paradiso, and D. De Rossi, "New generation of wearable goniometers for motion capture systems," *Journal of neuroengineering and rehabilitation*, vol. 11, no. 1, p. 56, 2014.

[97] R. R. Fletcher, K. Dobson, M. S. Goodwin, H. Eydgahi, O. Wilder-Smith, D. Fernholz, Y. Kuboyama, E. B. Hedman, M.-Z. Poh, and R. W. Picard, "icalm: Wearable sensor and network architecture for wirelessly communicating and logging autonomic activity," *IEEE Transactions on Information Technology in Biomedicine*, vol. 14, no. 2, pp. 215–223, 2010.

[98] G. López, V. Custodio, and J. I. Moreno, "Lobin: E-textile and wireless-sensor-network-based platform for healthcare monitoring in future hospital environments," *IEEE Transactions on Information Technology in Biomedicine*, vol. 14, no. 6, pp. 1446–1458, 2010.

[99] G. Ngai, S. C. Chan, V. T. Ng, J. C. Cheung, S. S. Choy, W. W. Lau, and J. T. Tse, "i* catch: a scalable plug-n-play wearable computing framework for novices and children," in *Proceedings*

of the SIGCHI Conference on Human Factors in Computing Systems, pp. 443–452, ACM, 2010.

[100] S. Coyle, K.-T. Lau, N. Moyna, D. O'Gorman, D. Diamond, F. Di Francesco, D. Costanzo, P. Salvo, M. G. Trivella, D. E. De Rossi, *et al.*, "Biotex—biosensing textiles for personalised healthcare management," *IEEE Transactions on Information Technology in Biomedicine*, vol. 14, no. 2, pp. 364–370, 2010.

[101] Analog Devices, *Digital Accelerometer Datasheet ADXL345*, 2013. Revision 0.

[102] *ITG-3200 Product Specification.*

[103] T. P. Chenal, J. C. Case, J. Paik, and R. K. Kramer, "Variable stiffness fabrics with embedded shape memory materials for wearable applications," in *Intelligent Robots and Systems (IROS 2014), 2014 IEEE/RSJ International Conference on*, pp. 2827–2831, IEEE, 2014.

[104] M. Yuen, A. Cherian, J. C. Case, J. Seipel, and R. K. Kramer, "Conformable actuation and sensing with robotic fabric," in *Intelligent Robots and Systems (IROS 2014), 2014 IEEE/RSJ International Conference on*, pp. 580–586, IEEE, 2014.

[105] M. Wehner, B. Quinlivan, P. M. Aubin, E. Martinez-Villalpando, M. Baumann, L. Stirling, K. Holt, R. Wood, and C. Walsh, "A lightweight soft exosuit for gait assistance," in *Robotics and Automation (ICRA), 2013 IEEE International Conference on*, pp. 3362–3369, IEEE, 2013.

[106] Y.-L. Park, B.-r. Chen, N. O. Pérez-Arancibia, D. Young, L. Stirling, R. J. Wood, E. C. Goldfield, and R. Nagpal, "Design and

control of a bio-inspired soft wearable robotic device for ankle–foot rehabilitation," *Bioinspiration & biomimetics*, vol. 9, no. 1, p. 016007, 2014.

[107] L. N. Awad, J. Bae, K. O'donnell, S. M. De Rossi, K. Hendron, L. H. Sloot, P. Kudzia, S. Allen, K. G. Holt, T. D. Ellis, *et al.*, "A soft robotic exosuit improves walking in patients after stroke," *Science Translational Medicine*, vol. 9, no. 400, p. eaai9084, 2017.

[108] C. M. Best, J. P. Wilson, and M. D. Killpack, "Control of a pneumatically actuated, fully inflatable, fabric-based, humanoid robot," in *Humanoid Robots (Humanoids), 2015 IEEE-RAS 15th International Conference on*, pp. 1133–1140, IEEE, 2015.

[109] S. E. Jacobs and D. L. Akin, "Human–robotic symbiosis to enable future planetary extravehicular activity," *Acta Astronautica*, vol. 66, no. 3, pp. 391–400, 2010.

[110] E. T. Roche, R. Wohlfarth, J. T. Overvelde, N. V. Vasilyev, F. A. Pigula, D. J. Mooney, K. Bertoldi, and C. J. Walsh, "A bioinspired soft actuated material," *Advanced Materials*, vol. 26, no. 8, pp. 1200–1206, 2014.

[111] O. Such, "Motion tolerance in wearable sensors-the challenge of motion artifact," in *2007 29th Annual International Conference of the IEEE Engineering in Medicine and Biology Society*, pp. 1542–1545, IEEE, 2007.

[112] R. Woodward, S. Shefelbine, and R. Vaidyanathan, "Pervasive motion tracking and muscle activity monitor," in *Computer-Based Medical Systems (CBMS), 2014 IEEE 27th International Symposium on*, pp. 421–426, IEEE, 2014.

[113] J. S. Lee, J. Heo, W. K. Lee, Y. G. Lim, Y. H. Kim, and K. S. Park, "Flexible capacitive electrodes for minimizing motion artifacts in ambulatory electrocardiograms," *Sensors*, vol. 14, no. 8, pp. 14732–14743, 2014.

[114] C. J. De Luca, L. D. Gilmore, M. Kuznetsov, and S. H. Roy, "Filtering the surface emg signal: Movement artifact and baseline noise contamination," *Journal of biomechanics*, vol. 43, no. 8, pp. 1573–1579, 2010.

[115] T. Tamura, Y. Maeda, M. Sekine, and M. Yoshida, "Wearable photoplethysmographic sensors—past and present," *Electronics*, vol. 3, no. 2, pp. 282–302, 2014.

[116] H. G. Kortier, V. I. Sluiter, D. Roetenberg, and P. H. Veltink, "Assessment of hand kinematics using inertial and magnetic sensors," *Journal of neuroengineering and rehabilitation*, vol. 11, no. 1, p. 70, 2014.

[117] K. K. P. Lukowicz, H. Junker, and G. Tröster, "Where am i: Recognizing on-body positions of wearable sensors," Springer.

[118] M. Kim, J. Lee, and K. Kim, "Tele-operation system with reliable grasping force estimation to compensate for the time-varying semg feature," in *Robotics and Automation (ICRA), 2016 IEEE International Conference on*, pp. 5561–5567, IEEE, 2016.

[119] S. Thiemjarus, "A device-orientation independent method for activity recognition," in *Body Sensor Networks (BSN), 2010 International Conference on*, pp. 19–23, IEEE, 2010.

[120] H. Harms, O. Amft, and G. Troster, "Influence of a loose-fitting sensing garment on posture recognition in rehabilitation," in

Biomedical Circuits and Systems Conference, 2008. BioCAS 2008. IEEE, pp. 353–356, IEEE, 2008.

[121] M. Yuen, H. Tonoyan, E. White, M. Telleria, and R. Kramer, "Fabric sensory sleeve for soft robot state estimation," in *Robotics and Automation (ICRA), 2017 IEEE International Conference on*, IEEE, 2017.

[122] K. Cherenack and L. van Pieterson, "Smart textiles: challenges and opportunities," *Journal of Applied Physics*, vol. 112, no. 9, p. 091301, 2012.

[123] J. Edmison, M. Jones, T. Lockhart, and T. Martin, "An e-textile system for motion analysis," *Studies in health technology and informatics*, vol. 108, p. 292, 2004.

[124] A. Leardini, L. Chiari, U. Della Croce, and A. Cappozzo, "Human movement analysis using stereophotogrammetry: Part 3. soft tissue artifact assessment and compensation," *Gait & posture*, vol. 21, no. 2, pp. 212–225, 2005.

[125] J. Fuller, L.-J. Liu, M. Murphy, and R. Mann, "A comparison of lower-extremity skeletal kinematics measured using skin-and pin-mounted markers," *Human movement science*, vol. 16, no. 2, pp. 219–242, 1997.

[126] J. P. Holden, J. A. Orsini, K. L. Siegel, T. M. Kepple, L. H. Gerber, and S. J. Stanhope, "Surface movement errors in shank kinematics and knee kinetics during gait," *Gait & Posture*, vol. 5, no. 3, pp. 217–227, 1997.

[127] R. Stagni, S. Fantozzi, A. Cappello, and A. Leardini, "Quantification of soft tissue artefact in motion analysis by combining

3d fluoroscopy and stereophotogrammetry: a study on two subjects," *Clinical Biomechanics*, vol. 20, no. 3, pp. 320–329, 2005.

[128] K. Manal, I. McClay, S. Stanhope, J. Richards, and B. Galinat, "Comparison of surface mounted markers and attachment methods in estimating tibial rotations during walking: an in vivo study," *Gait & posture*, vol. 11, no. 1, pp. 38–45, 2000.

[129] L. Cheze, B. Fregly, and J. Dimnet, "A solidification procedure to facilitate kinematic analyses based on video system data," *Journal of biomechanics*, vol. 28, no. 7, pp. 879–884, 1995.

[130] M. Loper, N. Mahmood, and M. J. Black, "Mosh: Motion and shape capture from sparse markers," *ACM Transactions on Graphics (TOG)*, vol. 33, no. 6, p. 220, 2014.

[131] M. S. Andersen, M. Damsgaard, and J. Rasmussen, "Kinematic analysis of over-determinate biomechanical systems," *Computer Methods in Biomechanics and Biomedical Engineering*, vol. 12, no. 4, pp. 371–384, 2009.

[132] R. Paradiso, G. Loriga, and N. Taccini, "A wearable health care system based on knitted integrated sensors," *IEEE transactions on Information Technology in biomedicine*, vol. 9, no. 3, pp. 337–344, 2005.

[133] E. Wressle, C. Engstrand, and A.-K. Granérus, "Living with parkinson's disease: elderly patients' and relatives' perspective on daily living," *Australian Occupational Therapy Journal*, vol. 54, no. 2, pp. 131–139, 2007.

[134] Z. Shen, J. Yi, X. Li, M. H. P. Lo, M. Z. Chen, Y. Hu, and Z. Wang, "A soft stretchable bending sensor and data glove applications," *Robotics and biomimetics*, vol. 3, no. 1, p. 22, 2016.

[135] W. Xu, N. Umetani, Q. Chao, J. Mao, X. Jin, and X. Tong, "Sensitivity-optimized rigging for example-based real-time clothing synthesis.," *ACM Trans. Graph.*, vol. 33, no. 4, pp. 107–1, 2014.

[136] S. Min and M. Tianlu, "Cloth animation based on particle model with constraint," in *Workshop on Digital Media and Digital Content Management*, pp. 141–145, 2011.

[137] V. Petrík, V. Smutnỳ, P. Krsek, and V. Hlaváč, "Physics-based model of a rectangular garment for robotic folding," in *Intelligent Robots and Systems (IROS), 2016 IEEE/RSJ International Conference on*, pp. 951–956, IEEE, 2016.

[138] H. Harms, O. Amft, and G. Tröster, "Estimating posture-recognition performance in sensing garments using geometric wrinkle modeling," *IEEE Transactions on Information Technology in Biomedicine*, vol. 14, pp. 1436–1445, Nov 2010.

[139] H. Li and Y. Wan, "An object-oriented system for dynamics-based 3d cloth simulation," in *International Conference on Information Science and Technology*, pp. 539–545, 2012.

[140] M. Tang, R. Tong, R. Narain, C. Meng, and D. Manocha, "A gpu-based streaming algorithm for high-resolution cloth simulation," in *Computer Graphics Forum*, vol. 32, pp. 21–30, Wiley Online Library, 2013.

[141] B. Chen and M. Govindaraj, "A physically based model of fabric drape using flexible shell theory," *Textile Research Journal*, vol. 65, no. 6, pp. 324–330, 1995.

[142] M. Magno, C. Spagnol, L. Benini, and E. Popovici, "A low power wireless node for contact and contactless heart monitoring," *Microelectronics Journal*, vol. 45, no. 12, pp. 1656–1664, 2014.

[143] S. Särkkä, *Bayesian filtering and smoothing*, vol. 3. Cambridge University Press, 2013.

[144] G. Clifford, J. Behar, Q. Li, and I. Rezek, "Signal quality indices and data fusion for determining clinical acceptability of electrocardiograms," *Physiological measurement*, vol. 33, no. 9, p. 1419, 2012.

[145] S. Choi and Z. Jiang, "A novel wearable sensor device with conductive fabric and pvdf film for monitoring cardiorespiratory signals," *Sensors and Actuators A: Physical*, vol. 128, no. 2, pp. 317–326, 2006.

[146] K. Li and S. Warren, "A wireless reflectance pulse oximeter with digital baseline control for unfiltered photoplethysmograms," *IEEE transactions on biomedical circuits and systems*, vol. 6, no. 3, pp. 269–278, 2012.

[147] D. Martínez-Gómez, G. Welk, M. Calle, A. Marcos, O. Veiga, A. S. Group, *et al.*, "Preliminary evidence of physical activity levels measured by accelerometer in spanish adolescents; the afinos study," *Nutricion hospitalaria*, vol. 24, no. 2, 2009.

[148] S. Butterworth, "On the theory of filter amplifiers," *Wireless Engineer*, vol. 7, no. 6, pp. 536–541, 1930.

[149] R. M. Wiard, O. T. Inan, B. Argyres, M. Etemadi, G. T. Kovacs, and L. Giovangrandi, "Automatic detection of motion artifacts in the ballistocardiogram measured on a modified bathroom scale,"

Medical & biological engineering & computing, vol. 49, no. 2, pp. 213–220, 2011.

[150] H. H. Asada, H.-H. Jiang, and P. Gibbs, "Active noise cancellation using mems accelerometers for motion-tolerant wearable biosensors," in *Engineering in Medicine and Biology Society, 2004. IEMBS'04. 26th Annual International Conference of the IEEE*, vol. 1, pp. 2157–2160, IEEE, 2004.

[151] L. B. Wood and H. H. Asada, "Low variance adaptive filter for cancelling motion artifact in wearable photoplethysmogram sensor signals," in *Engineering in Medicine and Biology Society, 2007. EMBS 2007. 29th Annual International Conference of the IEEE*, pp. 652–655, IEEE, 2007.

[152] P. Wei, R. Guo, J. Zhang, and Y. Zhang, "A new wristband wearable sensor using adaptive reduction filter to reduce motion artifact," in *Information Technology and Applications in Biomedicine, 2008. ITAB 2008. International Conference on*, pp. 278–281, IEEE, 2008.

[153] P. Gibbs and H. H. Asada, "Reducing motion artifact in wearable bio-sensors using mems accelerometers for active noise cancellation," in *American Control Conference, 2005. Proceedings of the 2005*, pp. 1581–1586, IEEE, 2005.

[154] R. Yousefi, M. Nourani, S. Ostadabbas, and I. Panahi, "A motion-tolerant adaptive algorithm for wearable photoplethysmographic biosensors," *IEEE journal of biomedical and health informatics*, vol. 18, no. 2, pp. 670–681, 2014.

[155] B. Widrow, J. R. Glover, J. M. McCool, J. Kaunitz, C. S. Williams, R. H. Hearn, J. R. Zeidler, J. E. Dong, and R. C.

Goodlin, "Adaptive noise cancelling: Principles and applications," *Proceedings of the IEEE*, vol. 63, no. 12, pp. 1692–1716, 1975.

[156] N. V. Thakor and Y.-S. Zhu, "Applications of adaptive filtering to ecg analysis: noise cancellation and arrhythmia detection," *IEEE transactions on biomedical engineering*, vol. 38, no. 8, pp. 785–794, 1991.

[157] H. Han, M.-J. Kim, and J. Kim, "Development of real-time motion artifact reduction algorithm for a wearable photoplethysmography," in *Engineering in Medicine and Biology Society, 2007. EMBS 2007. 29th Annual International Conference of the IEEE*, pp. 1538–1541, IEEE, 2007.

[158] S. Haykin and B. Widrow, *Least-mean-square adaptive filters*, vol. 31. John Wiley & Sons, 2003.

[159] W. De Clercq, A. Vergult, B. Vanrumste, W. Van Paesschen, and S. Van Huffel, "Canonical correlation analysis applied to remove muscle artifacts from the electroencephalogram," *IEEE transactions on Biomedical Engineering*, vol. 53, no. 12, pp. 2583–2587, 2006.

[160] P. S. Diniz, *Adaptive filtering*. Springer, 1997.

[161] H. Saito, T. Watanabe, and A. Arifin, "Ankle and knee joint angle measurements during gait with wearable sensor system for rehabilitation," in *World Congress on Medical Physics and Biomedical Engineering, September 7-12, 2009, Munich, Germany*, pp. 506–509, Springer, 2009.

[162] I. Cikajlo, Z. Matjačić, and T. Bajd, "Efficient fes triggering applying kalman filter during sensory supported treadmill walk-

ing," *Journal of medical engineering & technology*, vol. 32, no. 2, pp. 133–144, 2008.

[163] B. Lee, J. Han, H. J. Baek, J. H. Shin, K. S. Park, and W. J. Yi, "Improved elimination of motion artifacts from a photoplethysmographic signal using a kalman smoother with simultaneous accelerometry," *Physiological measurement*, vol. 31, no. 12, p. 1585, 2010.

[164] K. T. Sweeney, H. Ayaz, T. E. Ward, M. Izzetoglu, S. F. McLoone, and B. Onaral, "A methodology for validating artifact removal techniques for physiological signals," *IEEE transactions on information technology in biomedicine*, vol. 16, no. 5, pp. 918–926, 2012.

[165] F. Widjaja, C. Y. Shee, W. T. Latt, W. L. Au, P. Poignet, and W. T. Ang, "Kalman filtering of accelerometer and electromyography (emg) data in pathological tremor sensing system," in *Robotics and Automation, 2008. ICRA 2008. IEEE International Conference on*, pp. 3250–3255, IEEE, 2008.

[166] A. Hermanis, R. Cacurs, and M. Greitans, "Acceleration and magnetic sensor network for shape sensing," *IEEE Sensors Journal*, vol. 16, no. 5, pp. 1271–1280, 2016.

[167] D. Loebis, R. Sutton, J. Chudley, and W. Naeem, "Adaptive tuning of a kalman filter via fuzzy logic for an intelligent auv navigation system," *Control engineering practice*, vol. 12, no. 12, pp. 1531–1539, 2004.

[168] G. Ligorio and A. M. Sabatini, "A novel kalman filter for human motion tracking with an inertial-based dynamic inclinometer,"

IEEE Transactions on Biomedical Engineering, vol. 62, no. 8, pp. 2033–2043, 2015.

[169] R. Takeda, G. Lisco, T. Fujisawa, L. Gastaldi, H. Tohyama, and S. Tadano, "Drift removal for improving the accuracy of gait parameters using wearable sensor systems," *Sensors*, vol. 14, no. 12, pp. 23230–23247, 2014.

[170] H. Tan, A. M. Wilson, and J. Lowe, "Measurement of stride parameters using a wearable gps and inertial measurement unit," *Journal of biomechanics*, vol. 41, no. 7, pp. 1398–1406, 2008.

[171] M. Andriluka, S. Roth, and B. Schiele, "Pictorial structures revisited: People detection and articulated pose estimation," in *Computer Vision and Pattern Recognition, 2009. CVPR 2009. IEEE Conference on*, pp. 1014–1021, IEEE, 2009.

[172] N. J. Gordon, D. J. Salmond, and A. F. Smith, "Novel approach to nonlinear/non-gaussian bayesian state estimation," in *IEE Proceedings F (Radar and Signal Processing)*, vol. 140, pp. 107–113, IET, 1993.

[173] H. Tanizaki, *Nonlinear filters: estimation and applications*. Springer Science & Business Media, 2013.

[174] A. V. Oppenheim and R. W. Schafer, "Digital signal processing," 1975.

[175] S. Vijayakumar, A. D'souza, and S. Schaal, "Incremental online learning in high dimensions," *Neural computation*, vol. 17, no. 12, pp. 2602–2634, 2005.

[176] T. Hastie and C. Loader, "Local regression: Automatic kernel carpentry," *Statistical Science*, pp. 120–129, 1993.

[177] M. Howard and Y. Nakamura, "Locally weighted least squares temporal difference learning," in *European Symposium on Artificial Neural Networks*, 2013.

[178] S. Schaal and C. G. Atkeson, "Receptive field weighted regression," *ATR Human Information Processing Laboratories, Tech. Rep. TR-H-209*, 1997.

[179] R. J. Carroll, D. Ruppert, L. A. Stefanski, and C. M. Crainiceanu, *Measurement Error in Nonlinear Models: A Modern Perspective*. Chapman and Hall, 2006.

[180] R. H. Williams, D. W. Zimmerman, and B. D. Zumbo, "Impact of measurement error on statistical power: Review of an old paradox," *The Journal of Experimental Education*, vol. 63, no. 4, pp. 363–370, 1995.

[181] S. Park, E. Serpedin, and K. Qaraqe, "Gaussian assumption: The least favorable but the most useful [lecture notes]," *IEEE Signal Processing Magazine*, vol. 30, no. 3, pp. 183–186, 2013.

[182] W. A. Fuller, *Measurement error models*, vol. 305. John Wiley & Sons, 2009.

[183] Y. Nievergelt, "Total least squares, state of the art in numerical analysis," *SIAM Review*, vol. 36, no. 2, pp. 258–264, 1994.

[184] G. H. Golub and C. F. Van Loan, "An analysis of the total least squares problem," *SIAM Journal on Numerical Analysis*, vol. 17, no. 6, pp. 883–893, 1980.

[185] I. Markovsky and S. Van Huffel, "Overview of total least-squares methods," *Signal processing*, vol. 87, no. 10, pp. 2283–2302, 2007.

[186] W. Gander, *The Singular Value Decomposition*. Swiss Federal Institute of Technology in Zurich, 2008.

[187] C. M. Shakarji and V. Srinivasan, "Theory and algorithms for weighted total least-squares fitting of lines, planes, and parallel planes to support tolerancing standards," *Journal of Computing and Information Science in Engineering*, vol. 13, no. 3, p. 031008, 2013. Weighted Total Least Squares.

[188] S. Van Huffel and J. Vandewalle, "Analysis and solution of the nongeneric total least squares problem," *SIAM journal on matrix analysis and applications*, vol. 9, no. 3, pp. 360–372, 1988.

[189] W. S. Cleveland and S. J. Devlin, "Locally weighted regression: An approach to regression analysis by local fitting," *Journal of the American Statistical Association*, vol. 83, no. 403, pp. 596–610, 1988.

[190] S. S. Keerthi and C.-J. Lin, "Asymptotic behaviors of support vector machines with gaussian kernel," *Neural computation*, vol. 15, no. 7, pp. 1667–1689, 2003.

[191] J. Fan and Y. K. Truong, "Nonparametric regression with errors in variables," *The Annals of Statistics*, pp. 1900–1925, 1993.

[192] K. B. Petersen, M. S. Pedersen, *et al.*, "The Matrix Cookbook," *Technical University of Denmark*, vol. 7, p. 15, 2008.

[193] T. Linz, C. Kallmayer, R. Aschenbrenner, and H. Reichl, "Embroidering electrical interconnects with conductive yarn for the integration of flexible electronic modules into fabric," in *IEEE International Symposium on Wearable Computers*, pp. 86–89, IEEE, 2005.

[194] M. V. Albert, K. Kording, M. Herrmann, and A. Jayaraman, "Fall classification by machine learning using mobile phones," vol. 7, no. 5, p. e36556, 2012.

[195] K. Tuck, "Tilt sensing using linear accelerometers," *Freescale Semiconductor Application Note AN3107*, 2007.

[196] A. Ghazy and D. J. Bergstrom, "Numerical simulation of the influence of fabric's motion on protective clothing performance during flash fire exposure," *Heat and Mass Transfer*, vol. 6, no. 49, pp. 775–788, 2013.

[197] T. Demura, S.-i. Demura, M. Uchiyama, and H. Sugiura, "Examination of factors affecting gait properties in healthy older adults: focusing on knee extension strength, visual acuity, and knee joint pain," *Journal of Geriatric Physical Therapy*, vol. 37, no. 2, pp. 52–57, 2014.

[198] T. Hortobágyi, M. Lesinski, M. Gäbler, J. M. VanSwearingen, D. Malatesta, and U. Granacher, "Effects of three types of exercise interventions on healthy old adults' gait speed: a systematic review and meta-analysis," *Sports medicine (Auckland, NZ)*, vol. 45, p. 1627, 2015.

[199] J. Shim, L. G. Carlton, and Y.-H. Kwon, "Perception of kinematic characteristics of tennis strokes for anticipating stroke type and direction," *Research quarterly for exercise and sport*, vol. 77, no. 3, pp. 326–339, 2006.

[200] H. Hoffmann, "Kernel pca for novelty detection," *Pattern Recognition*, vol. 40, no. 3, pp. 863–874, 2007.

[201] N. Lawrence, "Probabilistic non-linear principal component analysis with gaussian process latent variable models," *Journal of machine learning research*, vol. 6, no. Nov, pp. 1783–1816, 2005.

[202] P. Meinicke, S. Klanke, R. Memisevic, and H. Ritter, "Principal surfaces from unsupervised kernel regression," *IEEE Transactions on Pattern Analysis and Machine Intelligence*, vol. 27, no. 9, pp. 1379–1391, 2005.

[203] S. Klanke and H. Ritter, "Variants of unsupervised kernel regression: General cost functions," *Neurocomputing*, vol. 70, no. 7, pp. 1289–1303, 2007.

[204] S. Valle, W. Li, and S. J. Qin, "Selection of the number of principal components: the variance of the reconstruction error criterion with a comparison to other methods," *Industrial & Engineering Chemistry Research*, vol. 38, no. 11, pp. 4389–4401, 1999.

[205] E. A. Nadaraya, "On estimating regression," *Theory of Probability & Its Applications*, vol. 9, no. 1, pp. 141–142, 1964.

[206] G. S. Watson, "Smooth regression analysis," *Sankhyā: The Indian Journal of Statistics, Series A*, pp. 359–372, 1964.

[207] J. Steffen, S. Klanke, S. Vijayakumar, and H. Ritter, "Towards semi-supervised manifold learning: UKR with structural hints," in *International Workshop on Self-Organizing Maps*, pp. 298–306, Springer, 2009.

[208] S. Klanke, "Learning manifolds with the parametrized self-organizing map and unsupervised kernel regression," 2007.

[209] D. W. Scott, *Multivariate density estimation: theory, practice, and visualization*. John Wiley & Sons, 2015.

[210] B. Michael and M. Howard, "Learning predictive movement models from fabric-mounted wearable sensors," *IEEE Transactions on Neural Systems and Rehabilitation Engineering*, vol. 24, no. 12, pp. 1395–1404, 2016.

[211] T. Oberg, A. Karsznia, and K. Oberg, "Basic gait parameters: reference data for normal subjects, 10-79 years of age.," *Journal of rehabilitation research and development*, vol. 30, no. 2, p. 210, 1993.

[212] D. Roetenberg, H. Luinge, and P. Slycke, "Xsens mvn: full 6dof human motion tracking using miniature inertial sensors," *Xsens Motion Technologies BV, Tech. Rep*, 2009.

[213] IvenSense, *ITG-3200 Product Specification*, 1.4 ed., 2010.

[214] Adafruit Industries, *Adafruit BNO055 Orientation Sensor*, 2010.

[215] Y. Ding *et al.*, "Imu-based iterative control for hip extension assistance with a soft exosuit," pp. 3501–3508, IEEE, 2016.

[216] S. Arlot, A. Celisse, *et al.*, "A survey of cross-validation procedures for model selection," *Statistics surveys*, vol. 4, pp. 40–79, 2010.

[217] J. Hamill and K. M. Knutzen, *Biomechanical basis of human movement*. Lippincott Williams & Wilkins, 2006.

[218] J. James *et al.*, "Movement-based interactive dance performance," in *ACM Int. Conf. on Multimedia*, pp. 470–480, 2006.

[219] S. C. Minton, *Choreography: a basic approach using improvisation*. Human Kinetics, 2007.

[220] F. Chen, Y. Liu, and H. Hu, "An experimental study on vibration isolation performance of weft-knitted spacer fabrics," *Textile Research Journal*, p. 0040517515622149, 2016.

[221] J. R. Wright, M. K. Burns, E. James, M. R. Sloan, and K. E. Evans, "On the design and characterisation of low-stiffness auxetic yarns and fabrics," *Textile Research Journal*, vol. 82, no. 7, pp. 645–654, 2012.

[222] S. Cooper, *Staging dance*. Routledge, 2016.

[223] C.-C. Yang and Y.-L. Hsu, "A review of accelerometry-based wearable motion detectors for physical activity monitoring," *Sensors*, vol. 10, no. 8, pp. 7772–7788, 2010.

[224] C. Cortes and V. Vapnik, "Support-vector networks," *Machine learning*, vol. 20, no. 3, pp. 273–297, 1995.

[225] I. Guyon and A. Elisseeff, "An introduction to variable and feature selection," *Journal of machine learning research*, vol. 3, no. Mar, pp. 1157–1182, 2003.

[226] I. T. Jolliffe, "Principal component analysis and factor analysis," *Principal component analysis*, pp. 150–166, 2002.

[227] A. Subasi, "Classification of emg signals using pso optimized svm for diagnosis of neuromuscular disorders," *Computers in biology and medicine*, vol. 43, no. 5, pp. 576–586, 2013.

[228] M. I. Mandel and D. Ellis, "Song-level features and support vector machines for music classification.," in *ISMIR*, vol. 2005, pp. 594–599, 2005.

[229] L. L. Andersen, C. H. Andersen, O. S. Mortensen, O. M. Poulsen, I. B. T. Bjornlund, and M. K. Zebis, "Muscle activation and

perceived loading during rehabilitation exercises: comparison of dumbbells and elastic resistance," *Physical therapy*, vol. 90, no. 4, p. 538, 2010.

[230] C. Peng, J. Cheng, and Q. Cheng, "A supervised learning model for high-dimensional and large-scale data," *ACM Transactions on Intelligent Systems and Technology (TIST)*, vol. 8, no. 2, p. 30, 2016.

[231] M. Galar, A. Fernández, E. Barrenechea, H. Bustince, and F. Herrera, "An overview of ensemble methods for binary classifiers in multi-class problems: Experimental study on one-vs-one and one-vs-all schemes," *Pattern Recognition*, vol. 44, no. 8, pp. 1761–1776, 2011.

[232] H. Banaee, M. U. Ahmed, and A. Loutfi, "Data mining for wearable sensors in health monitoring systems: a review of recent trends and challenges," *Sensors*, vol. 13, no. 12, pp. 17472–17500, 2013.

[233] F. Attal, S. Mohammed, M. Dedabrishvili, F. Chamroukhi, L. Oukhellou, and Y. Amirat, "Physical human activity recognition using wearable sensors," *Sensors*, vol. 15, no. 12, pp. 31314–31338, 2015.

[234] K. Watanabe, Y. Kurihara, and H. Tanaka, "Ubiquitous health monitoring at home–sensing of human biosignals on flooring, on tatami mat, in the bathtub, and in the lavatory," *IEEE Sensors Journal*, vol. 9, no. 12, pp. 1847–1855, 2009.

[235] G. Singh, T. A. Chen, R. Robucci, C. Patel, and N. Banerjee, "distratto: Impaired driving detection using textile sensors," *Sensors*, vol. 16, no. 8, pp. 2666–2673, 2016.

[236] A. Pantelopoulos and N. G. Bourbakis, "A survey on wearable sensor-based systems for health monitoring and prognosis," *IEEE Transactions on Systems, Man, and Cybernetics, Part C (Applications and Reviews)*, vol. 40, no. 1, pp. 1–12, 2010.

[237] S. Saha, H. Cano-Garcia, I. Sotiriou, O. Lipscombe, I. Gouzouasis, M. Koutsoupidou, G. Palikaras, R. Mackenzie, T. Reeve, P. Kosmas, *et al.*, "A glucose sensing system based on transmission measurements at millimetre waves using micro strip patch antennas," *Scientific reports*, vol. 7, no. 1, p. 6855, 2017.